ABSTRACT

Title of Dissertation: SOFT AQUEOUS STRUCTURES WITH SMART SKINS OR MEMBRANES: REGULATING THE RELEASE OF SOLUTES

Sai Nikhil Subraveti,
Doctor of Philosophy, 2022

Directed By: Professor Srinivasa R. Raghavan,
Department of Chemical and Biomolecular Engineering

In nature, various soft materials have a water-rich core covered by a hydrophobic layer, i.e., a membrane or skin. These 'smart' or 'adaptive' membranes regulate the molecules that can enter or leave the core. Membranes enclose cells (microscale structures) as well as vesicles in the cells (nanoscale structures). At the macroscale, fruits and vegetables, as well as the human body are covered with skins. Currently, researchers are developing many soft, aqueous materials across length scales, including hydrogels, capsules, and vesicles, which are being used in areas such as drug delivery, pharmaceutics, and cosmetics. *In this study, we will explore the synthesis of 'smart' skins or membranes around these structures with a goal of regulating solute release.*

In our first study, we put forward a simple technique for synthesizing a hydrophobic skin to cover any hydrogel. An analogy is made to the peelable skin around fruits and vegetables. To make the skin, we employ an inside-out polymerization, where one component of the polymerization (the initiator) is present only in the gel core while other components (the monomers) are present only in the external medium. The thin polymeric skin (~ 10 to 100 μm in thickness) grows outward from the core in a few minutes. We show that the skin prevents the gel from swelling in water and also from drying in air. Hydrophilic solutes are *completely prevented from leaking out* into the external solution, while harmful microbes are prevented by the skin from attacking the gels. The properties of the skin are tunable, including its thickness and its

mechanical properties. A polyurethane skin is elastomeric, transparent, and peelable from the core hydrogel. Conversely, other skins can be hard and brittle (glass-like).

Next, we alter the recipe for the skin around hydrogels by *incorporating redox-responsive monomers*. In the presence of an oxidizing agent, the initially hydrophobic skin becomes hydrophilic, thereby 'turning on' the release of solutes out of the gel. The release rate of various solutes can be easily controlled by changing the parameters such as solute loading, skin thickness as well as the concentration of oxidative species in the external medium. Conversely, solute release can also be 'turned off' at a later time by adding a reducing agent that reverts the skin to its hydrophobic state. Thus, our smart skin enables the *on-off release of solutes out of a gel*, and this concept is likely to be useful in many applications.

Lastly, we turn our attention to smaller nanocontainers, i.e., vesicles. We have come up with a way to make the membranes of vesicles responsive to multiple stimuli such as reactive oxygen species (ROS), temperature and ultraviolet (UV) light. The vesicle membrane is formed by a combination of cationic and anionic surfactant molecules, and the stimuli alter the geometry of these molecules. In turn, the vesicles are converted into micelles, resulting in the burst release of solutes out of the vesicle core. High-energy radiation used in cancer treatment is known to generate ROS – so, one application of these 'smart' vesicles could be in the radiation-induced burst-release of chemotherapeutic drugs, which could increase the effectiveness of cancer treatment.

SOFT AQUEOUS STRUCTURES WITH SMART SKINS OR MEMBRANES: REGULATING THE RELEASE OF SOLUTES

by

Sai Nikhil Subraveti

Dissertation submitted to the Faculty of the Graduate School of the
University of Maryland, College Park, in partial fulfillment
of the requirements for the degree of
Doctor of Philosophy
2022

Advisory Committee:

Professor Srinivasa R. Raghavan, Dept. of Chemical & Biomolecular Engineering, Chair
Professor Peter Kofinas, Dept. of Chemical & Biomolecular Engineering
Professor Robert M. Briber, Dept. of Materials Science & Engineering
Professor Chen Zhang, Dept. of Chemical & Biomolecular Engineering
Professor Ian White, Fischell Department of Bioengineering, Dean's Representative

This dissertation is dedicated to my parents and my brother,
for their constant support and unconditional love.

Acknowledgements

I express my deepest gratitude to my advisor Prof. Srinivasa Raghavan for allowing me to pursue doctoral studies in his group. This successful endeavor would not have been possible without his continual encouragement to explore different research topics. His vision, research approach, ability to mentor students, and methodology to present research work with utmost clarity have deeply inspired me. I wish to carry forward these invaluable lessons throughout my scientific career. In all, I could not have asked for a better advisor and mentor for my doctoral studies.

Besides my advisor, I would like to thank the rest of my committee: Prof. Peter Kofinas, Prof. Robert Briber, Prof. Chen Zhang, and Prof. Ian White for their valuable advice and feedback on my research projects. Especially, I am very grateful to Prof. Kofinas and Prof. Briber for their guidance, and insights provided during the polymer group meetings. I would like to extend my sincere thanks to Prof. Narottam Lamichhane for his advice and discussions related to the vesicles work. I would also like to appreciate Prof. Wen-An Chiou for his assistance with the electron microscopy experiments.

I am highly indebted to my roommates: Mrinalgouda Patil, Koushik Marepally, Abhishek Shastry, Shashank Maurya, and Animesh Shastry for making my journey of five years at Maryland fabulous. I appreciate all the stimulating discussions we had over the years, and more importantly, I thoroughly enjoyed playing cricket and badminton with them. I would especially like to acknowledge Mrinal and Koushik for their help with everything outside of research. I am also thankful to my colleagues from Dr. Raghavan's group, both present and past, for all the help

I received related to my research activities. Specifically, I would like to thank Hema Choudhary and Leah Borden for their moral support and friendship throughout the years. Many thanks to Faraz Ahmed Burni for imparting his knowledge through the late-night feedback sessions. I am also thankful to Dr. Niti Agrawal, Dr. Sohyun Ahn, Dr. Ben Thompson, Sairam Ganesh, Medha Rath, Wenhao Xu, Uma Kokilepersaud, and my undergrads Morine Nader, Sebastian Peters, and Luxman Maheswaran.

Finally, I would like to express my appreciation to my parents. Words cannot express my gratitude for their unconditional love, support, and numerous sacrifices. The value of education that they instilled in me at a young age is the primary reason I am where I am today. Moreover, I could not have possibly undertaken this journey without the help and unwavering support from my brother Dr. Gokul Subraveti.

Table of Contents

List of Figures

List of Abbreviations

ROS	Reactive oxygen species
UV	Ultraviolet
AAm	Acrylamide
NIPA	N – Isopropyl acrylamide
PEGDA	Polyethylene glycol diacrylate
BIS	N,N′-methylenebisacrylamide
LCST	Lower critical solution temperature
UDA	Urethane diacrylate
SEM	Scanning electron microscopy
PEGDMA	Polyethylene glycol dimethacrylate
UHA	Urethane hexa-acrylate
SA	Sodium acrylate
DI	Deionized
HCl	Hydrochloric acid
DC	Direct current
LED	Light emitting diode
MTEMA	2-(methylthio)ethyl methacrylate
EDX	Energy-dispersive X-ray
H_2O_2	Hydrogen peroxide
MSEMA	2-(methylsulfinyl)ethyl methacrylate

VitC	Vitamin C
FTIR	Fourier-transform infrared
PDST	(4-Phenylthiophenyl)diphenylsulfonium triflate
SDBS	Sodium dodecylbenzenesulfonate
DLS	Dynamic light scattering
Vis	Visible
OD	Optical density
Ca^{2+}	Calcium ions
Cu^{2+}	Copper ions
Fe^{3+}	Iron ions
3-D	Three dimensional
EGDMA	Ethylene glycol dimethacrylate
HMPP	2-hydroxy-2-methyl-propiophenone
CPP	Critical packing parameter
LPTBP	lithium phenyl-2,4,6-trimethyl-benzoylphosphinate
$CaCl_2$	calcium chloride dihydrate
•OH	Hydroxyl radicals
O_2^-	Superoxide
$^1O_2$	Singlet oxygen
DNA	Deoxyribonucleic acid
IRG	Irgacure 2959
TEMED	N,N,N′,N′-tetramethyl-ethylenediamine

NaCl	Sodium chloride
NBS	N-bromosuccinimide
CTAT	hexadecyl trimethylammonium p-toluenesulfonate
ODPI	p-octyloxydiphenyliodonium hexafluoroantimonate
Na_2HPO_4	Disodium hydrogen phosphate
TEM	Transmission electron microscope
SEC	Size-exclusion chromatography
MWCO	Molecular weight cut-off
SFL	Stop-flow lithography
PDMS	Polydimethylsiloxane
Se	Selenium
Te	Tellurium
RT	Radiation therapy
NSCLC	Non-small cell lung cancer

Chapter 1
Introduction and Overview

1.1 Problem Description and Motivation

Aqueous structures made from polymers, colloids, and amphiphilic molecules are routinely used in various industrial formulations for encapsulating small-molecule solutes such as drugs, agrochemicals, flavor-ingredients, or cosmetic agents.[1-7] Two examples of these are polymer hydrogels and lipid or surfactant vesicles. Hydrogels can be made at the macroscale (~ 1 cm) or at the microscale (10 to 100 μm) while vesicles are typically at the nanoscale (~ 100 nm). The problem with all these structures is that the moment they are placed in contact with water, the solutes will rapidly leak of by diffusion. Ideally, there should be a way to regulate the release of solutes – i.e., to ensure zero release until the desired time, and thereafter, for the release to be 'switched on'. This release should either occur at a controlled rate over some time, or as a burst. Moreover, it would be even better if this was a repeatable switch, i.e., if the release could be cycled many times between the on and off states. Such a perfect, cyclical on-off release of contents from hydrogels or vesicles has never been achieved to our knowledge.

There have been many reports demonstrating the pulsatile on-off release of solutes from some gels, e.g., in the case of thermosensitive poly(*N*-isopropylacrylamide) (NIPA) hydrogels by cycling temperature.[8-10] However, in all these studies, solute release in the 'off' state (where there is supposed to be no release) is not zero. Thus, given time (say a few hours or a day) most of the solute would still leak out of the gel in the 'off' state. Thus, none of these gels can ensure a 'hermetic' seal for solutes. Recently, our lab demonstrated a hermetic seal of small-molecule

solutes in a gel for the first time, and this was done by creating a wax shell around the gel.[11] For this, the gel was dropped into molten paraffin (or other) wax for a few seconds, which resulted in an opaque wax shell around the gel. The wax shell, being hydrophobic, served as a perfect barrier to solutes in the gel, and thus zero release out of the gel could be ensured for months. Furthermore, the release could be "switched on" by melting the wax by heat. However, the downsides to wax shells are that they are opaque and relatively thick. Moreover, the release cannot be "switched off" i.e., once the wax melts, the release cannot be stopped. Hence, there is still an unmet need to achieve perfect cyclical on-off release of small molecule solutes from aqueous structures.

1.2 Proposed Approach

The overall goals of this work are to create *'smart' skins or membranes around aqueous structures, i.e., hydrogels and vesicles.* Thereby, the release of solutes from the aqueous core can be regulated by external stimuli. We are aimed to achieve some of the idealized release profiles, including a hermetic seal followed by burst release, or a cyclical on-off release. Three examples of smart skins/membranes are described in this dissertation:

1.2.1 Hydrogels with Protective Skins

In Chapter 3, we describe a simple technique for synthesizing a protective polymer skin around any hydrogel (macro or micro scale) (Figure 1.1A). We employ an inside-out polymerization, where the hydrogel cores are loaded with one component of the polymerization (the initiator) and then placed in a solution containing the other components (the monomers). The key to our technique is that the initiator is chosen in such a way that it is soluble both in water and in the organic monomer. Conversely, the organic monomer is chosen to be a viscous

liquid that is completely insoluble in water. Upon polymerization, a thin polymeric skin encompasses the gel core. Figure 1.1A shows that the skin formed is thin and hydrophobic, and it completely prevents solute release (i.e., provides a hermetic seal). It is also peelable, and when peeled off, the contents are released in a burst due to diffusion of solutes. Figure 1.1B shows the idealized release profile (hermetic seal followed by burst release) for this skin-covered hydrogel system.

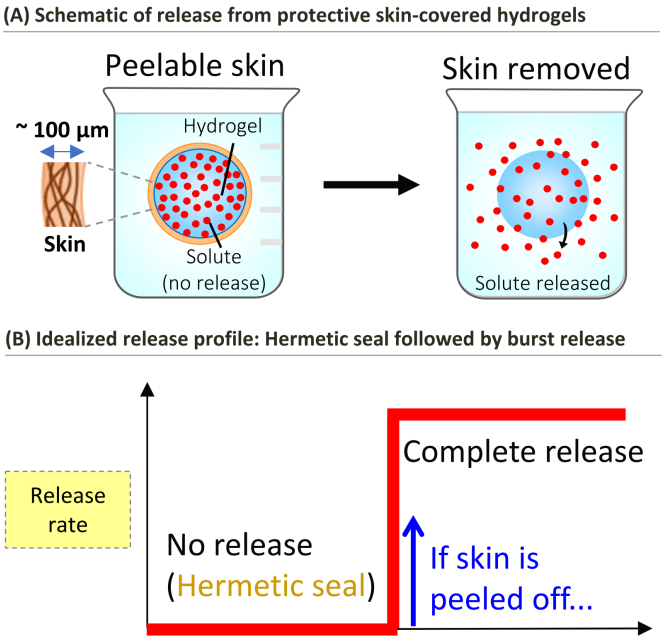

Figure 1.1. Solute release from hydrogels with protective skins. (A) Schematics of release from protective skin-covered hydrogels before and after peeling the skin. (B) Idealized release profile using the skin-covered hydrogel: hermetic seal with intact skin, followed by burst release once the skin is peeled off.

1.2.2 On-Off Release from Smart Skin-Covered Hydrogels

In Chapter 4, we describe a 'second-generation' smart skin around hydrogels (macro or micro scale) that is similar to the one above but enables idealized cyclical on-off release (Figure 1.2B). This skin is made with redox-responsive monomers. Initially, the skin is hydrophobic, and it hermetically seals the solute from releasing out of the gels. Oxidizing agents make the skin

hydrophilic and thereby switch on the release of contents, as shown in Figure 1.2A. The skin is then reverted to its hydrophobic form by using reducing agents. We also extend our technique of forming skin-covered hydrogels to create free-standing flat smart polymer membranes that exhibit redox-responsive on-off flux of small molecule solutes across the membranes.

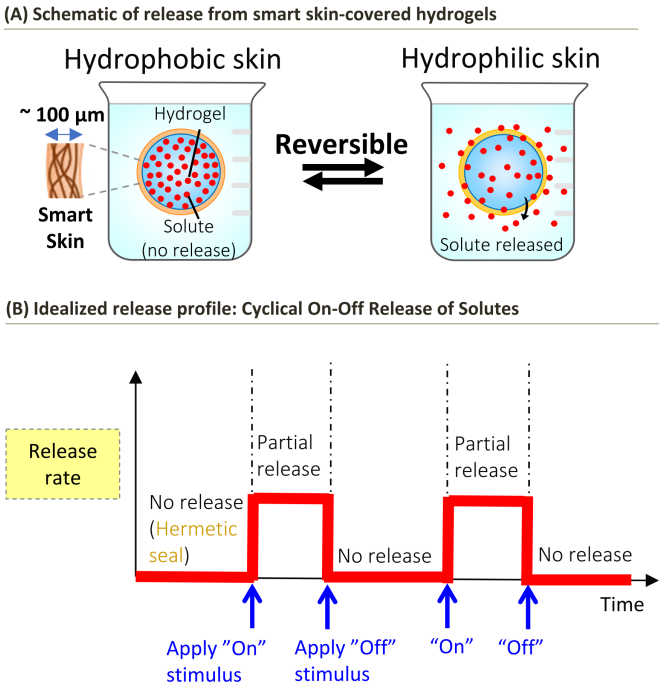

Figure 1.2. Solute release from smart-skin covered hydrogels. (A) A schematic of on-off release of solutes by reversibly converting the chemistry of the skin from a hydrophobic to a hydrophilic form. (B) Idealized release profile for smart-skin covered hydrogels: cyclical on-off release of solutes upon applying stimuli.

1.2.3 Smart Membranes Around Vesicles

Finally, in Chapter 5, we demonstrate the synthesis of smart membranes around vesicles (nano scale) that can be disrupted by UV light or by reactive oxygen species (ROS) or by temperature, thereby enabling a burst-release of solutes (Figure 1.3A). The vesicles are made from low-cost, commercially available amphiphilic molecules. Initially, the solutes encapsulated in these vesicles are released very slowly via diffusion with almost negligible release rates

(Figure 1.3B). However, upon applying stimuli such as temperature, ROS, or UV, burst-release is achieved because the molecules in the vesicle membrane are induced to change their geometry, and in turn they reassemble into micelles, which are smaller and have a hydrophobic core.

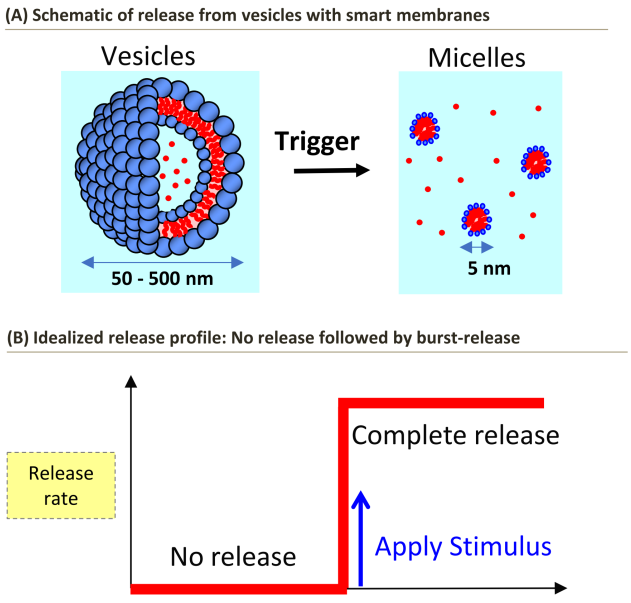

Figure 1.3. Solute release from vesicles with smart membranes. (A) A schematic of burst-release from vesicles with smart membranes due to their transformation to smaller micelles upon applying a trigger. (B) Idealized release profile of hermetic seal followed by burst release is achieved by the self-assembly transformation from vesicles to micelles.

1.3 Significance of This Work

The significance of this work is that it seeks to overcome the limitations associated with solute release from aqueous structures such as hydrogels and vesicles. By having smart skins/membranes around these structures, idealized solute release profiles that are generally considered impossible to achieve with small-molecule solutes can now be realized. Our approaches can be applied to a wide of range of solutes, and can thereby impact a wide array of

practical applications. These include delivery of drugs or other therapeutics (pharmaceutical industries), delivery of cosmetic or hydration agents (skin-care and cosmetics industries), delivery of agrochemicals or pesticides (agricultural industries), and delivery of flavor or nutritional ingredients (food industries). Importantly, our approaches to make skins/membranes use low-cost, commercially available precursors, and should therefore be scalable. Other broader impacts from the studies in Chapters 3-5 include:

- In Chapter 3, the hydrophobic skin around hydrogels serves as a protective barrier. While this protection prevents hydrogels from drying out and from swelling in water, it also protects the gels from harmful chemical and biological attack (e.g., from strong acids and mold). Overall, the presence of the skin improves the shelf life of the hydrogels and their long-term stability in aqueous fluids or when exposed to air. Stable hydrogels could be valuable in fields such as soft robotics, soft electronics, and as biomedical implants.

- The smart skin in Chapter 4 enables on-off release of hydrophilic small-molecule solutes from hydrogels. Moreover, extension of our technique to synthesize flat free-standing smart membranes is demonstrated. Such smart polymer membranes could be employed in applications such as separations, water purification and coatings for agriculture.

- Lastly, the vesicles with 'smart' membranes from Chapter 5, with their ability to transform to smaller micelles in the presence of ROS could be useful in the context of cancer treatment. It is well known that high-energy radiation such as X-rays and gamma rays that are used for radiation therapy generate ROS at the tumor site, and in fact, it is these ROS that are supposed to kill the tumor cells.[12] Loading chemotherapeutic drugs into these ROS-

responsive vesicles, and then radiating the tumor site would also simultaneously induce vesicles to release their payload into the tumor. Because radiation is already localized, there will be no systemic release of the payload to other healthy tissues. Thus, we could synergistically combine radiation and chemotherapy in a single step and thereby make cancer treatment more effective.

Chapter 2

Background

2.1 Smart Membranes or Skins in Nature

A variety of soft aqueous materials found in nature have water-rich cores covered by membranes or skins, as shown in Figure 2.1. These include structures across different length scales, ranging from the nanoscale (e.g., organelles in cells) to the microscale (e.g., cells) to the macroscale (e.g., fruits and vegetables, animals). The membranes and skins are 'smart' or 'adaptive': i.e., they tightly regulate the transport of materials into or out of the cores.[13,14] By doing so, they protect the interiors from toxic substances and other physical attacks.

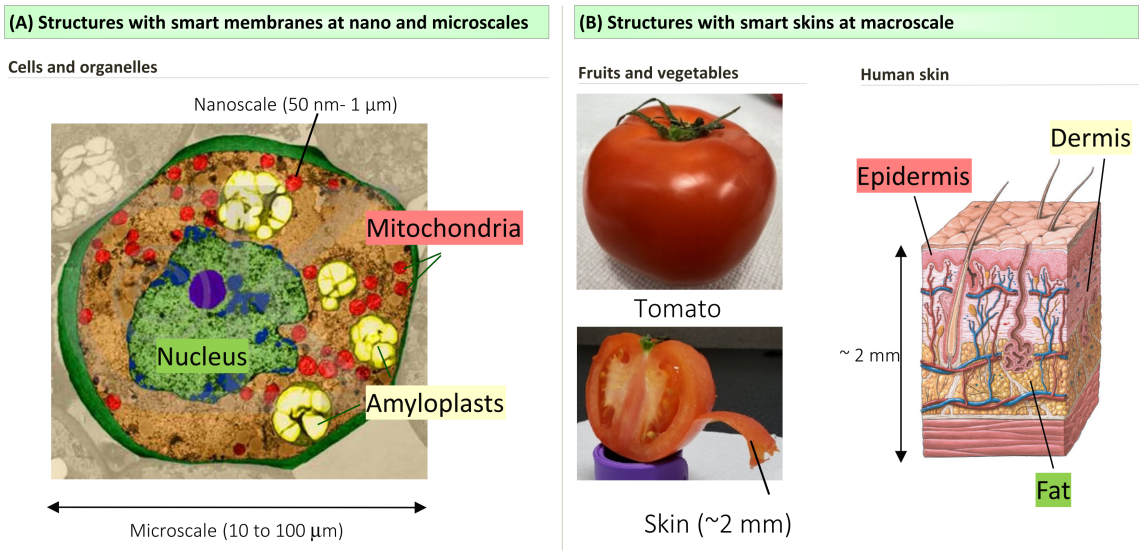

Figure 2.1. Soft natural aqueous structures with smart skins or membranes. (A) A eukaryotic cell (microscale) with organelles (nanoscale compartments). Image adapted from Lu et al.[15] (B) A tomato (example for fruits and vegetables) with the skin partially peeled off, and a schematic of human skin. The latter is adapted from Igarashi et al.[16]

Cell membranes are made of lipids and membrane proteins and they perform complex and sophisticated functions. For example, they control the precise movement of ions into or out of cells.[17] Many processes such as immune responses and muscle contraction are mediated by the flow of ions across cell membranes. Proteins that are involved in the transport of ions across membranes fall into two categories: ion channels and ion pumps (Figure 2.2). Ion channels allow passive transport of ions through the membrane down the concentration gradient, while ion pumps actively push the ions against their concentration gradients.[18] Both ion pumps and ion channels can contain gates that regulate the flow of ions when needed upon receiving activation signals.[19]

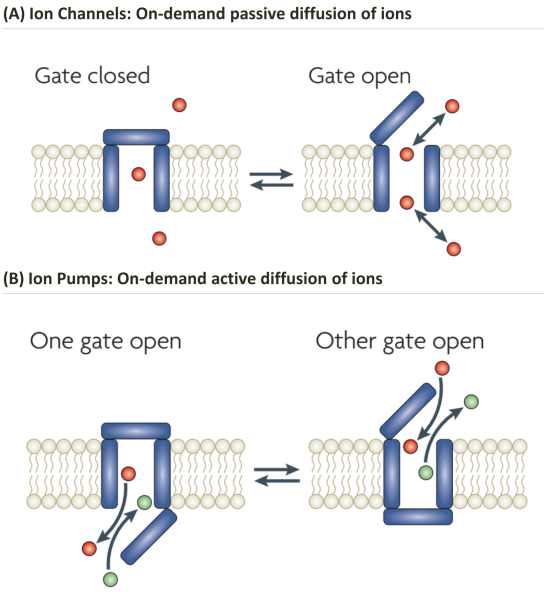

Figure 2.2. Ion channels and ion pumps in cell membranes for the transport of ions. (A) Schematic of an ion channel through which ions (red spheres) move passively. (B) Schematic of an ion pump through which ions can move actively against their gradient. Adapted from Gadsby et al.[18]

At the macroscale, the skin around humans (as well as other mammals) is the largest organ in the body. It has three main layers: epidermis, dermis and the subcutaneous (fat) layer as shown in Figure 2.1B. In addition to its protective functions,[20] another important function of the skin is in thermoregulation (ability to maintain body temperature within certain boundaries). Perspiration or the process of sweating from the skin surface plays a vital role in thermoregulation.[21] The release of water and sodium chloride in the form of sweat is an adaptive response to environmental conditions.[22]

2.2 Soft Aqueous Materials

Soft materials are those that are easily deformable by thermal or mechanical forces.[23] They are present everywhere, from foods we eat to consumer and industrial products such as toothpaste, paints, gels, and adhesives. Moreover, living creatures, including humans, are made of soft materials. Primarily, soft materials are made from building blocks such as amphiphiles, polymers and colloidal nanoparticles (Figure 2.3). These building blocks share a common characteristic of having the propensity to self-assemble into mesoscopic structures that are much larger than individual atoms and yet smaller than macroscopic sizes.[24] Self-assembly refers to the spontaneous organization of precursors into well-defined ordered structures, driven by the thermodynamics of the overall system.[25,26] A few notable examples of soft materials formed by the self-assembly of building blocks include gels, vesicles, micelles, and liquid crystals.[27]

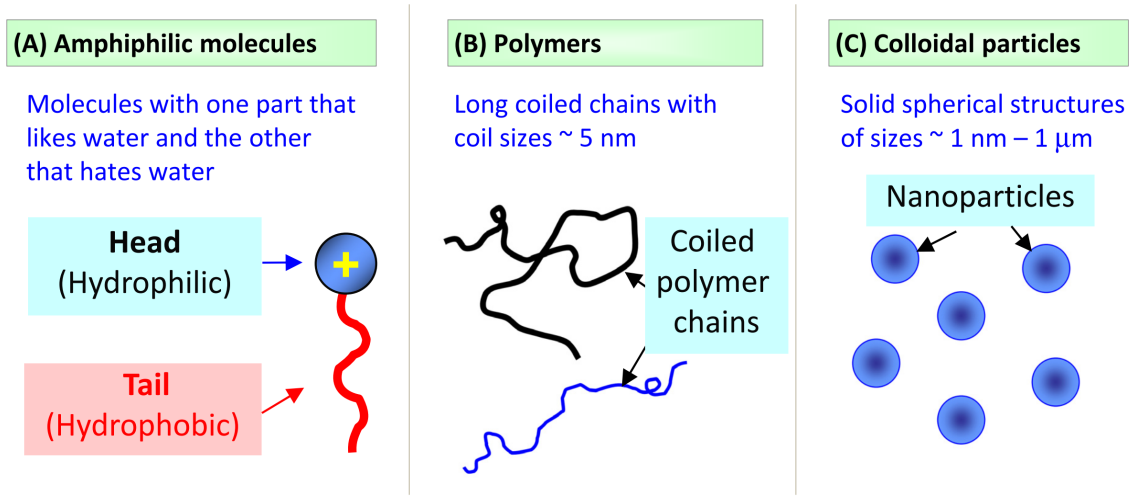

Figure 2.3. Building blocks of soft materials. (A) Amphiphilic molecules with hydrophilic head groups (blue) and hydrophobic tails (red). (B) Polymers, shown as long coiled chains. (C) Colloidal or nanoparticles shown by blue spheres.

Soft materials exhibit some unique properties such as viscoelasticity. As an example, silly putty behaves like a solid at short timescales (it can be bounced on a hard surface), but like a liquid at long timescales (it flows slowly in a container). Another example is toothpaste, which behaves like a solid at rest when placed on a toothbrush, whereas it flows like a liquid when squeezed out from the tube. This property of the same material to behave as either a solid or a liquid is termed as viscoelasticity. Another characteristic property of soft materials due to their having nanoscale or microscale structure (i.e., in the size range of 1 nm – 1 µm) is their ability to scatter radiation such as light. Light scattering is what makes milk turbid and why the path of a laser pointer appears bright and distinct in a micellar solution (Tyndall effect). Examples of soft aqueous materials that are of interest in this study include polymer hydrogels and surfactant vesicles. These have become very popular due to their simplicity and utility in the biomedical, agricultural, food, cosmetics, and textile industries.[1-7]

2.3 Polymer Hydrogels

Gels are three-dimensional networks of polymer chains connected by crosslinks.[28,29] They show elastic (solid-like) behavior with an infinite viscosity and a finite shear modulus. Gels containing water are termed hydrogels whereas those containing oil are called organogels.[30,31] In hydrogels, the presence of hydrophilic functional groups attached to the polymer chains give them the ability to absorb water, while the crosslinks prevent them from dissolving in water. Figure 2.4A shows an example of the widely used gelatin hydrogel (Jell-O) that is commonly consumed as a dessert. Figure 2.4B shows the schematic of a hydrogel at the nanoscale showing a crosslinked polymer network having a characteristic pore or mesh size.[32] Typically, this mesh size ranges from 5-100 nm.[33]

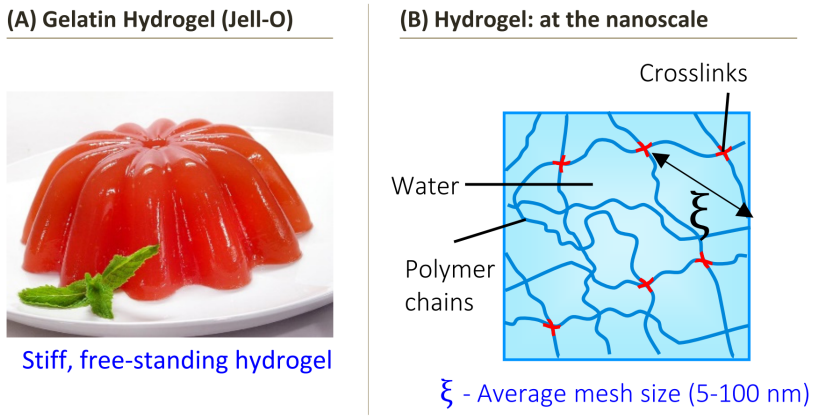

Figure 2.4. Common hydrogel and its nanoscale structure. (A) A gelatin hydrogel (Jell-O) (https://www.cookingchanneltv.com/recipes/watermelon-limeade-jello-2120124) (B) Schematic of a hydrogel at the nanoscale showing the crosslinked polymer network, which is characterized by its mesh size.

The extent to which gels swell in a solvent is determined by the equilibrium between the osmotic pressure inside the gel and the elastic pressure of the polymer chains.[34] For gels with

non-ionic polymer chains, the swelling extent is predicted by the Flory-Rehner equation, which is given by:

$$-\left[\ln\left(1-\phi_{\mathrm{p}}\right)+\phi_{\mathrm{p}}\right]=\chi\phi_{\mathrm{p}}^{2}+V_{\mathrm{s}}\cdot\nu\cdot\left(\phi_{\mathrm{p}}^{\frac{1}{3}}-\frac{\phi_{\mathrm{p}}}{2}\right) \qquad (2.1)$$

Here, ϕ_{p} is the volume fraction of the polymer in the swollen gel, χ is the polymer-solvent interaction parameter, V_{s} is the molar volume of the solvent, and ν is the density of crosslinks in the gel. If the polymer likes the solvent, $\chi < 0.5$ and if the polymer hates the solvent, $\chi > 0.5$. One trend from the above equation is that if $\chi < 0.5$, then ϕ_{p} will be low, implying that the gel will swell appreciably in water. Secondly, if the density of crosslinks ν is low, then again ϕ_{p} will be low and the gel will swell significantly. Another point to note is that ionic gels swell much more than non-ionic gels due to the higher osmotic pressure arising from the presence of counterions and also from the electrostatic repulsions between the polymer backbones.[34]

Hydrogels can be made from a variety of common biopolymers such as alginate, chitosan, hyaluronic acid, agarose, and collagen, which are obtained from natural sources such as algae, animals, plants, and micro-organisms.[30,35] Biopolymer-based hydrogels have several advantages over the synthetic polymer-based hydrogels in terms of their inherent biocompatibility, abundance, safety, and low cost.[35] Among these, alginate hydrogels are of particular interest in this study.[36] Sodium alginate is an anionic polysaccharide that is isolated from brown algae.[37] It is a linear unbranched copolymer that is composed of (1,4)-linked β-D-mannuronic acid (M) and α-L-guluronic acid (G) residues. These M and G residues are covalently bonded together in blocks or sequences. Alginates have different ratios of M to G blocks depending on their sources.[38,39] Alginate hydrogels are formed when the carboxylate

groups on G blocks are complexed with multivalent cations such as calcium (Ca^{2+}), copper (Cu^{2+}) or iron (Fe^{3+}) through electrostatic interactions[37,40] to form egg-box junctions (Figure 2.5A). By simply dropping a solution of sodium alginate into a solution containing cations like Ca^{2+}, alginate hydrogels can be made (Figure 2.5B).

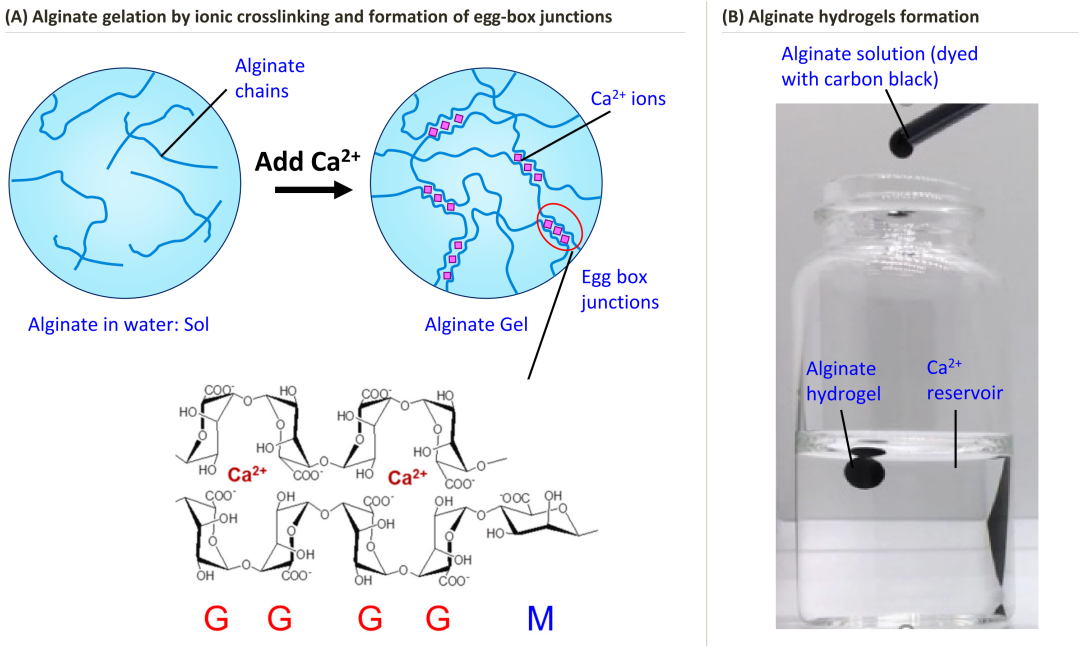

Figure 2.5. Alginate and its gelation process. (A) Alginate in water is initially a sol, but once Ca^{2+} ions are added, it becomes a gel due to electrostatic complexation of negatively charged alginate chains with the Ca^{2+} (at "egg-box" junctions). Alginate chains have G and M blocks and only the G blocks take part in forming these junctions. (B) Alginate gels are created by simply dropping an alginate solution into a Ca^{2+} containing reservoir.

As an alternative to biopolymer-based hydrogels, synthetic hydrogels can be formed through free radical polymerization.[28,29] This process involves the reaction of hydrophilic monomers with multi-functional covalent crosslinkers in the presence of thermal or UV initiators. Typical monomers include those with acrylate, vinyl, or methacrylate groups such as acrylamide (AAm), N-isopropyl acrylamide (NIPA). Common difunctional crosslinkers include

polyethylene glycol diacrylate (PEGDA) and N,N′-methylenebisacrylamide (BIS). Their structures are shown in the Figure 2.6.

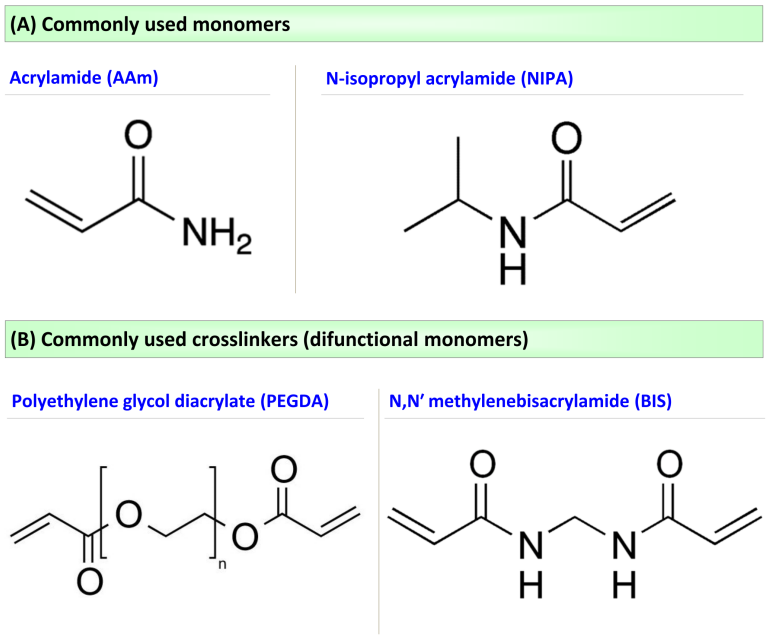

Figure 2.6. Examples of monomers and crosslinkers used for synthesizing synthetic hydrogels. (A) Acrylamide (AAm), (B) N-isopropyl acrylamide (NIPA), (C) Polyethylene glycol diacrylate (PEGDA), and (D) N,N′-methylenebisacrylamide (BIS).

Hydrogel synthesis involves preparing a prepolymer solution (sol) containing the monomer, crosslinker, and the initiator in water (Figure 2.7). Next, the prepolymer solution is subjected to heat or UV light, which causes the initiator to dissociate into free radicals. The free radicals interact with the carbon-carbon double bonds on the monomers and crosslinkers to begin the process of chain growth. A monomer such as AAm, with just one carbon-carbon double bond forms only linear chains. However, crosslinkers such as BIS and PEGDA with two carbon-carbon double bonds act as crosslinkers to connect one growing chain to another, creating a

three-dimensional (3-D) network of polymers. This polymer network entraps the water to form the gel: note that the gel holds its weight on inversion of the vial in Figure 2.7.

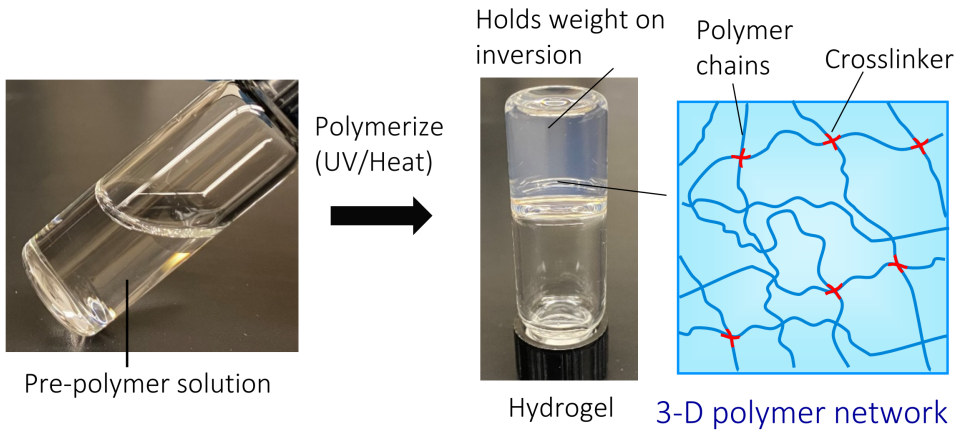

Figure 2.7. Synthetic hydrogel synthesis. A prepolymer solution of monomer, crosslinker and initiator is subjected to UV light or heat to form the hydrogel by free-radical polymerization. A schematic of the gel (right) shows the polymer chains being crosslinked into a 3-D network.

Hydrogels can encapsulate a wide range of hydrophilic solutes in their 3-D network. Release of solutes from the gel is primarily dictated by the mesh size of the network (Figure 2.4B), which is typically in the range of 5-100 nm.[33] For solutes that are smaller than the mesh size ($r_{solute}/r_{mesh} < 1$), the solute is easily released from the gel into the external medium by passive diffusion. If the solute and the polymer backbone experience attractive interactions, the solute release can be slightly slowed down. Conversely, for solutes that are closer to the mesh size ($r_{solute}/r_{mesh} \sim 1$), slow and controlled release can be achieved due to steric hindrance. Solutes that are much larger than the mesh size ($r_{solute}/r_{mesh} >> 1$) can be permanently entrapped in the gel.[33]

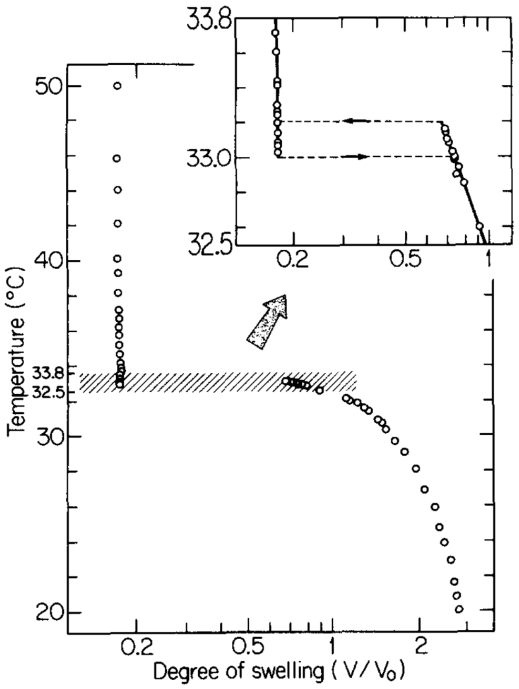

Figure 2.8. Volume change of NIPA gels on heating. When heated to a temperature above its LCST (32°C), NIPA gels shrink drastically. Adapted from Hirokawa et al.[41]

Hydrogels can be designed to respond to external stimuli such as temperature, pH, and light.[28,29,42,43] As an example, gels of NIPA respond to temperature.[44] Below 32°C, the isopropyl groups on NIPA chains are hydrated, and the gel is in a swollen state. On the contrary, when heated above 32°C, which is the lower critical solution temperature (LCST) of NIPA, the isopropyl groups become more hydrophobic and the NIPA chains undergo a coil-to-globule transition.[41,44] This results in water being released out of the gel, with a sharp reduction in the overall gel volume (Figure 2.8). The drastic shrinkage of NIPA gels in response to temperature is widely utilized in several applications.

2.4 Vesicles and Their Self-Assembly

Vesicles are another important class of soft materials, made from two-tailed lipids or from a combination of oppositely-charged single-tailed surfactants.[45] They are containers with an aqueous core surrounded by a bilayer (Figure 2.9). Hydrophilic solutes can be encapsulated in the aqueous core, as shown in the figure.

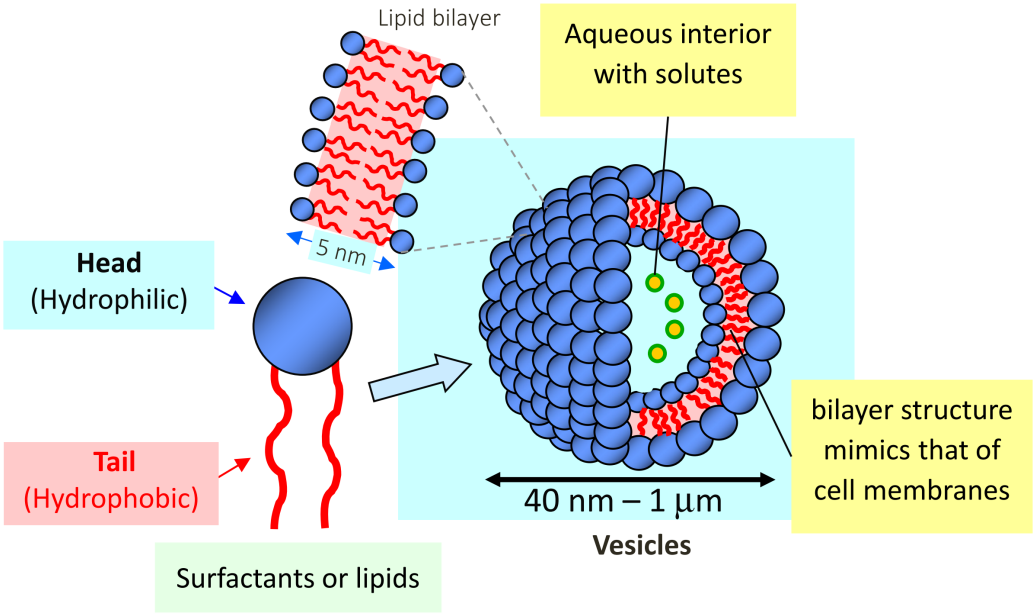

Figure 2.9. Structure of vesicles formed by amphiphilic molecules. The vesicles have an aqueous core surrounded by a lipid bilayer. They are formed by amphiphilic molecules such as surfactants or lipids, which have hydrophilic heads and hydrophobic tails.

Amphiphilic molecules have distinct hydrophilic head groups covalently bonded to hydrophobic tail(s), as shown in Figure 2.9. Due to their amphiphilic nature, when such molecules are added to water, their headgroups will prefer to associate with water, whereas their hydrophobic tails will tend to shield themselves from water. This results in self-assembly, i.e., spontaneous aggregation into structures such as micelles and vesicles.[45] The main driving force

for this self-assembly comes from the hydrophobic effect. When hydrophobes are in water, the hydrogen-bonding between water molecules is disrupted, resulting in a cage-like structure (clathrate) around the hydrophobes. In this cage, the water molecules are highly ordered, which is an unfavorable low-entropy state.[45] In turn, the hydrophobes associate and minimize their contact with water, which is the hydrohobic effect. Water molecules will then become disordered, thereby increasing the entropy of the system.

The shape and size of self-assemblies depends on the amphiphile's geometry. This correlation is expressed by the critical packing parameter (CPP), defined as:

$$\mathrm{CPP} = \frac{a_{\mathrm{tail}}}{a_{\mathrm{hg}}} \tag{2.2}$$

where a_{tail} is the cross-sectional area of the tail and a_{hg} is the effective headgroup area.[46,47] The higher the CPP, the greater the curvature of the self-assembled structure, as shown in Figure 2.10. If the CPP is less than 1/3, it implies that the amphiphile is shaped like a cone, and if so, spherical micelles will be formed. If the CPP is increased to a range between 1/3 and 1/2, the amphiphile assumes a truncated-cone geometry and it will then form cylindrical micelles. A further increase in CPP to a range between 1/2 and 1 makes the amphiphile assume a cylindrical geometry and in that case bilayer structures such as vesicles will be formed.[45]

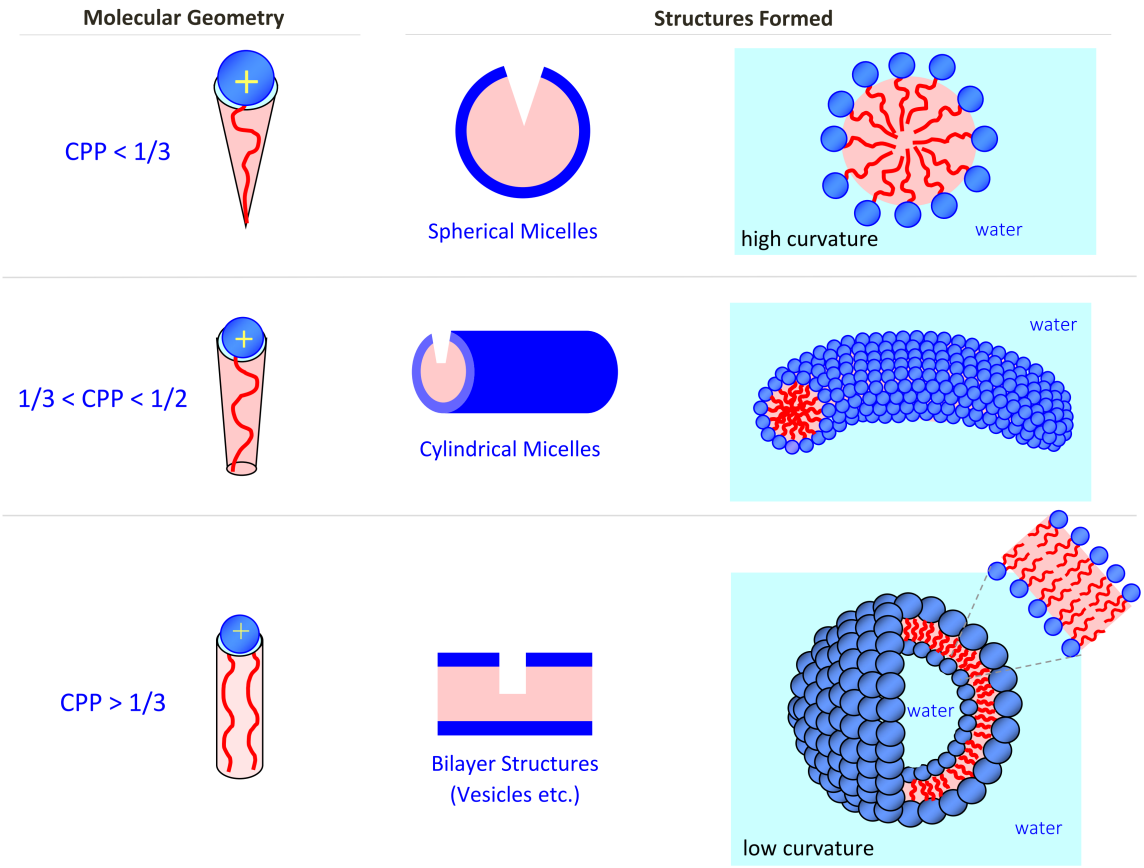

Figure 2.10. Schematics showing how the geometry of amphiphiles dictates the structures formed by self-assembly in water. The hydrophilic heads of the amphiphiles are shown in blue and the hydrophobic tails in red.

Vesicles are formed by lipids, which are biological constituents of cell membranes, and naturally have a cylindrical geometry due to their head and two tails (Figure 2.9). Lipid vesicles (also called liposomes) are biocompatible and biodegradable, but are relatively unstable. Moreover, to make unilamellar vesicles from lipids, high energy in the form of sonication or extrusion is required.[48] An alternative to liposomes is to combine single-tailed cationic and anionic surfactants. Such catanionic vesicles can be formed spontaneously by simple mixing of the surfactant solutions. They are unilamellar, with diameters around 100 nm and they remain stable for years. In our lab, we have had a long-standing interest in catanionic vesicles and have

been interested in creating vesicles that respond to various stimuli, with temperature, light, and pH being the most common ones.[49] A relatively new stimulus, reactive oxygen species (ROS), is gaining importance due to its crucial role in cell signaling pathways.[50]

2.5 ROS as a Stimulus and Thioether Chemistry

Reactive oxygen species (ROS) such as hydrogen peroxide (H_2O_2), hydroxyl radicals (•OH), superoxide (O_2^-), and singlet oxygen ($^1O_2$) are routinely generated in living organisms.[51-56] They are endogenously produced in the mitochondria and play a key role as signaling molecules in physiological processes such as apoptosis and cell proliferation.[51,53] High levels of ROS induce oxidative stresses and cause lethal damage to biomolecules such as proteins, DNA, and lipids. This in turn causes a series of diseases such as cardiovascular diseases, atherosclerosis, autoimmune diseases, and cancers. ROS levels are often unusually high in the tumor microenvironment when compared to normal tissues.[52] This makes ROS an important stimulus for targeted cancer therapy. It is well known that high-energy radiation such as X-rays and gamma rays that are used for radiation therapy generate ROS at the tumor site, and in fact, it is the ROS that is supposed to kill the tumor cells.[12]

Currently, ROS-responsive materials loaded with chemotherapeutics are being examined to combine radiation and chemotherapy in a single step to make cancer treatment more effective. Because radiation is already localized, there will be no systemic release of the payloads to other healthy tissues. ROS-responsive polymers, vesicles, and inorganic nanoparticles have been studied.[51-57]

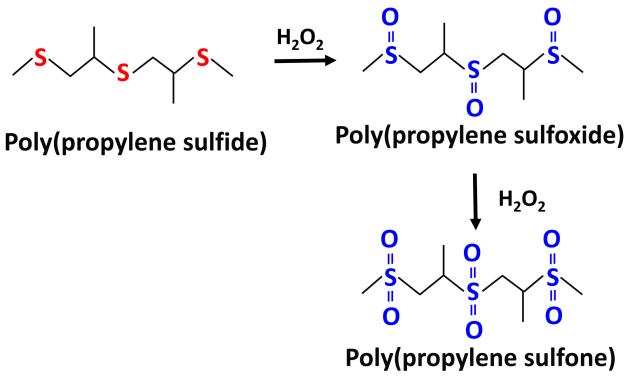

Figure 2.11. Steps in thioether oxidation by reactive oxygen species (ROS). The hydrophobic thioether groups (red) are converted to hydrophilic sulfoxide and sulfone groups (blue) in the presence of ROS such as hydrogen peroxide.

ROS-responsive chemistries include thioether, selenium, tellurium, thioketal, and arylboronic ester moieties. Thioether chemistry remains the simplest yet most-powerful among the above. A thioether-based polymer, polypropylene sulfide, was the first ROS responsive polymer reported in 2004 by Napoli *et al*.[58] In the presence of hydrogen peroxide, the hydrophobic thioether or sulfide groups on the polymer get oxidized to hydrophilic sulfoxides and ultimately to sulfones (Figure 2.11). Moreover, the reverse process of sulfoxide reduction to sulfide or thioether groups can be done using common reducing agents such as vitamin C, hydrazine, and lithium borohydride.[59,60] Thus, thioether chemistries have the potential to demonstrate reversible (redox) behavior.

2.6 Characterization technique: UV-Visible spectroscopy

UV-Vis spectroscopy is a common analytical technique in chemistry that is routinely used for quantitative determination of various ions or molecules that absorb energy in the visible (400 to 800 nm) and ultraviolet (200 to 400 nm) ranges.[61] Conjugated organic molecules, transition metal ions, and macromolecules are analyzed using this technique.

Electromagnetic waves (light) have a certain amount of energy based on their wavelength or frequency. When light in the UV-Vis range is incident on a sample, analyte molecules absorb the radiation of the incident photons and use this energy to promote electrons into higher energy states. Each molecule only absorbs energy at specific wavelengths and hence has a unique UV-Vis absorption spectrum. The absorbance peak in the spectrum is used to characterize the molecule. This absorbance A can be used to determine its concentration in solution using the Beer Lambert Law:[61]

$$A = \log_{10}\left(\frac{I_0}{I}\right) = \varepsilon \cdot c \cdot l \tag{2.3}$$

Here, I_0 is the intensity of the incident light, I is the transmitted intensity, ε is the molar absorptivity or extinction coefficient, c is the concentration of the molecule in mol/L, and l is the path length through the sample. Most of the commonly used dyes, drugs, and cosmetic agents have absorbances in the UV-Vis region and thus UV-Vis spectroscopy plays a vital role in studying their release from carriers.

Typically, a UV-Vis experiment involves adding a solution to a cuvette, which is then placed in the sample holder of a UV-Vis spectrometer. Light at a specified wavelength is passed through the sample and then a detector is used for converting the transmitted light into a readable electronic signal. The absorbance is then measured for different wavelengths of the light and the information is presented in the form of an absorbance spectrum with absorbance on the y-axis vs. the wavelength on the x-axis. These absorbances are then converted into concentrations using a standard curve for a given solute.

Chapter 3
Hydrogels with Protective Skins

The results presented in this chapter have been published in the following journal article: S. N. Subraveti and S. R. Raghavan, "A simple way to synthesize a protective "skin" around any hydrogel." *ACS Applied Materials & Interfaces*, 13 (31), 37645-37654 (**2021**)

3.1 Introduction

Hydrogels are water-swollen polymer networks that exhibit solid-like properties.[1,2,28,62] They are encountered in diverse fields including biomedicine (e.g., as scaffolds for tissue engineering),[62] pharmaceutics (e.g., as matrices for drug delivery),[1] and in the food industry where various edible materials are in the hydrogel state.[2] More recently, new applications for hydrogels are emerging in soft robotics and as biomedical devices that can be interfaced with the body.[63-67] In many of the above scenarios, the utility of hydrogels is limited by their tendency to dry out (dehydrate) when their surface is exposed to ambient air. For instance, consider a cube of gelatin gel (Jell-O) that is commonly made in homes as a dessert. If this gel is left on a countertop, it will appreciably dry out in less than a day and will lose its texture and taste. Similarly, Figure 3.1 shows that a gel of acrylamide (AAm) prepared in the lab as a 2 cm cube shrinks by more than half its original volume within 17 h.

As a counterpoint, consider various fruits or vegetables, examples of which (a mango, an orange, and a tomato) are shown in Figure 3.1. These are all soft materials that contain considerable water in them. We specifically focus on the tomato (Figure 3.1A), more than 60% of which is water (similar to many gels prepared in the lab). Despite its high water content, the tomato does not lose much water when left for a day on a countertop under ambient conditions.

Even after a week, the tomato is not significantly reduced in size, indicating that most of its water is intact. This remarkable ability of the tomato (and likewise, other fruits) to resist drying is due to the presence of an outer skin that covers its water-rich core.[68,69] This skin or *cuticle* is formed from wax-like polymers called cutin and cutan. Such polymers are synthesized by the epidermal cells of the fruit and together form a hydrophobic outer layer, which prevents the leakage of water and other small molecules from the core.[68,69] Figure 3.1A shows a cross-section of the tomato, highlighting its skin. Note that this skin can be peeled off and separated from the core. Generally, the skin is quite thin compared to the core, i.e., the skin thickness is typically about 1–10% of the fruit size. For example, around the tomato in Figure 3.1A (size ~ 1 to 5 cm), the skin is 1 to 2 mm thick. However, in some fruits like navel oranges, the skin can be thicker (3 to 5 mm) and it can be more robust compared to the softer core.

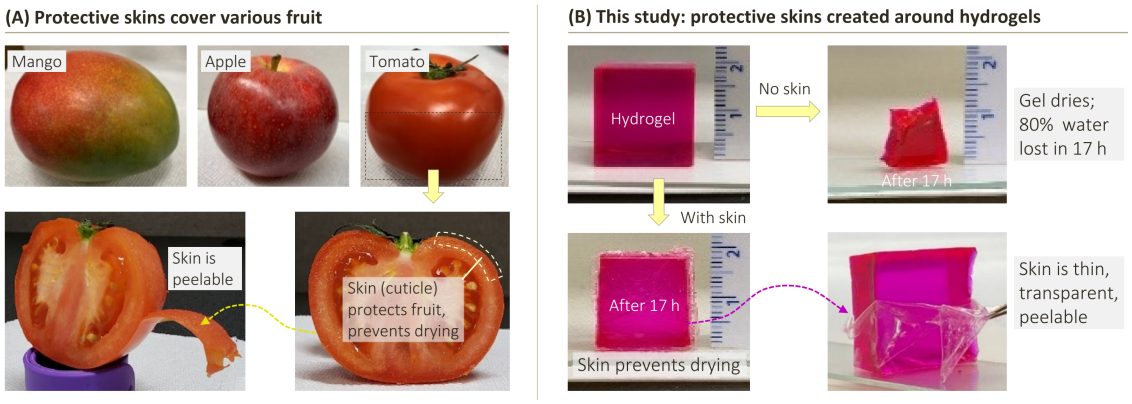

Figure 3.1. Natural inspiration for the approach outlined in this study. (A) Examples of fruits with a hydrophobic skin (cuticle), which include the mango, apple and tomato. A cut-section of the tomato is shown, highlighting the skin, which is also shown to be peelable. (B) A hydrogel in the shape of a cube dries appreciably when left exposed to ambient air for 17 h. However, if the same gel is enveloped in a thin, hydrophobic skin, the water loss is substantially reduced. The skin is thin, flexible and transparent, and it can be peeled off from the gel using tweezers.

The focus of this chapter is on creating a hydrophobic skin around a hydrogel. Could such a skin be formed, and if so would it be sufficient to inhibit drying? Recently, this problem has attracted the attention of several researchers who have attempted to attach thin hydrophobic layers to hydrogels.[70-83] This is challenging because of the chemical incompatibility (and thereby, a lack of interfacial adhesion) between hydrophobic materials and the water-filled gel. To solve the problem, some researchers have used coupling[74,77] or grafting agents,[71,76] which are chemicals that can form bonds between hydrophobic and hydrophilic materials. Others have treated hydrophobic polymers with oxygen plasma so as to introduce reactive groups into the chains before reacting with the gel.[73,79] Recently, Zhou *et al*.[80] reported a way to coat a specific type of hydrogel with an organogel via a co-polymerization technique. However, all these approaches are limited to specific chemistries of the gel, i.e., they cannot be applied widely to all gels. Most methods are complex, and some require access to sophisticated equipment such as an oxygen plasma generator. Moreover, in all these cases, once the hydrophobic layer is formed it cannot be separated from the underlying gel because of the strong bonding between the two. The ability to peel off and remove the skin as desired (much like in a fruit) could be important for many applications.

Here, we present a simple technique that allows any hydrogel regardless of composition, geometry, or mechanical properties to be encompassed in a peelable hydrophobic skin. The skin is synthesized in just a few minutes by an inside-out polymerization, which involves placing the hydrogel in a monomer liquid and irradiating with ultraviolet (UV) light. The key to our approach is that one component required for the polymerization (the initiator) is *present only in the hydrogel* at the start. This initiator is soluble in both the hydrogel and the external monomer,

but the *monomer is insoluble in water* and therefore cannot enter the hydrogel. When irradiated with UV light, the skin, i.e., a thin polymeric layer, grows outward from the hydrogel core. We will show that the thickness as well as the mechanical properties of the skin can be precisely controlled. A typical skin around the cube of AAm gel is shown in Figure 3.1B: note that the skin is transparent and peelable from the core. Such a skin inhibits transport from or into the gel: specifically, the gel stops swelling when placed in water and a gel left open to air loses very little water. Similarly, solutes (e.g., model drugs or proteins) can be stored in the gel core for long times, while harsh chemicals (e.g., acids) or contaminants (e.g., microbes) in the external solution are prevented from entering the gel. Likewise, *the solutes can be released into the external solution upon peeling off the skin*. On the whole, we believe the approach described in this chapter will prove useful to researchers and will help to further advance novel applications for hydrogels.

3.2 Experimental Section

Materials. The following were obtained from Sigma-Aldrich: the anionic biopolymer alginate (alginic acid sodium salt from brown algae, medium viscosity); the monomers acrylamide (AAm), sodium acrylate (SA), N,N′-methylene-bis(acrylamide) (BIS), polyethylene glycol diacrylate (PEGDA) (molecular weight of 550 Da), polyethylene glycol dimethacrylate (PEGDMA) (330 Da), methyl methacrylate, divinyl benzene, lauryl methacrylate and ethylene glycol dimethacrylate (EGDMA); the photoinitiators 2-hydroxy-2-methyl-propiophenone (HMPP) and lithium phenyl-2,4,6-trimethyl-benzoylphosphinate (LPTBP); the dyes calcein, methylene blue, and methyl red; the solvents ethanol and acetone, and the salts sodium chloride and calcium chloride dihydrate ($CaCl_2$). Sodium citrate was obtained from Fisher Scientific.

Several urethane-based monomers were gifts from Allnex: the urethane diacrylate (UDA; tradename Ebecryl 230) has an aliphatic urethane segment of 4858 Da and two acrylates at its ends, while the urethane hexa-acrylate (UHA; tradename Ebecryl 2221) has six acrylates connected to an aromatic urethane segment of 774 Da. The photoinitiator Irgacure 2959 (IRG) was obtained from BASF. The accelerant N,N,N′,N′-tetramethyl-ethylenediamine (TEMED) and the acid red 52 dye were purchased from TCI America. Aerosil R974, a hydrophobic fumed silica, was a gift from Degussa Corp. Deionized (DI) water was used in all experiments.

Preparation of Hydrogels. Alginate, AAm, and PEGDA gels were prepared in this study. To make alginate gels, 2 wt% of sodium alginate dissolved in DI water was added dropwise using a syringe into a 0.5 M $CaCl_2$ solution. The Ca^{2+} ions crosslinked the alginate chains, and thereby the liquid droplets were converted to spherical gels over an incubation time of 1 h. Gels with a diameter of 2–5 mm were created, depending on the diameter of the needle in the syringe. To make the AAm gel, a pre-gel solution containing 1 M AAm, 2.2 mol% BIS with respect to the monomer, and 3.4 mM of the LPTBP photoinitiator was first prepared in DI water (in terms of weights, these corresponded to 0.71 g AAm, 0.034 g BIS, and 0.01 g LPTBP in 10 mL of solution). This pre-gel mixture was then loaded into a mold (cuboidal or cylindrical) and irradiated with UV light for 1 min to make the gel. A variation of this recipe was used to make the AAm/SA gel: in this case, the total monomer in the pre-gel was again 1 M, but with a 9:1 molar ratio of AAm/SA (i.e., 0.64 g AAm and 0.094 g SA). In the case of the PEGDA gel, the pre-gel was composed of 10 wt% PEGDA and 0.1 wt% LPTBP in DI water.

Preparation of Skin-Covered Hydrogels. The procedure for growing a skin around the above hydrogels has been described above under Figure 3.2. First, a given gel was immersed for 5 min in a solution containing photoinitiator (0.5 wt% of IRG or 1 wt% of HMPP), 1 wt% of TEMED (accelerant), and solutes such as 1 mM of a dye (either acid red 52 or methyl red). Then, the gel was transferred to a liquid bath of an organic monomer such as UDA and UHA. Due to the high viscosity of the UDA and UHA liquids, the gel remained suspended in the monomer. The gel was then irradiated with UV light for a given period of time (typically 10 min) to form the skin, as shown in Figure 3.2. The UV Lamp used for polymerization was a 36 W nail-polish dryer from Melody Susie, which generated UV light at 365 nm. In the case of some monomers like PEGDMA, the liquid was not viscous enough to suspend the gel and therefore, 9 wt% of Aerosil R974 was added to increase the viscosity of the monomer prior to introduction of the gel.

Rheological Studies. An AR 2000 rheometer (TA Instruments) was utilized for performing the compression tests using a parallel plate geometry (20 mm diameter) at 25°C. Samples (4-mm diameter alginate gels with different skins) were placed at the center of the plates and studied under the squeeze/pull off test mode. Compression was done at a rate of 15% strain per minute. The normal force measured during compression was converted to stress by dividing the force by the initial cross-sectional area of the gel, and thus, plots of stress vs strain were obtained for each sample.

Optical Microscopy. Bright-field images of peeled skins of different thickness placed in ethanol were captured with a Zeiss Axiovert 135 TV optical microscope using a 2.5× objective. Ethanol

was used instead of water to match the refractive index of the skin. In water, the skin appeared opaque and its thickness could not be measured.

Scanning Electron Microscopy (SEM). The skin around a hydrogel was cut in half using a razor blade and then affixed to a viewing platform. Next, a drop of an ionic liquid (HILEM IL 1000) was added over the skin and was left for an hour before transferring to the SEM stage. The excess ionic liquid was removed by a piece of filter paper and the sample was analyzed using a Hitachi SU-70 field-emission SEM with an accelerating voltage of 5 kV.

Contact-Angle Measurements. Advancing contact angles for water droplets on polymer surfaces were estimated at room temperature using procedures reported elsewhere.[84] Droplets of deionized water (~ 100 μL) were injected out of a syringe onto the test surfaces, and images were captured using a Nikon D3400 camera. The images were analyzed subsequently using ImageJ. Five measurements were done on each sample.

Dye Release Experiments. Gels loaded with 1 mM acid red 52 dye (with and without the UDA skin) were placed in vials containing 5 mL of DI water at ambient conditions. To monitor the dye concentration in the external water, 1 mL samples were taken and analyzed using a Cary 50 UV-Vis spectrophotometer. Absorbance was measured at the absorption peak of the dye, which was 565 nm. The samples were then returned to the vials after the measurement. Cumulative dye release (%) was calculated by normalizing the dye concentration with that in the solution after two days. In the case of dye release in ethanol (Figure 3.7), since much of the dye remained in

the gel, the gel was transferred to DI water for two days to calculate the total dye corresponding to 100% release.

Electrical Tests. Gels of AAm were synthesized in the form of cylinders with a diameter of 0.5 cm and a length of 3 cm. They were incubated overnight in a 1 M NaCl solution to make them ionically conductive. One of the gels was then covered with a UDA skin as above. Graphite pencil leads were inserted into the AAm gels to establish connections with the electrical circuit components. The gels with pencil leads were then connected to red LED bulbs and to a DC power supply (Agilent E3612A) set at 10 V with the help of copper wires. The current flowing through the circuit was recorded at various times (every 2 h over a period of a day), with the power supply being turned off between measurements. As long as the current was non-zero, the LEDs would glow (see Figure 3.9).

3.3 Results and Discussion

3.3.1 Skin Synthesis

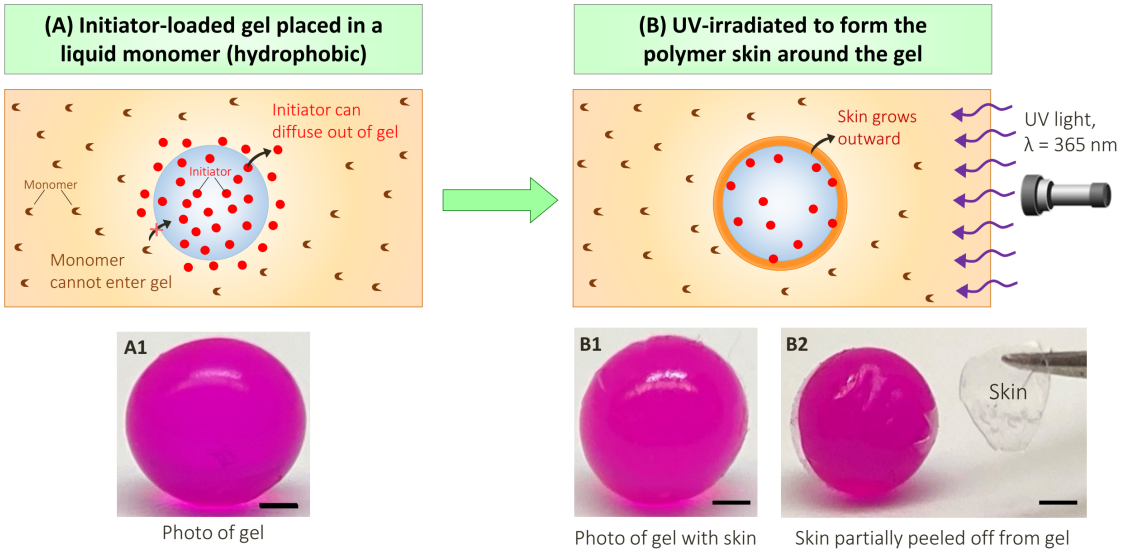

Figure 3.2. Procedure for synthesizing a skin around a hydrogel. (A) Initiator-loaded hydrogel (Photo A1) is placed in a monomer (UDA) solution. The initiator is chosen to be soluble in the monomer, whereas the monomer is insoluble in water. Thus, the initiator can diffuse out of the gel whereas the monomer cannot enter into the gel. (B) Upon irradiation with UV light at 365 nm, a skin (polymer of UDA) grows outward. Photos B1 and B2 show that the skin is thin and transparent. To show it clearly, the skin is partially peeled off using tweezers. Scale bars: 1 mm.

The procedure for covering a hydrogel with a hydrophobic skin is shown schematically in Figure 3.2. A spherical gel of alginate (4 mm in diameter) is the starting point. This gel is made by dropping a 2% sodium-alginate solution into 0.5 M calcium chloride using a syringe. The alginate chains in a given drop are crosslinked into a network by divalent Ca^{2+} ions, thereby forming a transparent spherical gel with a diameter of ~ 4 mm.[10] We included 0.05% of acid-red dye to provide visual clarity to the gel. To form a skin around this gel, we first incubate it in an aqueous solution containing 0.5% of a water-soluble photoinitiator (Irgacure 2959, a benzophenone derivative with an aqueous solubility of about 1 wt%). After 5 min, the initiator-

loaded gel (Photo A1) is placed in a liquid monomer, in this case an oligomeric urethane diacrylate (UDA).

There are a few key considerations in selecting the initiator and monomer. The initiator should be *soluble both in water and in the organic monomer*, which is the case for the Irgacure 2959 mentioned above. Conversely, the monomer should be a liquid that is insoluble in water, and the viscosity of this liquid should be high enough so that the gel remains suspended in it.[10] The UDA monomer is indeed a hydrophobic one and it also has sufficient viscosity because of its long urethane segment that has a molecular weight (MW) of 4858 Da.[85] The monomer also has two acrylate groups at its ends that allow the molecules to be crosslinked into a network. When the gel is placed in this monomer, the initiator diffuses out of the gel where it encounters the monomers (Figure 3.2A). We then expose the sample to UV light at a wavelength of 365 nm to trigger the free-radical polymerization (crosslinking) of the urethane. Note that polymer chains cannot form inside the gel because the monomer is insoluble in water. Thus, the polymer grows outward as a layer from the surface of the gel (Figure 3.2B). Ultimately, a thin, transparent polymer skin encases the gel core.

3.3.2 Skin Appearance, Thickness, and Microstructure

The polyurethane (UDA) skin in Figure 3.2B is a soft, peelable layer that can be easily separated from the gel using a tweezer (Photos B1 and B2). The skin thickness can be varied from ~ 10 to 200 μm depending on the duration of UV exposure. Figure 3.3A shows the skins formed under two different UV exposure times. These experiments were done with 4-mm alginate gels bearing 0.5% initiator. After 10 min of UV irradiation, a skin of 60 μm is detected

around the gel (Image A1). Increasing the UV irradiation time to 90 min leads to a thicker skin of 140 µm (Image A2). In both cases, note that the skin is very uniform in thickness. The uniformity is further confirmed by images from Scanning Electron Microscopy (SEM), which are shown in Figure 3.3B. Here, a skin is formed around an alginate gel (3 mm diameter) over 30 min of UV irradiation. The gel is then cut in half and the skin is detached from one half prior to SEM-imaging. We again find the skin to be uniform with a thickness of 100 µm. In addition to UV exposure time, the skin thickness can also be altered by chemical variables such as the initiator content.[10]

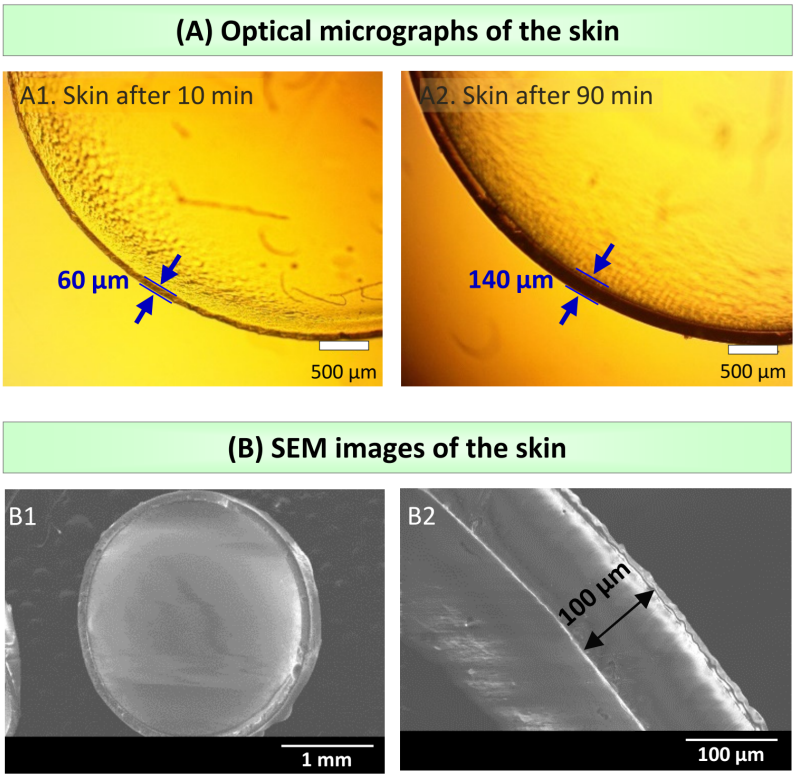

Figure 3.3. Visualizing the skin by microscopy techniques. (A) Optical micrographs of the UDA skin around a 4-mm alginate gel after 10 min (A1) and 90 min (A2) of UV irradiation. The images reveal the outward growth of the skin layer with time. (B) SEM images of the skin separated from a 3-mm alginate gel core after 30 min of UV irradiation. The higher magnification image (B2) shows the thickness of the skin to be 100 µm.

3.3.3 Skins Around Various Gels

Our technique for forming a skin around a hydrogel is simple and convenient. It can be used to encase any hydrogel of arbitrary composition, shape or mechanical properties. To demonstrate this, we prepared gels of alginate, acrylamide (AAm), and polyethylene glycol-diacrylate (PEGDA) and encased them all in polyurethane skins (Figure 3.4). The alginate gel in the shape of a sphere has been mentioned above. In the case of the AAm gel, it was made in the shape of a cube by adding an aqueous mixture of AAm, crosslinker, and photoinitiator into a cubic mold and inducing the mixture to polymerize by UV light. Similarly, the PEGDA gel was made in the shape of a cylinder by adding a mixture of PEGDA monomer (molecular weight 550 Da) and photoinitiator into a cylindrical mold and inducing UV-polymerization. At the PEGDA monomer content (10%) used, this gel was hard and brittle whereas the AAm and alginate gels were soft. The three gels (with acid-red dye for visual contrast) were then loaded with the Irgacure photoinitiator and placed in the UDA liquid monomer, followed by UV polymerization as discussed above (see Figure 3.2). All gels thus become uniformly encased in a thin polyurethane skin (Figure 3.4); in all cases, we have partially peeled the skins from the gels to indicate their presence. The examples above have been chosen to illustrate the diversity of gels that can be encased in skins by our technique, which include physical gels (alginate, crosslinked by ionic bonds) as well as chemical gels crosslinked by covalent bonds (AAm and PEGDA), and soft gels (alginate, AAm) as well as hard/brittle gels (PEGDA).

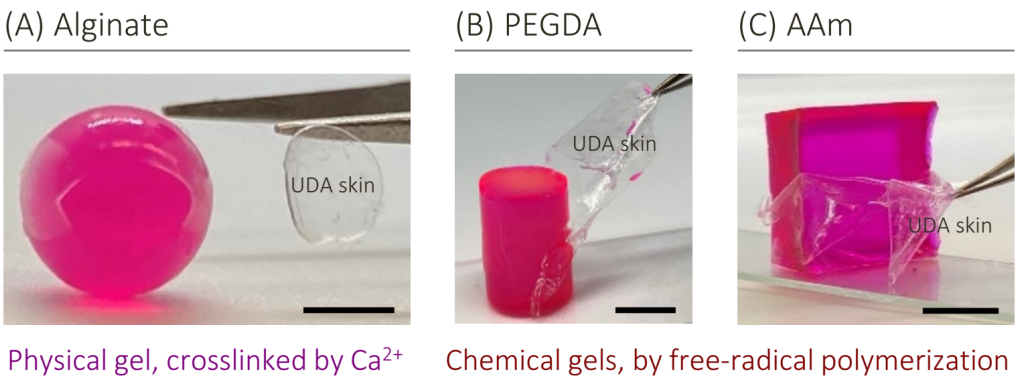

Figure 3.4. Skins around different hydrogels of various chemistries and shapes. A spherical alginate gel, a cylindrical PEGDA gel, and a cube-shaped AAm gel are all shown to be covered with thin UDA skins. The skins are partially peeled off using a tweezer to indicate their presence. Scale bars from (A) to (C): 2 mm, 8 mm, and 1 cm.

3.3.4 Soft and Hard Skins

In addition to thickness, we can change other physical properties of the skins around the gels. As noted above, any liquid monomer that is insoluble in water could be used to form a skin, and we have experimented with various UV-cross-linkable urethanes, acrylates, and methacrylates. An example is a skin formed from polyethylene glycol dimethacrylate (PEGDMA) of molecular weight 330 Da. When this monomer is polymerized, it forms a hard and brittle gel, so we examined if a hard PEGDMA skin could be formed around a soft gel such as an alginate sphere. To synthesize a PEGDMA skin, one modification had to be done to the procedure shown in Figure 3.2: the viscosity of the PEGDMA liquid is quite low and so it had to be increased to ensure that the alginate gel remains suspended in it. For this purpose, we added 9% of a fumed silica (Aerosil R974), which are a class of nanoparticles known to increase the viscosity of organic liquids.[86] The alginate gel could be suspended in this thickened PEGDMA and we were able to form a PEGDMA skin around it. As expected, this skin was hard and brittle.

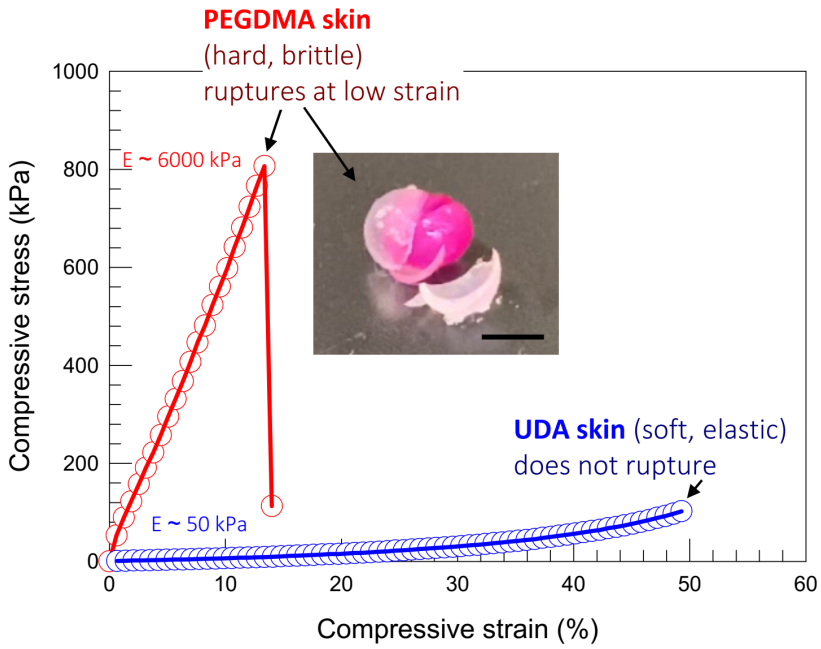

Figure 3.5. Contrasting the mechanical properties of hard and soft skins. Compressive stress vs. strain for alginate gels covered with UDA and PEGDMA skins. The gel with UDA skin has a compressive modulus $E \sim 50$ kPa and is intact even at 50% strain, i.e., the skin is soft and elastic. The gel with PEGDMA skin has $E \sim 6000$ kPa and ruptures at 14% strain, i.e., the skin is hard and brittle. The inset photo shows the latter after impact with a hammer: the brittle skin is broken while the gel is intact. Scale bar in photo: 4 mm.

Experiments demonstrate the differences in mechanical properties between the PEGDMA and the UDA skins. If the PEGDMA-covered alginate gel is placed on a benchtop and hit with a hammer, the skin cracks into pieces while the core gel remains intact (Figure 3.5 inset). In contrast, the polyurethane (UDA) skin is soft and elastomeric. When a UDA-covered gel is squeezed between one's fingers, it transforms from a sphere to a pancake shape. When the squeezing is stopped, the gel recovers quickly to its initial spherical shape. To quantify these differences, we tested the skin-covered gels under compression. Figure 3.5 plots the compressive stress vs. strain for the two cases. The gel with a UDA skin can be compressed by more than 50% without breaking. The compressive modulus E from the linear part of this curve is 50 kPa.

On the other hand, the gel with a PEGDMA skin has a modulus E of 6 MPa (120x higher) and this skin breaks when compressed by just 14%. This shows the hard and brittle nature of the PEGDMA skin compared to the soft and resilient UDA skin. Note from the above results that the mechanical properties of the skin can be varied *independently* from those of the underlying gel. Even if there is a mismatch in properties (e.g., if a soft gel is encased in a hard skin), the gel core and skin remain well-adhered to each other.

3.3.5 Skin Prevents Gel from Drying in Air and Swelling in Water

Next, we show that the presence of a skin allows hydrogels to resist dehydration as well as swelling in water (Figure 3.6). Dehydration studies were done with AAm gels having two types of skins, one of UDA (discussed above) and the other of a urethane hexa-acrylate (UHA), which provides a greater degree of crosslinking. Both skins were 150 μm in thickness. Figure 3.6A compares the drying under ambient air of the skin-covered and bare gels, which are all cubes with a length of 2 cm. These gels are otherwise identical and contain 15% polymer and 85% water. The gel-weight over time is plotted in Figure 3.6A as a ratio relative to the initial weight at $t = 0$. The bare gel (control) loses 80% of its weight within 17 h. Photo A4 in Figure 3.6A shows the shrivelled and irregular shape of this dehydrated gel relative to its initial state (Photo A3), with the mass that remains mostly containing the polymer. In contrast, the UHA skin-covered gel only loses about 2% of its weight in the same 17 h period. Photo A2 in Figure 3.6A of this gel after 17 h reveals a near-identical size and shape relative to its initial state (Photo A1). Similar results were also obtained with the UDA skin, but the weight loss over 17 h was slightly higher: at around 10% (photos shown earlier in Figure 3.1). The results confirm that a thin, hydrophobic skin

that is a fraction of the gel size is able to significantly inhibit water-loss (dehydration) from the gel. The better water-retention with a UHA vs. UDA skin is due to two reasons: the UHA is more crosslinked due to its six acrylates vs. two in UDA, and also the UHA is more hydrophobic. To test the latter point, we measured the contact angles of water droplets on pure films of UDA and UHA and found these to be 102° and 108°, respectively. Because both these values are above 90°, it confirms that the polymers are hydrophobic,[85] and moreover that UHA is more hydrophobic than UDA.

We then study the counterpart of the above phenomenon, which is whether the skin can inhibit swelling (entry of water) when a gel is placed in a water bath (Figure 3.6B). For better visualization of gel swelling, we made ionic gels by copolymerizing AAm (a nonionic monomer) with an anionic monomer, sodium acrylate (SA) in a 90:10 ratio of Aam/SA. It is well-known that ionic gels swell much more than nonionic ones due to the electrostatic repulsions between ionic groups along the polymer chains.[87] The gels were created as cylinders with a diameter of 0.5 cm and a length of 2 cm and were dyed red as before for clarity. Photo B1 shows a bare gel (control) on the left, and on the right is an identical gel with a UDA skin of 150 μm thickness. The gels were placed in water at ambient pH and temperature and their volumes over time were recorded. Figure 3.6B plots the gel volume as a ratio relative to its initial volume at $t = 0$. In a period of 12 h, the bare gel swells to 3x (i.e., 300%) of its original volume. However, the skin-covered gel does not swell at all over this time (and indeed, there is no swelling even over a period of days). The difference in sizes is shown by Photo B2, where the gels are removed from water and placed side-by-side for comparison. Another interesting point from this photo is that the red dye in the bare gel has

completely leaked out over 12 h and thus the gel appears nearly colorless. Conversely, none of the dye has leaked out of the skin-covered gel, which thus retains its vivid red color.

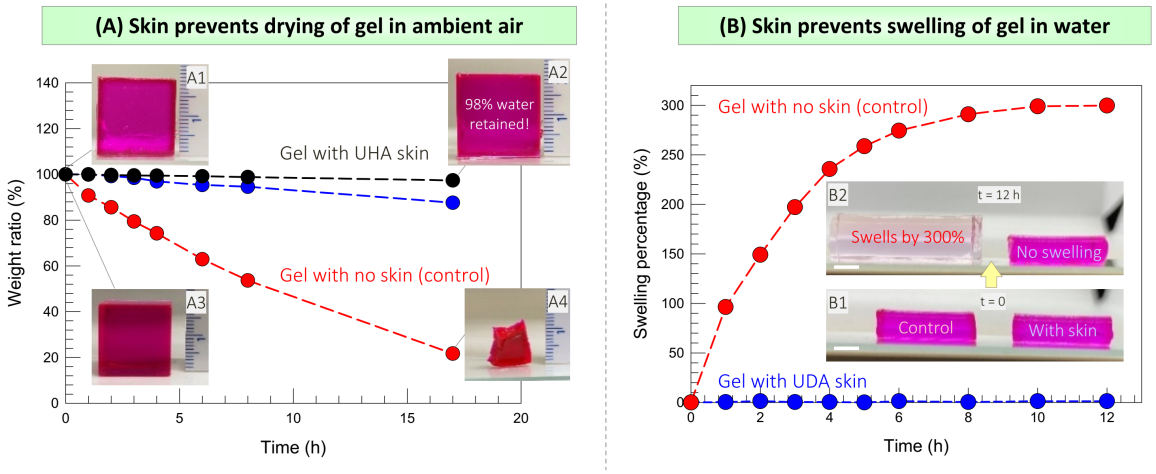

Figure 3.6. Testing the ability of the skin to prevent exit/entry of water from/into a gel. (A) AAm gels with UHA and UDA skins and an AAm gel without a skin are compared for their weight loss vs. time while drying under ambient conditions. The gel with the UHA skin retains 98% of its weight (compare Photos A1 vs. A2), the one with the UDA skin retains 90% of its weight, while the gel without a skin retains only 20% of its weight (compare Photos A3 vs. A4) over a 17 h period. (B) Gels of AAm-SA are made in the shape of cylinders, one with a UDA skin and the other with no skin. The gels are placed in DI water and the degree of swelling (ratio of swollen vs. original volume) is plotted vs. time. The bare gel (no skin) swells by 300% while the skin-covered gel does not swell at all (compare Photos B1 vs. B2). Scale bars in B1 and B2: 4 mm.

3.3.6 Skin Regulates Solute Transport Out of Gel

The ability of the skin to inhibit transport out of a gel is then studied further. We consider the case of small, hydrophilic solutes in the gel, such as the acid red 52 dye. 1 mM of this dye was loaded into spherical alginate gels (4 mm diameter). A bare alginate gel (without skin) served as the control while a second gel was encased in a UDA skin of 150 μm thickness. Both gels were separately placed in water baths at t = 0, and the dye in the solutions was monitored over time. Figure 3.7A plots the cumulative dye release (as a % of the total) vs. time. In less than 1 h, 80% of the dye is released out of the bare gel into the

external solution, and in 4 h, virtually all of the dye gets released. This is to be expected because the dye molecules are less than a nanometer in size, which is much smaller than the mesh size of the alginate gel (~ 20 nm).[88] Thus, dyes can easily diffuse out, and the rapid release of small solutes from gels is well-documented in the literature. However, in complete contrast, Figure 3.7A shows that there is absolutely no release of the dye from the skin-covered alginate gel even after a day.

The above finding is substantiated by the photos in Figure 3.7A. In the case of the bare gel (Photo A1), the solution after 4 h has a deep pink color, reflecting the release of dye from the gel to the solution. The bare gel, picked out of this solution by tweezers, has the same color as the solution, i.e., the dye has equilibrated between the gel and the solution (Photo A2). On the other hand, the skin-covered alginate gel (Photo A3) continues to have a bright-red color even after a day whereas the external solution remains colorless. This result is similar to that in Figure 3.6B where the dye did not leak out of a skin-covered AAm gel. Thus, the skin entirely prevents the release of solutes from all kinds of gels - even for solutes that are much smaller than the mesh size of the gel and are highly water-soluble (hydrophilic). We have confirmed the above finding for a variety of model solutes. The ability of the skin to provide a '*hermetic seal*',[11] i.e., to keep solutes encapsulated (preserved) for long times in water could be a significant benefit for pharmaceutical applications. Note also that the skin is much more stable to heat compared to the hydrogel. Thus, even if the skin-covered gel is heated to 90°C and held at that temperature for a day, the structure remains stable and there is no leakage of solute over this period. Additionally, this skin can be easily peeled off, as shown in Figures 3.2 and 3.4, to "*switch on*" *the burst-*

release of small molecule solutes. Once the skin is removed, the bare gel will release the small molecules rapidly as shown in Figure 3.7A (Photo A1).

The reason why the UDA skin is impermeable to solutes is likely because of its hydrophobic nature, as discussed above. In turn, solutes dissolved in the aqueous gel core will also not be able to pass through the UDA skin. However, we found that the UDA monomer is soluble in polar organic solvents such as ethanol and acetone. We therefore proceeded to examine if solute transport out of skin-covered gels could be mediated by ethanol (Figure 3.7B). The alginate gel with UDA skin releases none of its encapsulated dye in water (Photo B1), but when the same gel is placed in ethanol, some of the dye leaks out (Photo B2; note the pink color of the solution). The plot shows an *initial burst-release*, followed by the dye concentration saturating in the external solution by about 36 h. The cumulative amount of dye released corresponds to 60% of the dye in the gel. This equilibrium is established because ethanol is a poor solvent for alginate[89] and therefore the dye partitions between the water-rich alginate gel and the ethanol-rich external solution. A close examination of the skin-covered gel shows the UDA skin to have detached from the core (Photo B3). This occurs because the skin is swollen with the solvent whereas the alginate core shrinks (the core then drops to the bottom due to its weight, leaving a gap between the skin and the core at the top). Similar results have also been found in acetone. A key point from Figure 3.7B is that it is possible to regulate solute-release out of the gel by carefully choosing the skin-chemistry as well as the appropriate solvent.

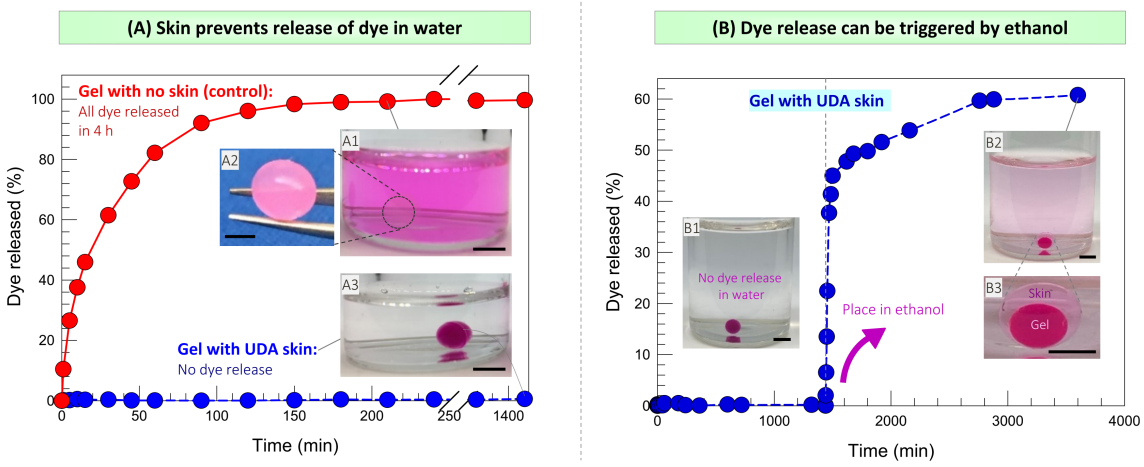

Figure 3.7. Testing solute release out of skin-covered gels in water and ethanol. (A) Cumulative solute release (% of total) vs. time from alginate gels (4 mm dia) with and without a UDA skin. The gels contain identical amounts of acid red 52 dye. All the dye is released from the bare gel in 8 h (Photos A1 and A2), and the solution thus exhibits a pink color. None of the dye is released from the skin-covered gel (Photo A3), with the solution remaining colorless even after a day. (Scale bars in photos: 2 mm) (B) The skin-covered gel that was initially in water is transferred to ethanol after 24 h. While no dye is released in water due to the hydrophobicity of the UDA skin (Photo B1), release does occur in ethanol (Photo B2) because the UDA is more compatible with ethanol and swells in this solvent (Photo B3). (Scale bars: 4 mm)

3.3.7 Skin Prevents Transport Into Gel

The skin also prevents transport of molecules or species from the external aqueous solution into the gel. For example, we have tested acids, bases, and chelators added to the water around a skin-covered alginate gel and in all cases, the skin protected the core gel from contact with the above species. An example is shown in Figure 3.8A, where gels loaded with a pH-indicating dye (methyl red), are placed in strong acid (1 M HCl). Initially, the gels show a yellow color from the dye because the water in them is at pH 7. Within a minute, the bare gel with no skin turns from yellow to red as the acid permeates into the gel. In contrast, the gel with a thin (150 μm) UDA skin retains its yellow color, indicating no contact with the acid whatsoever. Similarly, when a bare alginate gel is placed in a solution of chelators like sodium citrate, the Ca^{2+} crosslinks are removed by the chelator, causing the gel to dissolve away. Conversely, an

alginate gel with a UDA skin is completely resistant to chelation and remains intact in the presence of sodium citrate or other chelators. Lastly, microbes (specifically, mold) are known to attack and digest gels formed by polysaccharides like alginate.[90] Indeed, Figure 3.8B shows that a bare alginate gel stored in water at room temperature develops mold over a period of three months (Photo B2). For comparison, an alginate gel covered by a thin UDA skin and placed alongside in the same vial does not develop any mold over the same period. Thus, the skin is able to protect the alginate gel from microbes.

Collectively, the findings in Figures 3.6, 3.7 and 3.8 show that the hydrophobic skin can *tightly regulate transport into and out of a gel placed in water*. Solutes dissolved in an aqueous gel are prevented from leaking out. Harsh chemicals or microbes from an external aqueous solution are prevented from entering the gel. Also, water itself cannot enter or leave the gel, i.e., the gel will not swell and increase its volume. The lack of swelling also means that the mechanical properties of the gel will remain preserved when there is a skin. Conversely, when a bare gel swells, its mechanical properties such as the elastic modulus decrease with time, which might be undesirable in many applications.

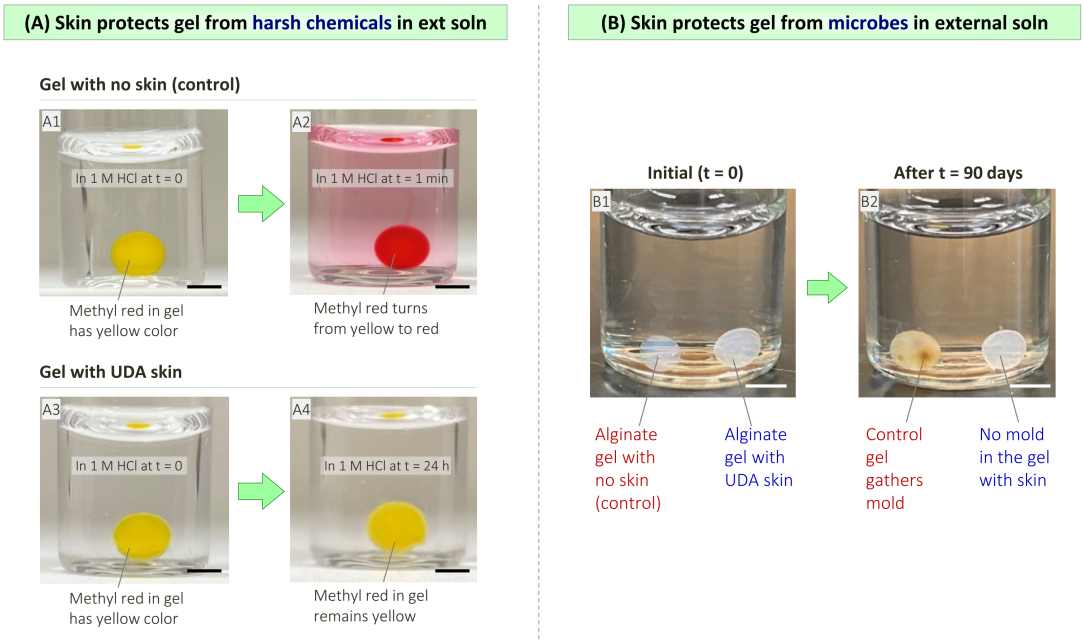

Figure 3.8. Testing the ability of the skin to protect a gel from harsh chemicals and microbes. (A) An alginate gel with no skin (Photo A1) and an identical one with a UDA skin (A3) are placed in strong acid (1 M HCl) at $t = 0$. The gels both contain the pH indicating dye, methyl-red, which has a yellow color at normal pH and a red color at acidic pH. Within a minute, the alginate gel turns red (A2) and the red color is also seen in the solution due to leakage of dye. Conversely, the skin-covered gel retains its yellow color even after 24 h (A4). (B) An alginate gel with no skin and an identical one with a UDA skin are left in water at $t = 0$ (Photo B1). Over time (90 days), the former gets attacked by mold (micro-organisms) because alginate is a polysaccharide and hence a source of nutrients for the mold (B2). Conversely, the skin-covered gel is protected from the mold. Scale bars in all photos: 4 mm.

3.3.8 Skin-Covered Gel as an Electric Conductor

Nowadays, gels are being evaluated in electronic sensors where they would be interfaced with skin (the gels would thus sense analytes present in the body). Gels are also being used as electrolytes in flexible batteries or as actuators in soft robots. In such futuristic applications, gels that can resist dehydration (when covered by a skin) can be advantageous. To explore this aspect, we have conducted a simple experiment where a cylindrical gel is used as the conduit or 'wire' in an electrical circuit (Figure 3.9). Here, the gel is used to connect a DC power source (10 V) to

a red light-emitting diode (LED). The control is an AAm gel loaded with 1 M NaCl (to ensure ionic conductivity), and this is compared with an identical gel covered by a thin (150 μm) UDA skin. At t = 0, both gels conduct electricity to the same extent and thus both LEDs light up (Figure 3.9A, Photos A1 and A3). The current I is recorded as a function of time t for the two cases (Figure 3.9B). As time progresses, the bare gel dries out and hence the resistance in the circuit increases. In turn, I drops sharply with t, until it reaches zero at t = 8 h, whereupon the LED stops glowing (Photo A2; note that the dried gel is appreciably shrunk compared to the initial gel in Photo A1). On the other hand, in the case of the skin-covered gel, the LED continues to glow even after 24 h (Photo A4). There is a drop in current in this case too, but it is comparatively small, with I at 24 h being 70% of its initial value (I_0). (Note that the drop in current is due to an increase in resistance $R = \rho L/A$, where ρ is the resistivity of the gel-wire, L its length, and A its cross-sectional area.[91] The loss of water from the gel impacts both its resistivity as well as its geometry.) In sum, the skin-covered gel retains its electrical functionality over a much longer time because of its ability to retain water. In a similar vein, we believe the ability to grow a skin around a gel will prove useful in many other scenarios.

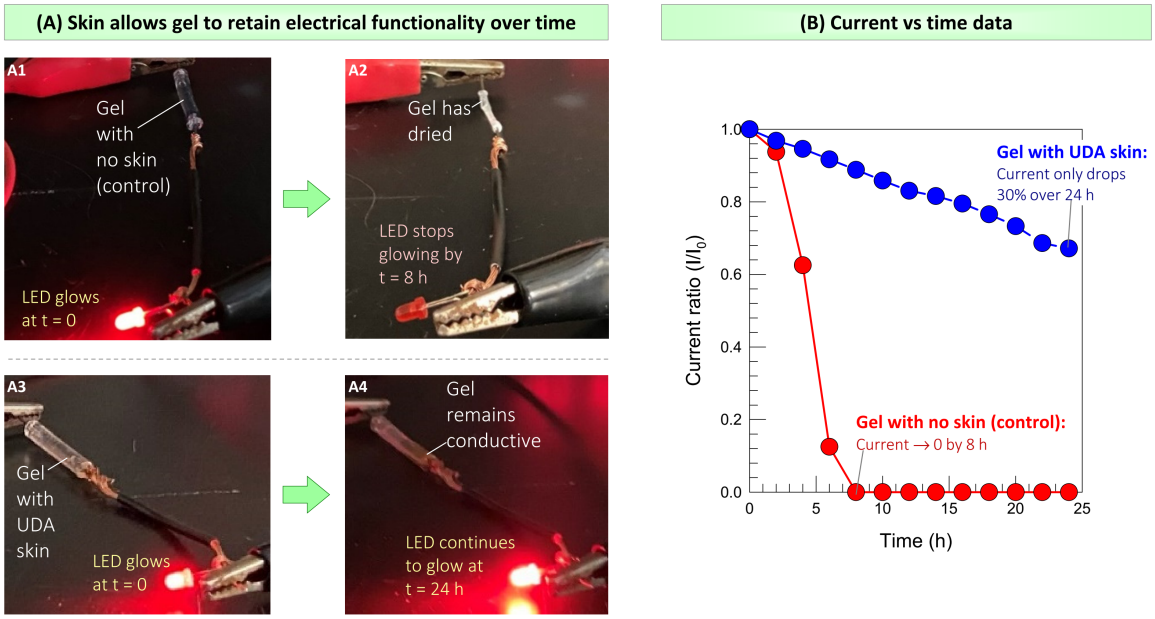

Figure 3.9. Testing a skin-covered gel as a conduit in an electric circuit. A DC power supply is connected to an LED with a cylindrical gel (3 cm long, 0.5 cm diameter) serving as an ionic conductor over a part of the circuit. (A) Photos of the experiment. For the control experiment, the bare gel with no skin is used (A1, A2) while in the second experiment, the gel with UDA skin is used (A3, A4). (B) Plots vs time t of the current I (normalized by I_0 at t = 0) for the two experiments. The current goes to zero for the bare gel by 8 h, whereas the current only drops by 30% over one day for the skin-covered gel. Correspondingly, the LED stops glowing in the case of the bare gel by the 8 h mark (A2) while it continues to glow even after 24 h (A4). The differences arise because the skin inhibits the drying of the gel.

3.4 Conclusions

We have devised a simple technique that permits any hydrogel to be enclosed in a hydrophobic skin. The technique is an 'inside-out' polymerization that requires an initiator-loaded gel to be placed in an organic (liquid) monomer. We choose the initiator to be *soluble in both the aqueous gel as well as in the monomer*, whereas the monomer is hydrophobic and thereby insoluble in the gel. Upon irradiation with UV light, a polymer skin grows around the gel. The entire process is convenient, quick, and performed under mild conditions. Skins can be formed around gels in various geometries, and the procedure works equally well for gels formed by physical or covalent bonds. Skin thickness can be easily controlled by the UV irradiation time; typically, we form a ~ 100 μm-thick skin around a gel of 3–5 mm size (i.e., the skin is 2–3% of the gel size) in 10 min of irradiation. The choice of organic monomer dictates the mechanical properties of the skin. With UDA as the monomer, the resulting polyurethane skin is transparent, elastomeric (soft and flexible), and can be peeled from the core gel using forceps. When PEGDMA is used as the monomer, a hard and brittle skin is formed around the gel core, which can be cracked open by impact with a hammer.

Due to its hydrophobic nature, the skin acts as a protective barrier around the core hydrogel. This protection allows the gel to resist dehydration when exposed to air and resist swelling when placed in water. Also, the skin allows hydrophilic cargo to be *hermetically sealed* in the gel and thus prevented from leaking out into water. The cargo can also be *released in a burst-release fashion when the skin is peeled off or when the external fluid is an organic solvent like ethanol*. The skin also protects the gel from chemical or biological attack (e.g., from strong acids and mold). Because the skin grows uniformly from the gel core, there is sufficient adhesion

between the gel and the skin, even though the former is hydrophilic and the latter hydrophobic; thus, the skin does not delaminate and expose the gel during any of the testing. When compared to alternative techniques, the advantage of the present technique lies in its simplicity (no need for plasma or other treatments to ensure adhesion between the gel and the skin); wide applicability (it can be used to protect any gel); and tunability (skin properties can be varied from soft to hard, etc. by simply varying the monomer used). Indeed, the variety of skins possible with our approach can be likened to the diverse skins seen around fruit or vegetables, which range from very soft and thin (mango, plum) to soft and thick (navel oranges) to hard and thick (avocadoes). Skin-encasing of gels could be useful in any application where the gel is exposed - either to air or aqueous fluids. Examples of the former include gels designed for soft-robotics or soft electronics; as an example, we have shown that a skin-covered gel maintains its electrical functionality in a circuit for long periods. Examples of the latter include gels intended for use as biomedical implants or drug-delivery depots.

Chapter 4
On-Off Release from Smart Skin-Covered Hydrogels

4.1 Introduction

Hydrogels are crosslinked polymer networks that retain high amounts of water due to the presence of hydrophilic functional groups on their polymeric backbones.[28-30] Owing to their high-water content (typically more than 70%), they have the capability to encapsulate a wide range of hydrophilic solutes. As a result, hydrogels are widely employed in the encapsulation of various substances such as small-molecule and macromolecular drugs in biomedical applications,[33,92] moisturizers and fragrances in cosmetic applications,[93] and fertilizers and pesticides in agricultural applications.[94,95] The release of these solutes from hydrogels is primarily dictated by two features: (1) the mesh sizes of the networks and (2) the interactions between the polymer chains and the solutes.[33] By carefully modulating these two features, hydrophilic solutes can be released in a controlled manner.

Mesh sizes of hydrogels are generally in the range of 5 to 100 nm.[33,96] If the solute size is smaller than this mesh size ($r_{solute}/r_{mesh} < 1$), the solute gets easily released into the external medium by diffusion. Most of the small molecule solutes including chemotherapeutic drugs, agrochemicals, and cosmetic agents fall under this category. In such cases of diffusion-limited release of small molecule solutes, it is worthy to note that the release cannot be extended beyond a few hours. Conversely, if the solutes are chosen in such a way that their sizes are closer to the mesh sizes ($r_{solute}/r_{mesh} \sim 1$), extended and controlled release of solutes can be achieved by slowing down the diffusion rate due to steric hindrance. This is the case for protein therapeutics

and many studies have shown extended release up to a period of a few weeks or a month.[97] On the other hand, if the solute size is much larger than the mesh size of the hydrogels ($r_{solute}/r_{mesh} > 1$), the solutes are permanently entrapped inside the network. Mammalian and bacterial cells (sizes ~ 1-10 μm) can be easily entrapped inside the hydrogel matrices in this way.[98] In addition to the mesh sizes, if the chemistry of the solute and polymer backbone are carefully tuned to exhibit attractive interactions such as covalent bonding, electrostatics, and van der Waals' interactions, the small-molecule or macromolecular solute release can be slowed down even further.[32] However, incorporating such attractive interactions involves a choice of specific chemistries of polymers corresponding to the solute of interest as well as complex chemical modifications, deeming them very difficult for scaling-up to commercial applications.

Recently, the controlled release of solutes from hydrogels has been faced with a major challenge of achieving an on-demand release of solutes. In particular, the release should be zero until a desired time, followed by the release to be 'switched on'. Likewise, the release should also be cyclable multiple times between the on and off states as and when needed. Figure 4.1A shows a schematic of such an ideal release rate profile with an initial no release region (indicated by a zero rate), followed by a partial release occurring at a certain rate when an "on" stimulus is applied. Later, the release should be stopped when an "off" stimulus is applied, and these on-off steps should be repeatable multiple times. A cumulative release profile (Figure 4.1B) of this idealized scenario is shown to exhibit a step-release pattern and it clearly illustrates each of the individual steps corresponding to the ideal release rate profile. Many pharmaceutical drugs including insulin and hormones require such on-demand pulsatile release profiles for achieving maximum therapeutic effects. In this regard, stimuli-responsive hydrogel systems that exhibit

physical changes in their water-swollen polymer networks in response to external stimuli such as temperature, pH, light, redox species, and ultrasound are being extensively studied.[10,44,99-101]

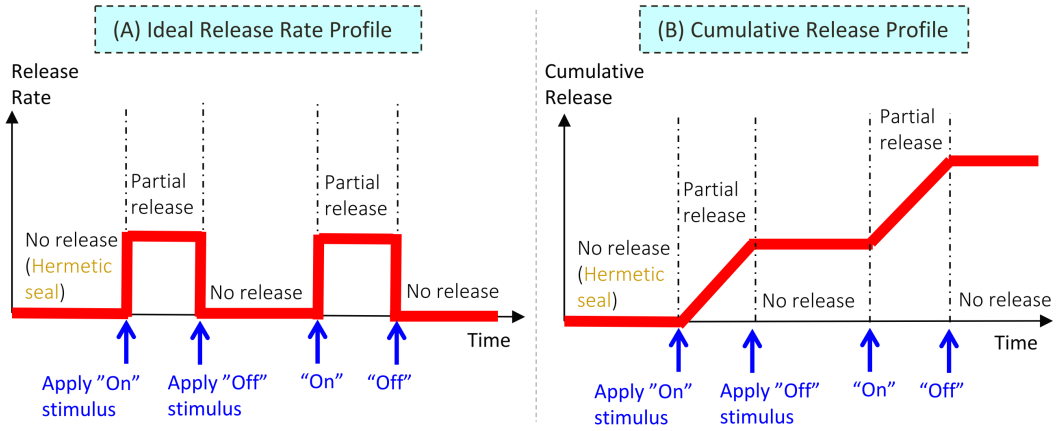

Figure 4.1. Schematics of idealized on-off release profiles. (A) Schematic of a solute release rate vs. time showing no release region (hermetic seal), followed by an on-off release by applying an "on" or "off" stimuli. (B) Schematic of cumulative solute release vs. time showing the step-like release profile with the initial no release region, followed by the on-off regions.

The ability of stimuli-responsive hydrogel systems to show dramatic changes in their mesh sizes due to their abrupt changes in the swelling behavior upon applying external stimuli is the most explored phenomenon for achieving the on-demand release of solutes. There have been few reports demonstrating the pulsatile on-off release of macromolecular solutes from some gels,[9,102-105] e.g., in the case of thermosensitive poly(N-isopropylacrylamide) hydrogels by cycling temperature.[103-105] However, in all these studies, solute release at the outset where there is supposed to be no release is still a finite value and not zero. Thus, given time (say a few hours or a day) most of the solute would still leak out of the gel in the initial 'off' state. This situation would be exacerbated if the small-molecule solutes are used due to their sizes being much

smaller than the mesh sizes of the gels.[106,107] Thus, none of these gels can ensure a truly on-demand and on-off release of solutes, especially the small-molecule solutes.

Recently, our lab demonstrated two simple ways to provide hermetic seal of small-molecule solutes in a gel, and this was done by either creating a wax shell around the gel[11] or by creating a hydrophobic protective polymer skin around the gel.[108] The wax shell and the protective skin, both being hydrophobic, served as perfect barriers to solutes in the gel, and thus zero release out of the gel could be ensured for months. Furthermore, the release could be "switched on" by either melting the wax by heat or by using a good solvent that swells the polymer skin. However, the drawbacks of these designs are that the release cannot be "switched off" i.e., once the wax melts or once the polymer skin is swollen in the solvent, the release cannot be stopped. Hence, there is still an unmet need to achieve on-demand and cyclical on-off release of small molecule solutes from hydrogels.

In this study, we have used a simple technique that we developed previously for covering hydrogels with protective hydrophobic polymer skins and altered the recipe to create hydrogels covered with smart skins. Specifically, we have incorporated a redox-responsive monomer, 2-(methylthio)ethyl methacrylate (MTEMA), that contains a thioether functional group.[109] Thioether-containing polymers are well studied in the field of redox responsive materials due to their ability to reversibly transition from a hydrophobic thioether form to a hydrophilic sulfoxide form in the presence of oxidizing and reducing agents.[51,52,59,109-111] Therefore, the initially hydrophobic skin will become hydrophilic in the presence of oxidizing agents, thereby 'turning on' the release of solutes out of the gel. Furthermore, we show that the rate of release can be

easily controlled by changing the thickness of the smart skin as well as the solute and the oxidizing agent concentrations. Conversely, solute release can also be 'turned off' at a later time by adding a reducing agent that reverts the skin to its hydrophobic state. Thus, our smart skin will enable the regulated (on-off) release of solutes out of a gel, and this concept is likely to be useful in many industrial applications. We further extend our technique to synthesize flat free standing smart polymer membranes that exhibit on-demand tunable permeability to small molecule solutes. These membranes again enable regulated redox responsive on-off flux of small molecule solutes. Such smart membranes can be employed for various applications such as chemical separations, controlled release, and water treatment.[19,112-114]

4.2 Experimental Section

Materials. The biopolymer alginate (alginic acid sodium salt from brown algae, medium viscosity); the monomer 2-(methylthio)ethyl methacrylate (MTEMA); the photoinitiator 2-hydroxy-2-methyl-propiophenone (HMPP); the accelerant N,N,N′,N′-tetramethyl-ethylenediamine (TEMED); the dyes methylene blue, brilliant yellow, and rhodamine 6G; the salt calcium chloride dihydrate ($CaCl_2$); the oxidant hydrogen peroxide solution (H_2O_2, 30 wt% in water); the reducing agent L-ascorbic acid or vitamin C (VitC); and the catalyst N-bromosuccinimide (NBS) were all obtained from Sigma-Aldrich. Urethane-based monomer was a gift from Allnex: the urethane diacrylate (UDA; tradename Ebecryl 230) consists of an aliphatic urethane segment of 4858 Da with two acrylates covalently bonded at its ends. The biopolymer agar (termed agar-agar) was also a gift from TIC Gums. The anionic acid red 52 dye was obtained from TCI America. The photoinitiator Irgacure 2959 (IRG) was purchased from BASF. Deionized (DI) water was used in all experiments.

Preparation of Hydrogels. To prepare spherical alginate hydrogels, 2 wt% of alginate solution in DI water was dropped into a 0.5 M $CaCl_2$ solution using a transfer pipette. The anionic alginate chains are electrostatically crosslinked with Ca^{2+} ions, and thus convert the liquid alginate droplets into spherical hydrogels after an incubation period of 30 minutes. The resulting gels had diameters of 2–5 mm, depending on the orifice dimensions of the pipette used.

To prepare cylindrical agar hydrogels, agar (5 wt%) was suspended in DI water and then heated to above 85 °C under constant stirring until the agar is completely dissolved. The viscous

agar solution was then poured into a cylindrical plastic container. Upon subsequent cooling to room temperature, cylindrical agarose gels were obtained.

Preparation of Smart-Skin Covered Hydrogels. The procedure for covering alginate hydrogels with smart-skins using an inside-out strategy has been outlined above in Figure 4.2A. First, a spherical alginate hydrogel was placed for a period of 10 min in an aqueous mixture consisting of 0.5 wt% photoinitiator (IRG or HMPP), 1 wt% accelerant (TEMED), along with solutes to be encapsulated such as 1mM of acid red 52 or 10 mM of methylene blue dyes. After which, the alginate gel was placed in a vial containing the organic monomer mixture: UDA and 20 wt% MTEMA (thioether-containing monomer) with respect to UDA. Note that the high viscosity of the mixture helps the gel to be suspended in the monomer mixture without setting at the bottom.[108] The vial containing the gel was then subjected to UV exposure (at 365 nm) for a specified time (typically 10 minutes) to form the smart-skins. A low-intensity 36 W UV lamp from Melody Susie was used for forming the smart skins.

Preparation of Smart-Membranes. The procedure for forming smart membranes is illustrated above in Figure 4.2B. First, a cylindrical agar hydrogel was placed in a solution containing 0.5% photoinitiator (IRG or HMPP) and 1 wt% accelerant (TEMED) for 10 min. Then, the agar hydrogel was placed in a plastic container and an organic monomer mixture (UDA and 20 wt% MTEMA with respect to UDA) was poured on top of the hydrogel. The gel with the organic mixture on top was then irradiated with UV light (at 365 nm) for 10 minutes to form the smart membranes. The excess monomer was pipetted out and the membrane was peeled off from the gel using the tweezers. The membrane was carefully wiped with kimwipes before usage.

Scanning Electron Microscopy (SEM) and Energy Dispersive X-ray Analysis (EDX). The smart skins were separated from the gels using tweezers and then pieces of the skins were cut out using razor blades. The skin pieces were then sputter-coated with gold and palladium to increase the conductivity of the material. Next, the SEM images of the skins were taken with a Tescan XEIA3 SEM machine operated at an accelerating voltage of 10 kV. The machine is also equipped with energy dispersive X-ray spectrometry (EDX) capability to probe the elemental compositions of the smart-skins.

Optical Microscopy. Smart skins of different thicknesses were first prepared by irradiating with UV light for 10 minutes and 30 minutes respectively. The skins were cut into two semi-hollow spherical halves using razor blades and were separated from the gels using tweezers. Optical images of the skins were then taken using a handheld Dino-Lite USB digital microscope purchased from Amazon at a magnification of 230x. The microscope came with a DinoCapture 2.0 software, which was used for measuring the thickness of the skins.

FTIR Spectroscopy. Fourier transform infrared spectroscopy (FTIR) studies were performed for the UDA, MTEMA, and MSEMA polymer samples. First, the monomers (UDA or MTEMA) were mixed with a 0.5% photoinitiator (HMPP) and 2 mL of the solutions were then poured into multiple Petri dishes. Each of the samples in Petri dishes was then polymerized by irradiating with UV light for 30 minutes. The resulting films of poly(UDA) and poly(MTEMA) were obtained. Some of the Poly(MTEMA) films were then placed in a 30% H_2O_2 solution for 10 minutes to form poly(MSEMA) films. Subsequently, a few of the poly(MSEMA) films were

placed in a solution containing 10% VitC and 0.5% NBS and were analyzed for the reduction of sulfoxide groups. FTIR spectra were obtained for all the polymer films using a Thermo Nicolet NEXUS 670 FTIR instrument with a spectral range of 4000–1000 cm^{-1}.

Dye Release Experiments. Skin-covered gels loaded with known amounts of the dyes (acid red 52 or methylene blue) were placed in vials containing 2 mL of DI water, or 2 mL of 30% H_2O_2 solution, or 2 mL of 10% VitC and 0.5% NBS solution for a given period of time, depending on the experiment. The dye concentration in the external solutions was monitored using a Cary 50 UV-Vis spectrometer by taking 1 mL samples at a time. The absorbance measurements were made at the absorption peaks of the dyes (565 nm for acid red 52 and 665 nm for methylene blue) using the Advanced Reads software. Immediately after the measurements were recorded, the samples were put back into their respective vials. Cumulative dye release (as a percentage of the initial loading) was calculated and plotted as a function of time.

For the smart-membrane dye release experiments, osmosis chambers were purchased from the Carolina company. The smart membranes were secured using binder clips in between the two sides of the chamber. On one side of the chamber (side 1), 2 mL of 1 mM acid red 52 solution was injected using a transfer pipette. On the other side (side 2), 2 mL solutions of DI water, or 30% H_2O_2, or 10% VitC, and 0.5% NBS were injected using pipettes, depending on the experiment. The dye concentration in the solutions loaded on side 2 was monitored using the UV-Vis spectrometer by following the same procedure as above.

4.3 Results and Discussion

4.3.1 Synthesis of Smart-Skins and Smart-Membranes

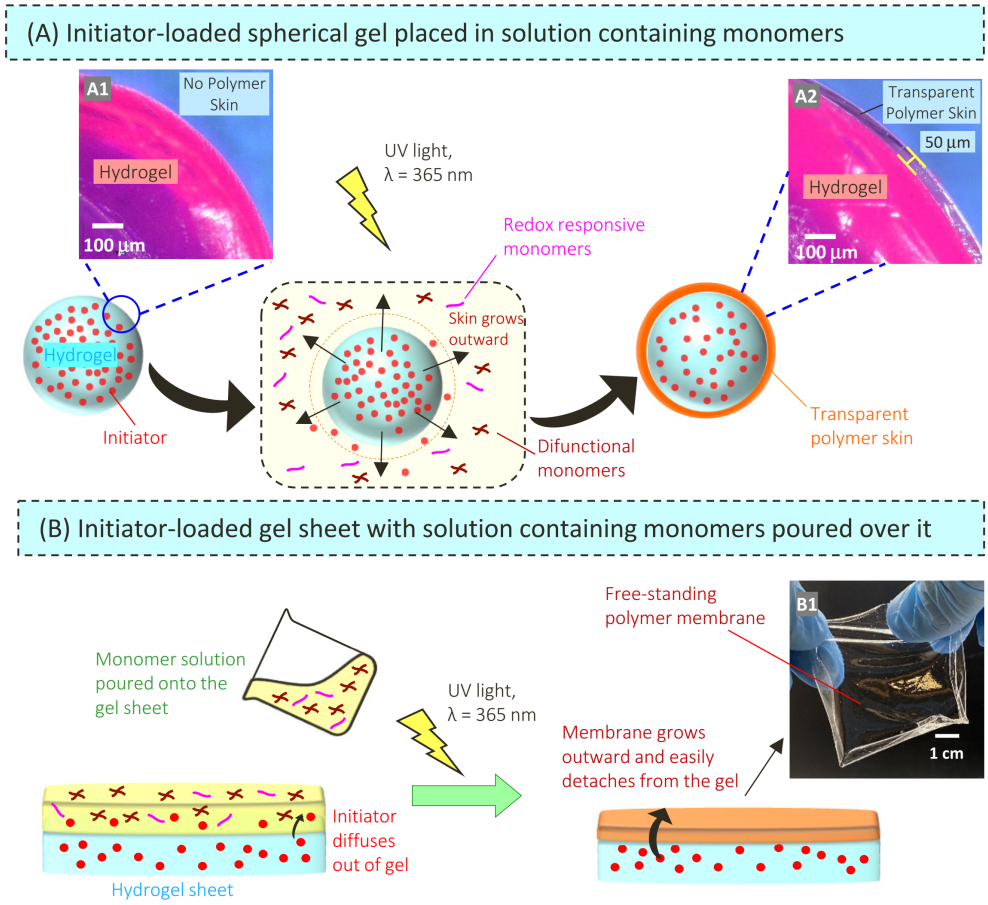

Figure 4.2. Procedure for forming smart-skins/membranes around hydrogels. (A) Initiator-loaded spherical alginate gel (Photo A1) is placed in a mixture of UDA and MTEMA monomers. The skin (copolymer of UDA and MTEMA) grows around the gel core upon UV irradiation and is transparent (Photo A2). (B) Monomer mixture (UDA and MTEMA) is poured on top of the initiator-loaded agar gel disc. Upon UV irradiation, a thin free-standing membrane is formed and it is easily detached from the gel (Photo B1).

Our procedure for synthesizing smart-skins around hydrogels is a modification of our earlier approach.[108] We begin with a spherical gel of alginate (3-4 mm in diameter) formed by dropping 2% sodium alginate into a 0.5 M calcium chloride solution using a pipette or a syringe (Photo A1). The gel is formed by complexation of anionic alginate chains with Ca^{2+} ions at egg-

box junctions.[36] This spherical gel is then loaded with 0.5% Irgacure 2959 (photoinitiator) and then placed in a mixture of liquid monomers (Figure 4.2A).[108] The monomer is an 80/20 mixture of a urethane diacrylate (UDA) and the redox-responsive 2-(methylthio)ethyl methacrylate (MTEMA). The initiator is *soluble in water and in the monomers, while the monomers are insoluble in water*. This ensures that a thin skin is formed concentrically around the spherical gel upon irradiation with UV light (Photo A2).

We also form free-standing membranes of UDA/MTEMA by using a gel of a different geometry (Figure 4.2B). For this, a gel of agar, a biopolymer extracted from red seaweeds,[96] is formed in a disc shape. A hot agar solution (~90°C) is added to a Petri dish. Upon cooling, agar chains form a network in which the crosslinks correspond to double-helical junctions of the chains. The agar gel is then loaded with 0.5% Irgacure 2959. We then pour the monomer mixture on the agar disc. Because the monomer is a viscous liquid, it spreads uniformly on the gel. We then irradiate the system with UV light to form a thin transparent membrane, which can be peeled off from the agar gel (Photo B1).

4.3.2 Smart-Skin Characterization

Scanning electron microscopy (SEM) images of a smart skin that was peeled off from a 3-mm alginate core are shown in Figure 4.3A. The skin, obtained after 10 min of UV irradiation, shows a smooth texture and is very uniform, with a thickness of 75 μm (Photo A2). Energy-dispersive x-ray (EDX) measurements on a region (red box in A2) of the skin confirms the presence of sulfur in the skin (by the K_α peak at 2.3 eV in the EDX spectrum in Figure 4.3B). Note that the elements C, O, N, and S are the only ones found in the EDX, which is as expected

from the structures of UDA and MTEMA. Moreover, from EDX, the sulfur content is calculated to be 11.5% by weight and 4.9% on an atomic basis (Table in Figure 4.3), which agrees with the sulfur percentages calculated from the monomer composition (80/20 UDA/MTEMA).

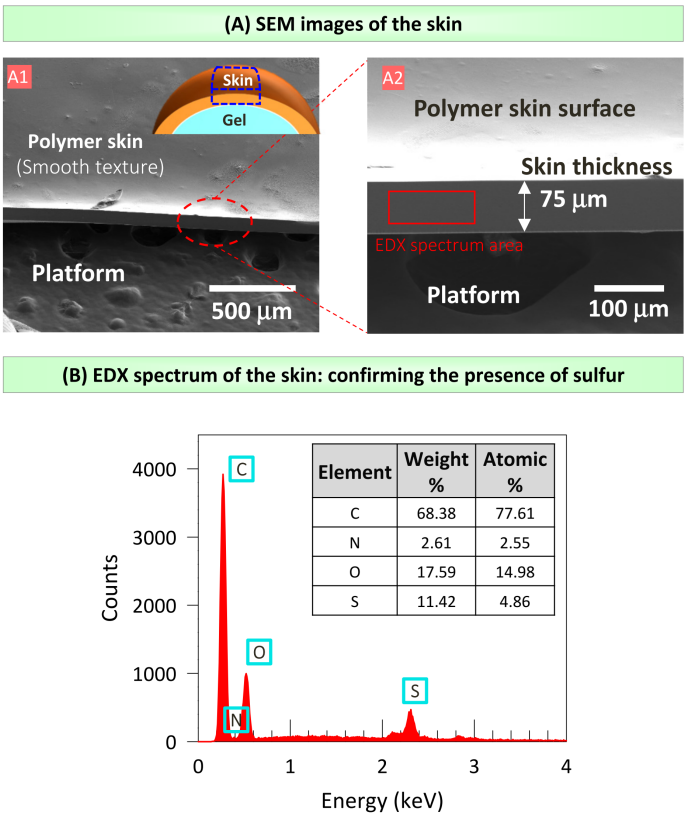

Figure 4.3. Smart-skin characterization using electron microscopy. The skin was formed around a 3-mm alginate gel with 10 min of UV-irradiation. (A) SEM images showing the smooth texture of the skin (Photo A1). The magnified image (Photo A2) shows the thickness to be 75 µm. (B) EDX spectra of the skin confirm the presence of sulfur (peak at 2.3 eV) in the skin at a weight% of 11.4% and atomic% of 4.9% (inset table).

We can control the thickness of the skin around alginate hydrogels from ~ 20 to 200 µm by simply varying the UV exposure time. As an example, Figure 4.4 shows the skins around alginate gels (4 mm diameter) loaded with 0.5% photoinitiator, followed by 10 and 30 min of UV irradiation. The skin thickness is 50 µm with a 10-min UV exposure whereas it increases to

120 µm when the UV exposure time is increased to 30 min. Such control over the thickness will be helpful in controlling the release of solutes from the skin-covered hydrogels.

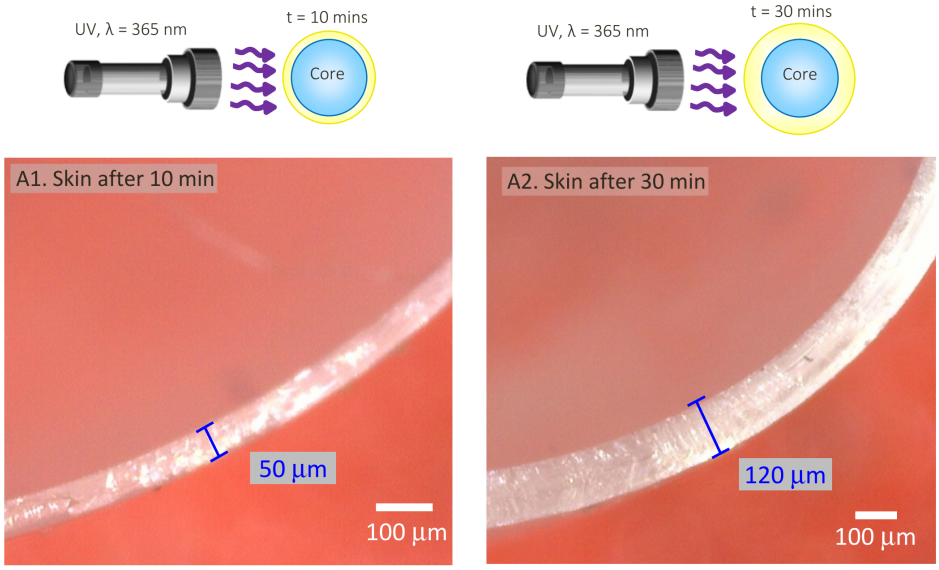

Figure 4.4. Smart-skin characterization by optical microscopy. Optical images of the skins around 4-mm alginate gels with 10 min (Photo A1) and 30 min (Photo A2) of UV exposure.

4.3.3 Thioether Redox Chemistry

The redox-responsive properties of our smart skin are due to the thioether groups on MTEMA units (Figure 4.5A). Thioethers are known to get oxidized to sulfoxides when exposed to oxidizing agents such as hydrogen peroxide (H_2O_2).[109] Note that poly(MTEMA) has a purely hydrocarbon backbone and is therefore hydrophobic and insoluble in water. When poly(MTEMA) is oxidized, its sulfoxide form, denoted as poly(MSEMA) in Figure 4.5A, is hydrophilic. The sulfoxides can also be reduced back to thioethers using reducing agents such as vitamin C (VitC).

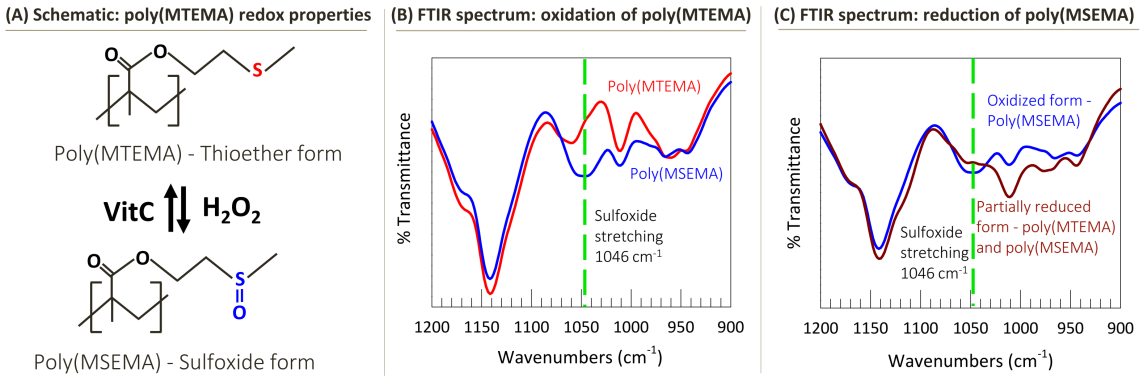

Figure 4.5. Thioether redox chemistry and its spectroscopic quantification. (A) In the presence of oxidizing agents such as H_2O_2, the thioether-bearing polymer, poly(MTEMA) is oxidized to its sulfoxide form, poly(MSEMA). The reaction can be reversed upon contact with reducing agents such as VitC. (B) FTIR spectra for a poly(MTEMA) film before and after placing in 30% H_2O_2. A strong sulfoxide stretching peak at 1046 cm^{-1} confirms the oxidation. (C) FTIR spectra for a poly(MSEMA) film before and after reduction with 10% Vit C. The peak at 1046 cm^{-1} is decreased, indicating that poly(MSEMA) is partially reduced to poly(MTEMA).

To confirm the oxidation reaction, we prepared a poly(MTEMA) film and exposed it to 30% H_2O_2. We studied the film by FTIR spectroscopy before and after oxidation. After oxidation, a characteristic peak for sulfoxide stretching is observable at 1046 cm^{-1} (Figure 4.5B), indicating the conversion of thioethers to sulfoxides, i.e., of the polymer to its hydrophilic form, poly(MSEMA). Next, we exposed the poly(MSEMA) to reducing conditions (10% VitC) and re-ran the FTIR. Previous studies had indicate that the yields of the reverse reaction are not very high.[59] Therefore, both the thioether and sulfoxide forms are expected to be present after reduction with VitC. Indeed, Figure 4.5C shows that the peak at 1046 cm^{-1} is decreased, indicating that some of the sulfoxides are converted back to thioethers, making the polymer less hydrophilic. Note that these experiments could not be done on the copolymer skin made from UDA and MTEMA because UDA has a strong peak at 1100 cm^{-1} that interferes with the sulfoxide peak (Figure 4.6).

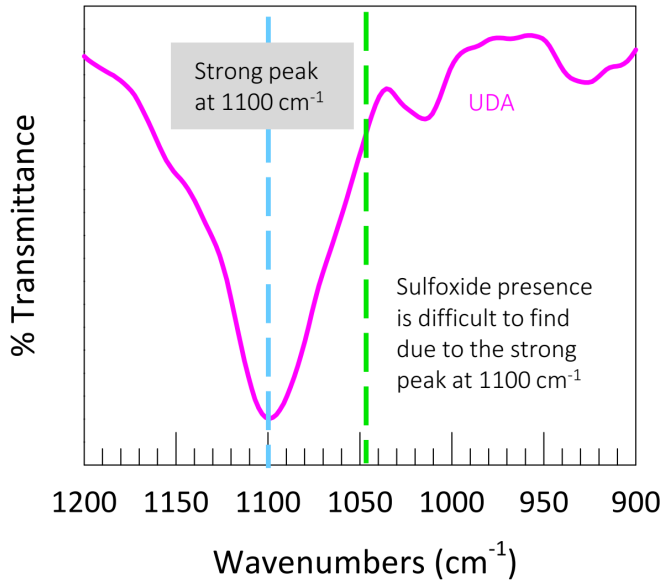

Figure 4.6. FTIR spectroscopy of UDA and the reduced MSEMA film. FTIR spectrum of a poly(UDA) film. The strong peak at 1100 cm^{-1} precludes analysis of a sulfoxide peak in the 1070-1030 cm^{-1} range.

4.3.4 Smart-Skin for 'Switching On' the Release of Solutes

We now discuss the release of hydrophilic solutes from skin-covered hydrogels. Specifically, we study a model hydrophilic solute, *viz*. acid red 52 (MW = 559 Da), which is an anionic dye with a molecular size ~ 0.5 nm. We loaded 1 mM of this dye into an alginate gel (4-mm diameter) and then covered it with a UDA/MTEMA skin (50 μm thickness) using the technique shown in Figure 4.2. This skin-covered gel was initially placed in a vial containing 2 mL of deionized (DI) water for 24 h. Figure 4.7 shows the cumulative dye concentration (as a percentage of the total dye) in the external solution as a function of time. Over the 24 h in DI water, we observe no dye release from the gel. This is consistent with the skin being hydrophobic with thioether moieties (MTEMA form), which completely block the release of the dye, even though its molecular size (0.5 nm) is much smaller than the mesh size of the alginate gel (expected to be ~ 20 nm).

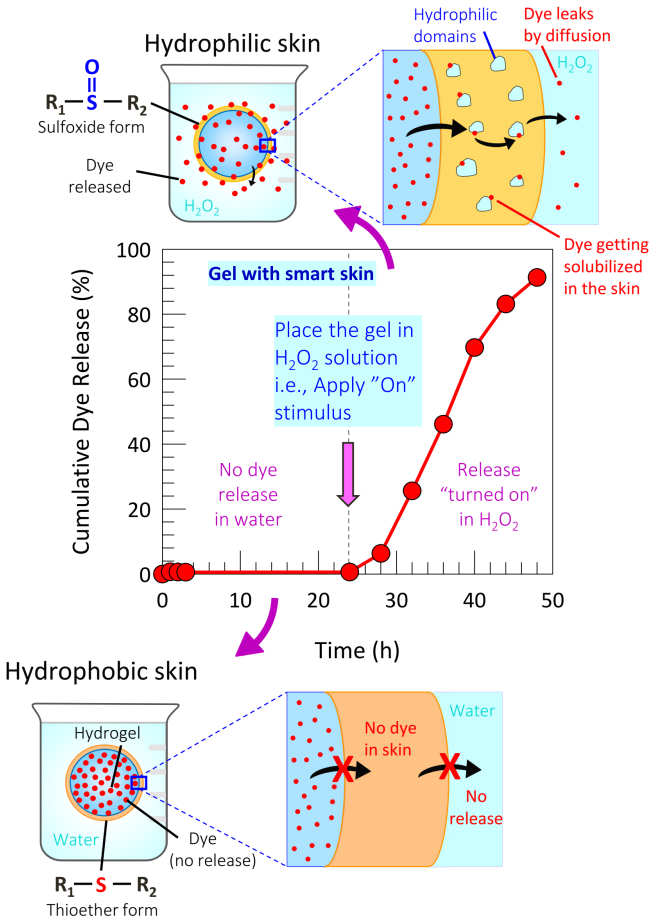

Figure 4.7. Release of an anionic solute from a smart-skin-covered hydrogel. Cumulative release (% of the loaded solute) vs. time for acid red 52 dye from an alginate gel covered with a smart skin. No dye gets released in water for a day, while the dye starts releasing upon transferring the gel to a 30% H_2O_2 solution. Schematics demonstrating that the release is "turned on" because the skin is converted from its hydrophobic (thioether) form to its hydrophilic (sulfoxide) form.

Next, the gel is transferred to a vial containing 2 mL of 30% H_2O_2 solution. We observe the release of dye to be "turned on" and it occurs in a steady fashion with 90% of the dye released over a period of a day. The release of dye can be attributed to the transformation of hydrophobic thioethers to hydrophilic sulfoxides in the skin. Note that there is no change in the core gel; all the action is in the thin surface layer – the smart skin – whose thickness is just 1% of the gel diameter.

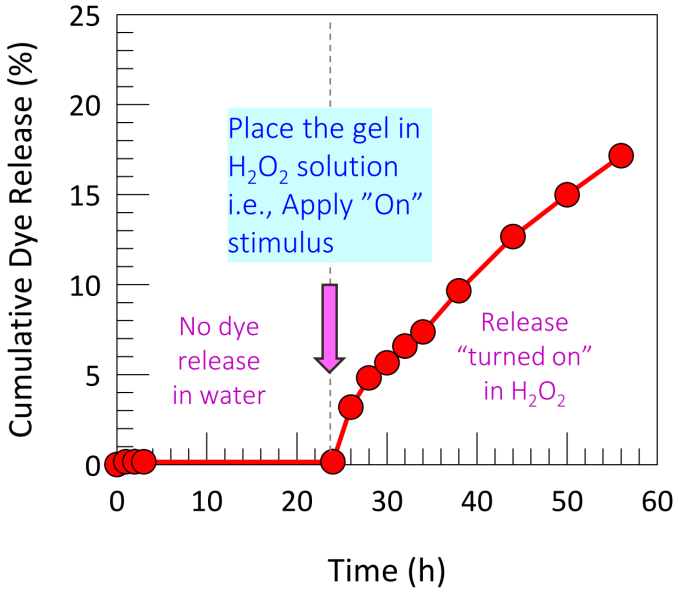

Figure 4.8. Release of a cationic solute from a smart-skin-covered hydrogel. Cumulative release (% of the loaded solute) vs. time for methylene blue dye from an alginate gel covered with a smart skin. No dye gets released in water for a day, whereas a steady release is seen upon transferring the gel to a 30% H_2O_2 solution.

To validate that the findings are universal and regardless of the charge of the hydrophilic solute, we further tested the release of cationic methylene blue dye (MW = 320 Da) from a skin-covered gel. This time, we loaded 10 mM of this dye into an alginate gel (4-mm diameter) and then covered it, as before, with a UDA/MTEMA skin (50 μm thickness). Figure 4.8 shows the plot of cumulative dye concentration vs. time. Once again, the release into DI water is zero, while 20% of the dye was released in 40 h of incubation in a 30% H_2O_2 solution. Note that the methylene blue dye release is much slower than that of the acid red 52, even though 10 times more dye was loaded in the gel. This delayed release may be due to the binding of anionic alginate chains to the cationic methylene blue molecules.

We then reverted to the acid red 52 (anionic dye) and studied the effects of parameters such as skin thickness, oxidant (H_2O_2) concentration, and dye concentration on the release. Keeping other variables constant, two 4-mm diameter alginate gels with different skin thicknesses (50 and 120 μm) were obtained by varying the UV exposure time from 10 to 30 min (Figure 4.4). Both these gels were loaded with 1 mM dye and placed in a 30% H_2O_2 solution. The release (Figure 4.9A) occurred from both the gels; however, the rate of release was much slower from the gel covered with the thicker skin (120 μm). The thicker skin provided more resistance to the release of hydrophilic solutes due to the increased residence time of solutes in the skin.

Next, we varied the concentration of H_2O_2 in the external solution, with all other parameters the same (1 mM dye, 4-mm gels, 50 μm skin). Figure 4.9B shows that ~100% of the dye was released in 1 day when the H_2O_2 was at 30%, whereas, when the H_2O_2 was dropped by half (15%), only 50% of the dye was released a day. In this case, it took more than 3 days to release ~100% of the dye. A further decrease in H_2O_2 to 10% resulted in less than 20% of the dye released in a day. This reduction in dye release is due to the slower conversion of thioether to sulfoxide groups, as noted in the literature.[115] Lastly, we did the release experiments for 1 mM and 10 mM dye concentrations with other parameters (4-mm gels, 50 μm skin, 30% H_2O_2) all fixed. A faster release is observed with the higher concentration, evidently due to a higher concentration gradient (Figure 4.9C).

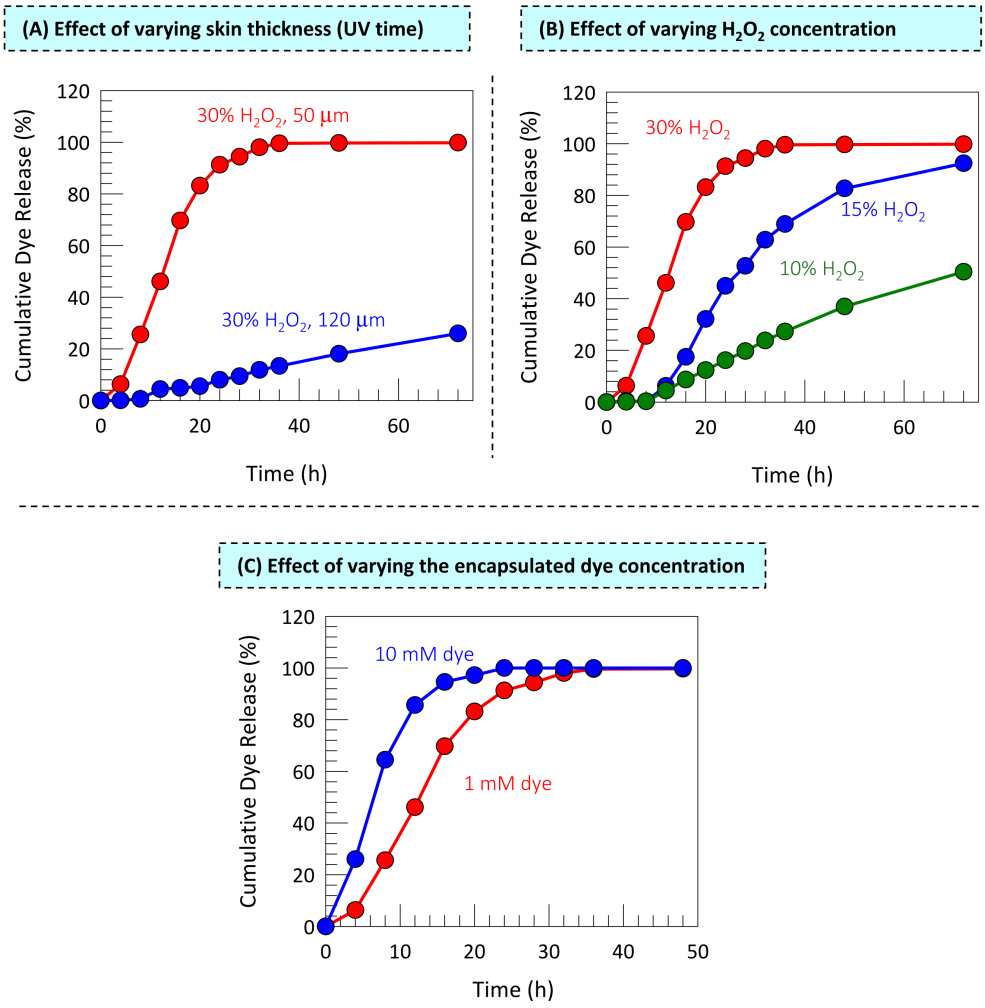

Figure 4.9. Tuning the kinetics of solute release. In all cases, release of the anionic dye (acid red 52) out of skin-covered alginate gels is studied. (A) Effect of skin thickness (this is tuned by the UV irradiation time). (B) Effect of H_2O_2 concentration in the external aqueous solution. (C) Effect of the encapsulated dye concentration.

Altogether, from findings in Figures 4.7, 4.8, and 4.9, we have demonstrated that release of solutes from smart-skin-covered gels can be switched on as needed. To our knowledge, such on-demand release has never been demonstrated with small, hydrophilic molecules. Next, we examine if the release can be switched both on and off.

4.3.5 Cyclical On-Off Release of Solutes from Smart-Skin Covered Gels

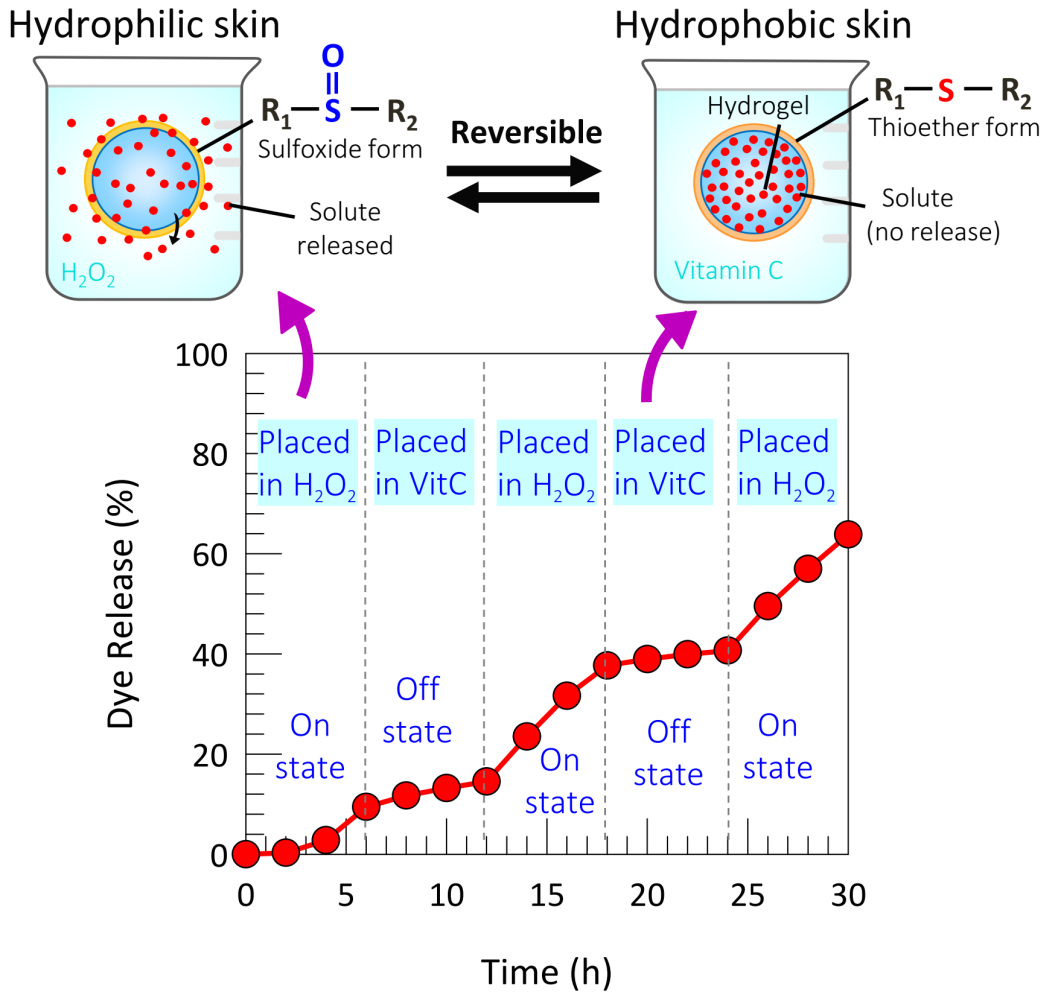

Figure 4.10. Cyclical release of solute from a smart-skin-covered hydrogel by toggling the redox state of MTEMA. Cumulative release of acid red 52 dye vs. time is shown from an alginate gel covered with a smart skin. Dye is released in the "ON" state (when the gel is exposed to the oxidant, H_2O_2) whereas release is negligible in the "OFF" state, when the gel is exposed to the reductant, VitC. The schematics indicate that the skin is in its hydrophilic (sulfoxide, MSEMA) form in the ON state and in its thioether (hydrophobic) form in the OFF state.

The smart-skin system, thus far, showed a one-way release, but we can do more. By simply changing the oxidation-reduction states of the sulfides on MTEMA units, we can go back and forth between a hydrophobic and a hydrophilic skin. Figure 4.10 shows a cyclical on-off release profile of the acid red 52 dye. For this experiment, a 4-mm alginate gel with a 50 μm skin was loaded with 1 mM dye. At $t = 0$, the hydrophobic skin (MTEMA form) was "switched ON" by placing it in a vial containing 30% H_2O_2. The oxidizing agent converts MTEMA into the hydrophilic (MSEMA) form. Over the next 6 h, some of the dye (10%) leaks out. Next, we placed the skin-covered gel in 10% VitC for 10 min, which is our way to "switch OFF" the release because VitC reduces some of the MSEMA back to MTEMA. The gel was then transferred to DI water. As expected, in this OFF state, there is negligible release of dye (only 4% in 6 h), indicating that the skin is sufficiently hydrophobic again.

Next, we repeated this process by returning the gel to the ON state (H_2O_2), and this again results in 30% of dye release over 6 h. Then, the gel was again switched OFF (VitC for 10 min, then put in DI water), and in this case, there was only 3% of release over 6 h. As a final step, we placed the gel back in H_2O_2 to switch it ON again, and in the last 6 h in Figure 4.10, 25% of the dye is released. Thus, our "smart skin" allows the release of solute from the gel to be switched on as needed and also switched off as needed.

4.3.6 On-Off Release of Solutes from Smart Membranes

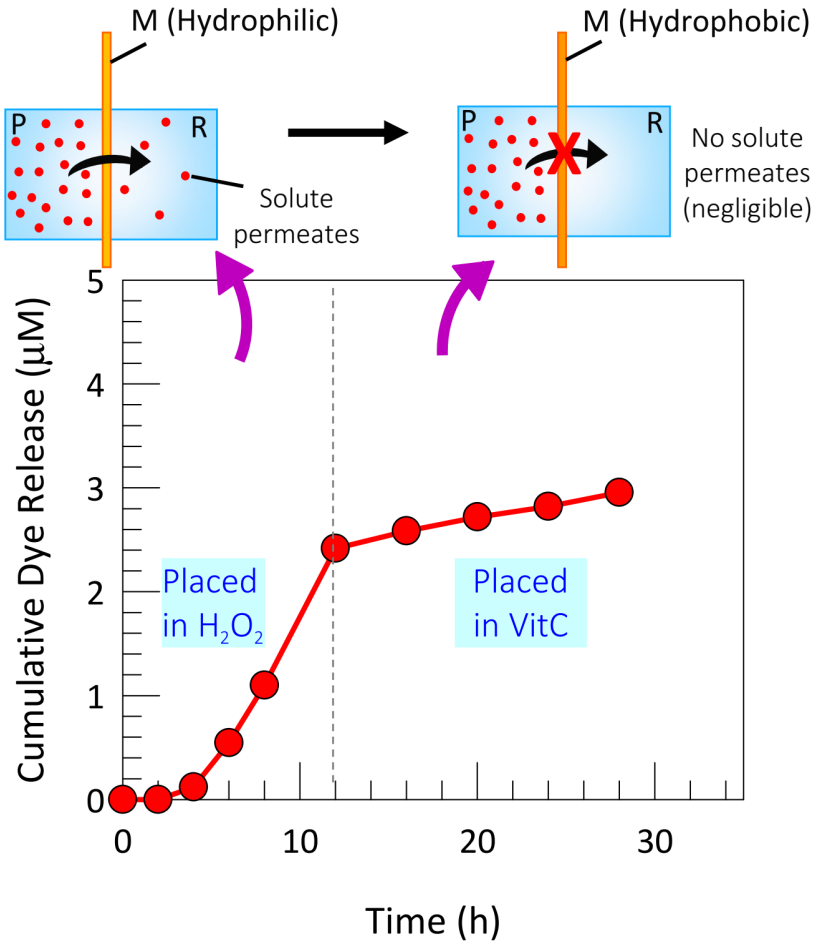

Figure 4.11. Smart-membranes and their ability to achieve on-off solute transport. Cumulative dye release (% of the loaded dye) vs. time (h) from a smart membrane. Fast transport occurs through the skin when injected with a 30% H_2O_2 solution due to the membrane being in the hydrophilic form, whereas slow transport or negligible release occurs after placing in a solution containing 10% vitamin C due to the skin being in the more hydrophobic form.

Finally, we show that the flat membranes made from UDA/MTEMA copolymers also demonstrate on-off release of solutes. For the experiment, we worked with a membrane of dimensions 12 cm × 5 cm × 50 µm, made as shown in Figure 4.2B. The membrane was then placed in an osmosis setup that has two chambers on either side. The permeate (P) side is filled with 1 mM dye and the retentate (R) side is filled with water (no dye). At this stage, the

hydrophobic membrane (M) does not let any of the dye through, despite the existence of a strong concentration gradient for the dye. Then, the water is replaced with 30% H_2O_2 solution. Figure 4.11 shows the dye concentration in the R chamber as a function of time. The oxidizer (which is only on one side of the membrane) slowly converts the membrane into a hydrophilic form. In 12 h, some dye is seen to permeate through to the R chamber.

At this point, the H_2O_2 solution was pipetted out from the R chamber, and it was filled with 10% VitC solution for 10 min and after which it was replaced with DI water. In the next 12 hours, very little dye is released into the R chamber, suggesting that the VitC has reduced some of the hydrophilic MSEMA groups back to MTEMA form. Thus, our approach can also be extended to on-off release from membranes, which could be useful in applications including separations, controlled release, and water treatment.[112-114]

4.4 Conclusions

In conclusion, we have designed smart-skin covered hydrogels with redox-responsive properties that allow *on-demand and cyclical on-off release of small molecule hydrophilic solutes* from the gel cores. At the outset, the solutes are completely sealed in the gel cores and are prevented by the skins from leaking out into the external aqueous solutions until desired periods of time. Moreover, the gels with smart skins have the ability to release their encapsulated solutes on-demand by applying an "on" switch via placing them in a solution containing oxidants such as hydrogen peroxide. Additionally, the rate of release can also be easily controlled by varying the parameters such as skin thickness, oxidant concentration as well as solute loading. Conversely, the solute release can also be stopped on-demand by applying an "off" switch via placing them in a solution containing reducing agents such as vitamin C. This process of switching on/off the release of solutes is repeatable and can be cycled multiple times between the on and the off states.

To achieve this, we have utilized an inside-out technique that we developed for enclosing hydrogels with hydrophobic polymer skins. This time, we have modified the chemistry of the skin to include functional polymers containing thioether moieties. Initially, the skin is hydrophobic, but in the presence of H_2O_2, the thioether groups are oxidized into hydrophilic sulfoxide groups, thus making the skin become hydrophilic and thereby allowing the solutes to be released. Moreover, in the presence of vitamin C, the sulfoxide groups are partially converted back to the thioether forms and thus allowing the solutes to be prevented from leaking out of the gels. By reversibly toggling the skin state from hydrophobic thioether form to hydrophilic sulfoxide form, on-demand and cyclical on-off release of various small molecule hydrophilic

solutes can be achieved. Such, a perfect hydrogel-based system with on-demand and on-off release capabilities is envisioned to be useful in many industrial applications.

We also extend the inside-out technique to form thin, freestanding, smart-polymer membranes with controlled thicknesses of ~10-200 μm. These membranes, like the skins, also allow on-demand and on-off transport of solutes from one-side to the other. This is achieved by selectively tuning their chemistry and with that their hydrophilicity using oxidizing and reducing agents. We envisage that these smart polymer membranes can be employed in several applications including chemical separations, controlled release drug delivery as well as water purification.

Chapter 5
Smart Membranes around Vesicles

5.1 Introduction

Molecular self-assembly is ubiquitous in nature and is centrally important to life itself.[116] It refers to a thermodynamically driven process of spontaneous organization of molecules into ordered aggregates, usually through non-covalent interactions. Many complex structures contained in a cell including folded proteins, functional nucleic acids, and lipid membranes are formed by this self-assembly process.[117] Likewise, amphiphilic molecules such as surfactants, lipids, or block-copolymers self-assemble in aqueous solutions to form diverse architectures, including spherical micelles, cylindrical micelles, and vesicles.[45] It turns out that the key to the formation of a particular self-assembled structure relies on the geometry of the amphiphilic molecule and can be quantified by a parameter known as the critical packing parameter (CPP).[45,118,119] This parameter is expressed as the ratio of the average cross-sectional area of the tail to the average cross-sectional area of the head group. For instance, if the CPP is less than 0.33, the amphiphile assumes a cone geometry and favors the formation of spherical micelles. On the other hand, if the CPP is higher and is in the range of 0.5 - 1, the amphiphile assumes a cylindrical geometry and bilayer structures, or vesicles are formed.

Vesicles are nanoscale hollow containers that consist of an aqueous interior core surrounded by a bilayer and are often made from lipids[4,120] or a combination of oppositely charged surfactants,[119,121,122] which have cylindrical geometries. The vesicles formed from lipids are generally biocompatible and biodegradable but often exhibit low stability as they are not equilibrium structures.[48] On the contrary, catanionic vesicles formed from oppositely charged

surfactants exhibit long-term stability.[119,121] Moreover, unilamellar catanionic vesicles form spontaneously when unequal ratios of cationic and anionic amphiphiles are simply mixed. In contrast, unilamellar vesicles made from lipids require high energy in the form of sonication or extrusion.[120] These are the key reasons why catanionic vesicles, with their long-term stability, low cost, and relative ease of preparation attract the attention of several researchers including our group.

Catanionic vesicles are of special interest for applications in a wide range of industries including pharmaceuticals, food, and cosmetics due to their ability to encapsulate a variety of substances such as drugs, perfumes, and organic chemicals.[121,123] More importantly, these self-assembled vesicle structures can be designed using stimuli-responsive amphiphiles, which can tune their geometry in response to external stimuli. This change in geometry in turn causes a transformation in the self-assembled structure to spherical or cylindrical micelles.[49,124] Furthermore, this transformation can result in the burst active release of the encapsulated substances upon activation of the trigger. In this regard, various stimuli such as temperature, light, and pH have been extensively studied.[49,124-127]

An additional relatively new stimulus, reactive oxygen species (ROS) is also gaining importance as it is commonly produced from various endogenous sources and it can also be produced exogenously through irradiation of photosensitizers.[128-131] ROS are highly reactive oxygen species including hydrogen peroxide (H_2O_2), hydroxyl radical (·OH), superoxide (O_2^-), and singlet oxygen ($^1O_2$). In living organisms, ROS are routinely generated at low levels in all cells and play a vital role in mediating several physiological processes including cell signaling,

protein function, and pathogen control.[55,57] However, increased levels of ROS are often observed locally in tumor microenvironments when compared to normal tissues. Therefore, it is not surprising that several ROS-responsive materials have been considered for cancer treatment. Various ROS responsive chemistries have been reported, such as thioether, selenium, tellurium, thioketal, and arylboronic ester.[51,52,58,132-134] Among these chemistries, the thioether group, beginning with the development of polypropylene sulfide in 2004,[58] remains the simplest yet powerful chemistry that is sensitive to ROS moieties. Thioether groups are known to undergo a transition from hydrophobic sulfide to hydrophilic sulfone or sulfoxide groups in the presence of ROS such as hydrogen peroxide and hydroxyl radicals due to oxidation.[51,52,55,58,132,133]

Several research groups have been successful in achieving the transformation of vesicles to micelles upon applying stimuli such as temperature, light, and pH.[49,124-127] However, to our knowledge, only a handful of articles are reported thus far demonstrating such a transformation using ROS as a trigger. One such study is a recent one by Guo *et al*.,[57] where they show ROS-induced vesicle to micelle transition with custom-synthesized selenium incorporated amphiphilic surfactants. All these systems relied on complicated synthesis procedures requiring adept knowledge of organic chemistry techniques. Hence, there is still a need to create simple ROS responsive vesicles made from commercially available organic molecules.

Moreover, in many pharmaceutical and biomedical applications, it is often desirable to have vesicles that are responsive to multiple stimuli instead of a single stimulus.[135-141] Having such multi-stimuli responsive systems could provide unique opportunities to tune the release profiles of active ingredients simply by adjusting the suitable combination of stimulus

conditions.[140] Previously studied multi-stimuli responsive vesicles thus far have involved complex modifications and organic synthesis of certain amphiphilic molecules to incorporate specific functional groups.[135-141] This makes it very difficult to reproduce these systems and to scale them up for commercial applications.

In this study, we have used two commercially available amphiphilic molecules for obtaining multi-stimuli responsive vesicles: the cationic PDST and the anionic SDBS. PDST is a commonly used photoinitiator and a photoacid generator for cationic polymerization of epoxy or vinyl ether functional groups.[142] On the other hand, SDBS is a commonly used anionic surfactant used in detergents and cleaning products. The concept we have explored is that molecules with sulfur-containing groups will be responsive to oxidative and reductive conditions. Here, a sulfide group is present in the hydrophobic tail of the cationic photoinitiator. Initially, PDST and SDBS assemble into vesicles when mixed in a certain ratio. In the presence of ROS (via the addition of H_2O_2), the vesicles are transformed into micelles. The reason for this transformation is believed to be due to the sulfide in the PDST tail being converted into a sulfone or sulfoxide; thus, the tail is no longer hydrophobic and PDST loses its amphiphilicity. The system will transition from PDST/SDBS vesicles to much smaller micelles (Figure 5.1).

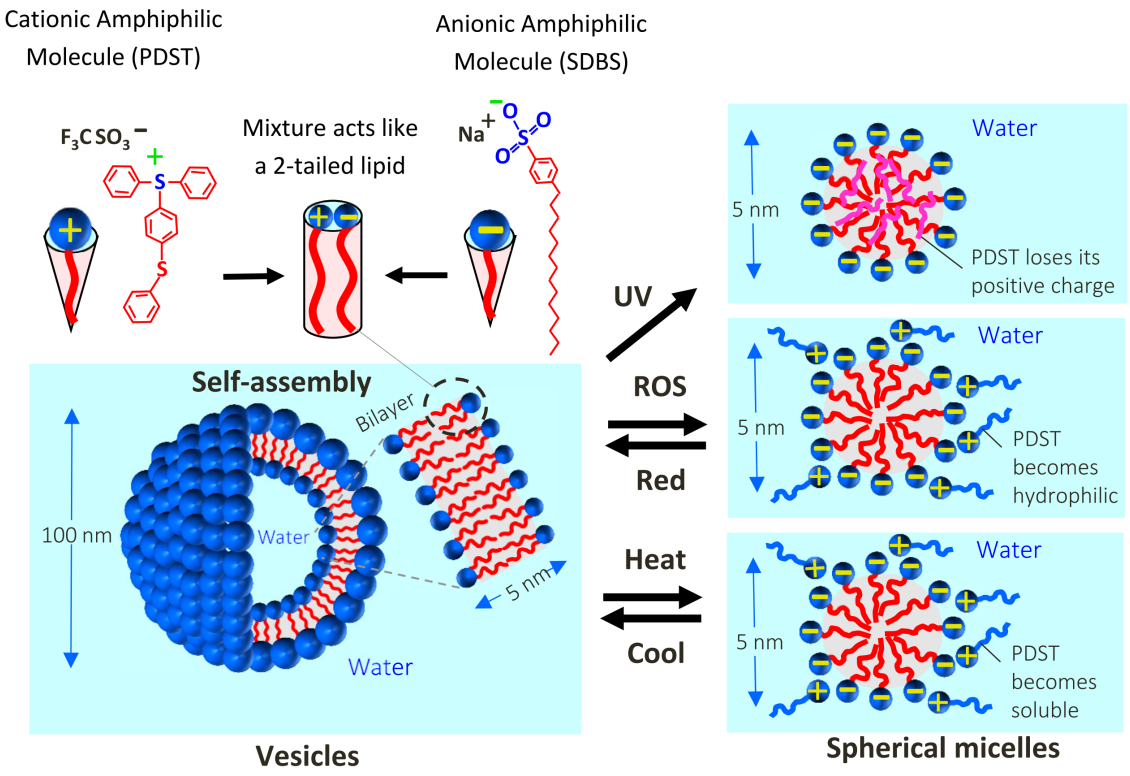

Figure 5.1. Multi-stimuli responsive catanionic vesicles. The vesicles are made by combining the cationic amphiphile PDST and the anionic surfactant SDBS. The mixture acts like a two-tailed lipid and self-assembles into "catanionic" vesicles with sizes ~ 100 nm. In the presence of UV, ROS, and temperature (heat), these vesicles are transformed into spherical micelles through different mechanisms. In the latter two cases, the micelles can be reverted to vesicles: by adding a reducing agent and by cooling, respectively.

Another interesting aspect about PDST is that it is also responsive to light and temperature, in addition to ROS. When UV light is irradiated, PDST loses its positive charge and is photolyzed into hydrophobic molecules.[143] Thus, UV will again induce a transition from PDST/SDBS vesicles to SDBS micelles, with the photolyzed PDST incorporated into the core of the micelles. Moreover, increasing the temperature of the system solubilizes the PDST in an aqueous buffer and therefore triggers the transformation of vesicles to micelles. Subsequently, we also show that the transformation from vesicles to micelles is both redox reversible and thermo-reversible (Figure 5.1). We also show the release of a model solute from these catanionic

vesicles before and after they are converted to micelles upon increasing the temperature. Moreover, as expected, *the burst release of a payload is achieved from micelles, whereas slow release is observed from vesicles*. Such stable, multi-responsive vesicles are desirable in many applications including drug delivery, and personal care.

5.2 Experimental Section

Materials. (4-Phenylthiophenyl)diphenylsulfonium triflate (PDST), hexadecyl trimethylammonium p-toluenesulfonate (CTAT), hydrogen peroxide (30 wt% in water), and hydrazine hydrate (50-60%) were purchased from Sigma-Aldrich. p-octyloxydiphenyliodonium hexafluoroantimonate (ODPI) was purchased from Gelest. Sodium dodecylbenzenesulfonate (SDBS) was obtained from TCI and glacial acetic acid was purchased from fisher chemical. Sodium phosphate, dibasic, anhydrous was used to prepare phosphate buffer solutions and was purchased from J.T. Baker. Ultrapure DI water was used in all experiments. Spectra-Por Float-A-Lyzer G2 dialysis inserts (MWCO = 100 kDa), and Sephadex G-50 (fine) were purchased from Sigma-Aldrich.

Sample Preparation. Stock solutions of SDBS were prepared first by mixing and dissolving known quantities in 50 mM Na_2HPO_4 buffer. For experiments involving the dye, 1mM Rhodamine 6G was added and mixed to this stock buffer solution containing SDBS. Next, PDST and SDBS catanionic vesicles/mixtures were prepared by adding known amounts of PDST powder to the above-prepared stock solution of SDBS at appropriate weight ratios with a total amphiphile concentration of 1wt%. These mixtures were stirred for 24 h using magnetic stirrers to ensure complete mixing and equilibration. Sample containing vials were stored in the dark at room temperature until further use.

Sample response to UV irradiation and turbidity measurements. The samples containing 1:9 and 2:8 weight ratio PDST-SDBS catanionic vesicles at 1% total concentration were subjected to UV light to study their transformation to micelles. 1.5 mL of samples were transferred into

polystyrene cuvettes and were then irradiated with an Oriel 200 W mercury arc UV lamp for a specific period under mild stirring. At any given time, the cuvettes containing the samples were taken and analyzed using a Cary 50 UV-Vis spectrometer. Absorbance or optical density was measured at a wavelength of 500 nm. The samples were then immediately placed back under the UV lamp until the samples completely became yellowish and clear. The measured optical density was then plotted as a function of UV irradiation time. Finally, they were returned to vials after the measurements for taking photos.

Sample response to H_2O_2 and Hydrazine hydrate. For studying the redox-response of 1:9 and 2:8 mixtures, known amounts of 30wt% H_2O_2 solution were first added to the previously prepared 1wt% 1:9 and 2:8 PDST-SDBS samples and mixed thoroughly using a vortex mixer. Glacial acetic acid at 1% concentration was then added to the samples for enhancing the rate of conversion of sulfide to sulfoxide groups.[115] After given amounts of H_2O_2 and 1% acetic acid was added, the samples were analyzed for turbidity or optical density using the Cary 50 UV-Vis spectrometer at a wavelength of 500 nm. For time-dependent ROS-response, known amounts of H_2O_2 were first added to the samples containing vesicles, followed by taking absorbance measurements as a function of time. Next, the reversibility of micelles to vesicles using hydrazine hydrate was analyzed. Briefly, 1:9 and 2:8 mixtures were diluted with 30% H_2O_2 to reach a final H_2O_2 concentration of 15 wt%. Then, glacial acetic acid was added at 1% and the samples were incubated for 2 days at room temperature to completely convert the vesicles to micelles. Subsequently, known amounts of hydrazine hydrate were added to the converted micelles and the solutions were mixed using a vortex mixer. The samples were then allowed to

equilibrate for 2 mins before taking absorbance measurements. The optical density was measured at 500 nm after given amounts of hydrazine were added.

Sample response to temperature. The temperature response of the 1:9 and 2:8 samples was recorded by heating the samples by placing them in a water bath, where the temperature was set using a Julabo water heater. Optical density measurements of the solutions were done using Cary 50 spectrometer equipped with a Peltier-controlled cell holder. Samples were placed in cuvettes and the optical density was measured at a wavelength of 500 nm as a function of temperature. After measurements were done, the samples were left at room temperature to study their thermo-reversible behavior.

Dynamic Light Scattering (DLS) and zeta potential measurements. The particle size distribution and zeta potential of PDST-SDBS vesicles were determined using a Malvern Zetasizer Nano ZS90 instrument. 1 mL of the samples were loaded into a polystyrene cuvette and a disposable folded capillary cell (DTS1070, Malvern) for size and zeta potential measurements respectively. The zeta cell and the cuvette containing the samples were then placed into the sample holder of the instrument and the sample was allowed to equilibrate for 120 seconds at 25 °C. Next, the sample properties were measured by the software three times. In the case of zeta potential, the average zeta potential value of the three measurements was reported.

Cryo-TEM. The sample was pipetted onto the surface of an ultra-flat holey carbon-film coated copper grid (400 mesh, Protochips). After removing the excess solution, the sample was frozen

quickly by plunging into liquid ethane using a Gatan Cryoplunge 3 system to form a vitrified specimen. The frozen specimen was then transferred to a cryo-TEM holder using a cryo-workstation (Gatan) filled with liquid nitrogen. Subsequently, the cryo-TEM holder with the specimen was inserted into the TEM column and the morphology of the specimen was examined with the JEM 2100 LaB6 TEM (JEOL) instrument at an accelerating voltage of 100 kV.

Dye release experiments. The 2:8 catanionic vesicles samples that were loaded with 1mM Rhodamine 6G cationic dye were the starting point for the dye release experiments. To remove free solute, the solution was purified using a size-exclusion chromatography column (SEC) packed with fine Sephadex G50 resin. However, there was negligible separation observed using the SEC column because most of the dye was strongly bound to the 2:8 anionic vesicles using electrostatic attractions. Therefore, this separation step is unnecessary and could be omitted. To monitor the release of the Rhodamine 6G dye from the vesicles at room temperature and at 60 °C, 1.5 mL samples were first injected into the Float-A-Lyzer G2 dialysis inserts (MWCO: 100 kDa), which were placed into a 200 mL beaker containing 150 mL of 50 mM phosphate buffer equilibrated to 25 °C and 60 °C respectively. Note that 100 kDa MWCO dialysis inserts were used to allow the dye bound to 2:8 micelles to easily leak out (due to their large size) into the external buffer solution. 1 mL samples were collected periodically from the external buffer solution and the absorbance was measured at the peak wavelength of 530 nm. After measurement, the samples were returned to the vials. These absorption measurements were then converted into concentrations using a standard curve for the Rhodamine 6G dye. Cumulative dye release (%) was then calculated by normalizing the dye concentration with that in the solution after equilibration for 2 days at 60 °C.

5.3 Results and Discussion

5.3.1 Phase Behavior of Catanionic Vesicles

The multi-stimuli responsive vesicles are made by simple mixing of the cationic amphiphile PDST and the anionic surfactant SDBS in a phosphate buffer. Note that PDST (Figure 5.1) has a hydrophobic tail with a thioether group. PDST is found to be insoluble in water, but when mixed with SDBS in a 50 mM phosphate buffer (pH 7.4), we obtain vesicles at certain weight ratios, as shown by Figure 5.2A. Here, we fix the total concentration at 1 wt% and vary the weight ratio of PDST:SDBS. A buffer solution is used instead of DI water to maintain a stable pH.[49] Between PDST:SDBS ratios of 1:9 to 5:5 respectively, the samples appear bluish, turbid, and homogeneous, indicating the presence of vesicles. This bluish appearance is due to a well-studied light scattering phenomenon called the Tyndall effect.[124] Dynamic light scattering (DLS) measurements (Figure 5.2B) reveal that the average hydrodynamic diameters D_h of the vesicles are 145, 120, and 145 nm for the 1:9, 2:8, and 3:7 samples. As the SDBS weight fraction increases, the polydispersity increases.

The zeta potentials for these mixtures are plotted in Figure 5.2C and are found to be strongly negative ($|\zeta| > 50$ mV). The net anionic charge is to be expected because the samples have far more SDBS than PDST molecules (e.g., in the 4:6 PDST:SDBS sample, the molar ratio is 1:2.2, i.e., there are twice as many SDBS molecules for every PDST). Also, as expected, as the PDST fraction increases, the zeta potential becomes less negative. However, samples at PDST-SDBS ratios of 6:4 and higher exhibit phase separation (a solid precipitate) or coacervation (Figure 5.2A). The phase separation indicates that too high a fraction of PDST (a relatively hydrophobic amphiphile) cannot be accommodated in the self-assemblies.

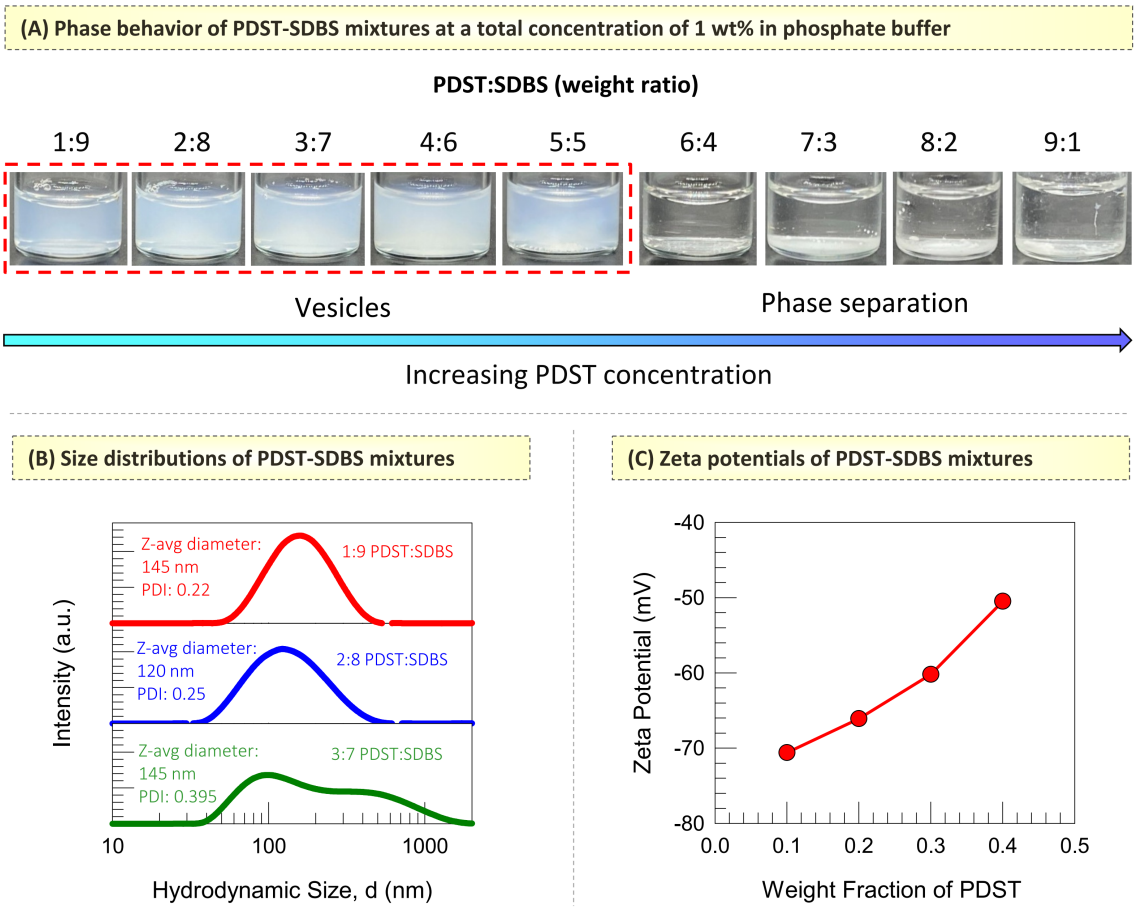

Figure 5.2. Phase-behavior of PDST-SDBS mixtures and characterization of their vesicles. (A) Phase behavior of 1% PDST-SDBS in phosphate buffer. Between 1:9 and 5:5, vesicles are formed (bluish samples). At higher PDST, phase separation occurs. (B) Size distributions from DLS of the 1:9, 2:8, and 3:7 PDST-SDBS vesicles. (C) Zeta potentials of PDST-SDBS mixtures with increasing weight fraction of PDST.

The PDST:SDBS vesicles were further analyzed for their stability. The 1:9 and 2:8 vesicle samples remain stable for over six months at room temperature (Figure 5.3). Both the average size and optical density (OD) are almost unchanged. Such long-term stability is commonly reported for catanionic vesicles. Images from cryo-transmission electron microscopy (cryo-TEM)[144,145] also confirm the presence of unilamellar vesicles in the samples and will be

shown later in Figure 5.7. The rest of our studies in this Chapter are mostly done with the 1:9 and 2:8 samples.

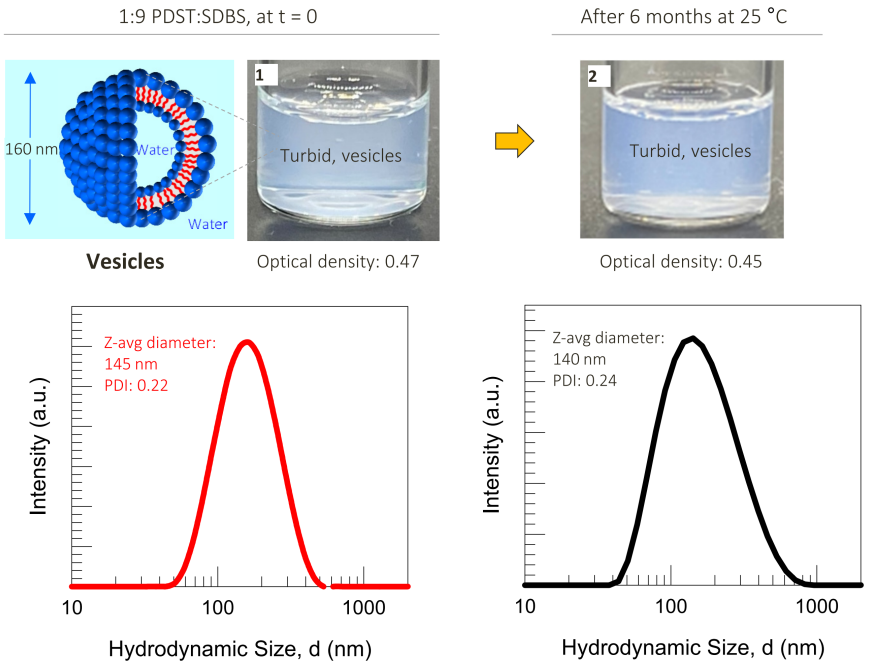

Figure 5.3. Long-term stability of PDST:SDBS vesicles. Photos are shown of a 1% mixture of 1:9 PDST:SDBS vesicles. The sample as prepared (t = 0) is turbid and bluish, with DLS revealing an average diameter of 145 nm and UV-Vis giving an optical density (OD) of 0.47 (Photo 1). After six months of storage at 25°C, the sample still appears the same, with virtually the same size and OD (Photo 2). This shows the long-term stability of these catanionic vesicles.

5.3.2 Light-Induced Vesicle to Micelle Transition

We now discuss the effects of different stimuli such as light, ROS, and temperature on these vesicles. First, we study UV light-irradiation (Figure 5.4). As shown in Photos A1 and B1, the 1:9 and 2:8 samples are initially bluish. The OD (measure of turbidity) at a wavelength of 500 nm is plotted as a function of UV irradiation time. Within 20 min, the OD of the 1:9 sample reaches a minimum and the sample becomes clear (Photo A2). The 2:8 sample also gradually

decreases in OD (over 2 h) and becomes clear. This loss in turbidity points to a structural transition from vesicles to much smaller structures, most likely micelles.[49,57,124] DLS experiments on these clear samples did not provide a clear estimate of micellar size, likely due to the low intensity of scattered light. Generally, spherical micelles are expected to be around 5 nm in diameter.

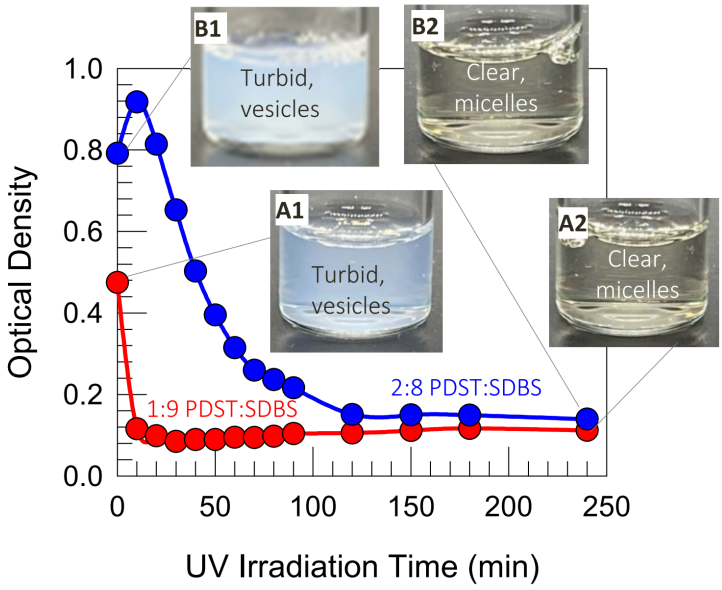

Figure 5.4. Light-induced transformation of vesicles to micelles detected by turbidity measurements. Optical density (OD) at 500 nm is plotted for 1% mixtures of 1:9 and 2:8 PDST:SDBS vesicles as a function of the UV-irradiation time. Initially, both samples are bluish, indicating vesicles (Photos A1 and B1). After 250 min, the samples are both clear, indicating conversion to small micelles (Photos A2 and B2).

The mechanism behind the above UV-induced vesicle-to-micelle transition can be explained based on the photochemistry of PDST, which is a triaryl sulfonium salt. Figure 5.5A shows that UV induces photolysis of PDST into hydrophobic byproducts and an acid.[143,146] This chemical change drastically alters the geometry of PDST. It goes from being a cationic amphiphile (blue head, red hydrophobic tail) to uncharged hydrophobic byproducts (pink tails).

In turn, vesicles can no longer exist and the system transitions to micelles.[49,57,124] Note that the generation of acid does not alter the pH of the samples because they were prepared in phosphate buffer; thus, the pH remains constant at 7.4 before and after the UV irradiation.

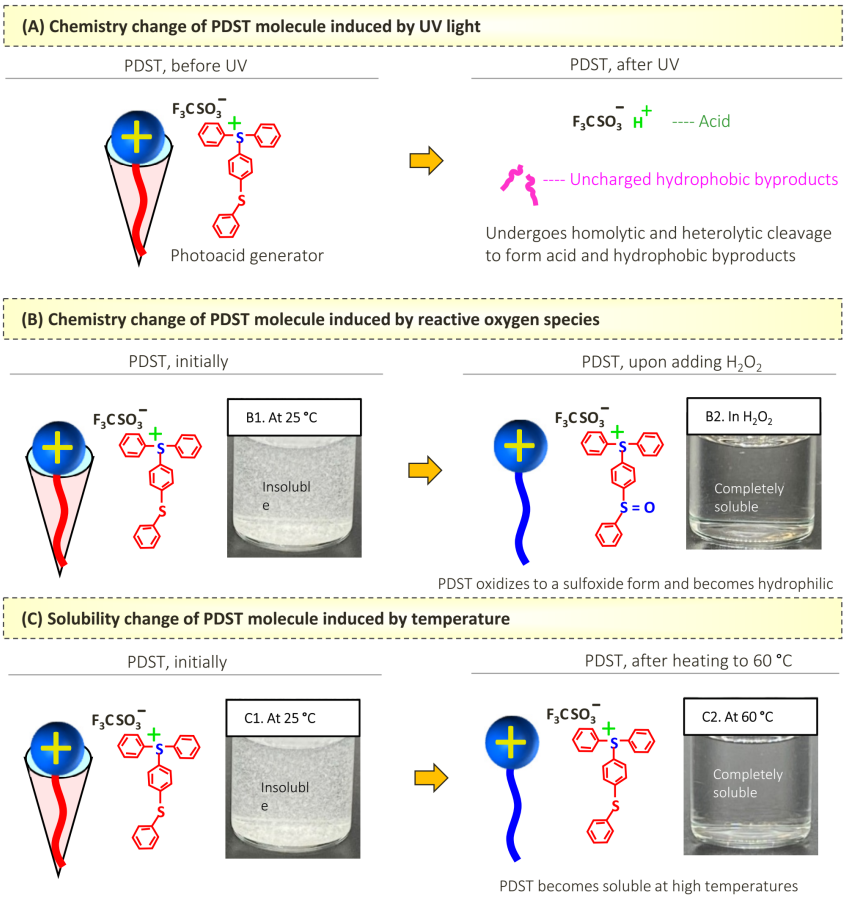

Figure 5.5. Effects of UV, ROS, and temperature on the PDST molecule and the resulting change in molecular geometry. (A) UV irradiation photolyzes PDST to acid and hydrophobic byproducts (pink tails). (B) ROS (H_2O_2) convert PDST from insoluble (Photo B1) to soluble (Photo B2) in buffer at room temperature. This is because the hydrophobic thioethers in PDST are oxidized to hydrophilic sulfoxides (tail shown to change from red to blue). (C) Temperature (heating) induces PDST to convert from insoluble (Photo C1) in buffer at room temperature to soluble (Photo C2) at 60°C. This is again because the tail of PDST changes from hydrophobic to hydrophilic (red to blue).

The concept of critical packing parameter (CPP) is useful in understanding the self-assembly transformation. CPP is the ratio of the average area of the tail region (a_{tail}) to the

effective area of the head group (a_{hg}).[45,118,119] Note that a_{hg} includes contributions from electrostatic and/or steric repulsions. A CPP ~ 1/3 implies the formation of spherical micelles; a CPP between 1/3 and ½ implies cylindrical micelles; and a CPP between ½ and 1 results in vesicles or bilayers. For instance, SDBS alone forms spherical micelles because it is negatively charged and therefore has a large a_{hg} which makes SDBS cone-shaped and thus a CPP ~ 1/3. When PDST is added to SDBS, a_{hg} decreases due to the formation of ion pairs, while a_{tail} also increases due to the PDST-SDBS pair acting like a two-tailed lipid (Figure 5.1). Consequently, the CPP increases to ~ 1, favoring vesicles. When PDST is photolyzed, the loss of charge will eliminate the ion-pairing. Thus, the CPP will simply become that of SDBS, i.e., ~ 1/3, and this will favor spherical micelles (Figure 5.1). The uncharged hydrophobic by-products of PDST photolysis are likely to be embedded in the core of the SDBS micelles.

5.3.3 ROS-Induced Vesicle to Micelle Transition

Next, we proceeded to study the effect of reactive oxygen species (ROS) on the vesicles. PDST has a thioether group which is known to be oxidized to hydrophilic sulfone or sulfoxide by ROS such as hydrogen peroxide (H_2O_2),[51,52,55,58,132,133] as shown by Figure 5.5B. Figure 5.6A shows photos of 1:9 PDST:SDBS vesicles with increasing concentration of H_2O_2 at room temperature (the images were taken immediately after H_2O_2 addition). The turbidity decreases as H_2O_2 is increased, and above 6% H_2O_2 the sample is completely transparent, indicating the transformation of vesicles to smaller micelles.

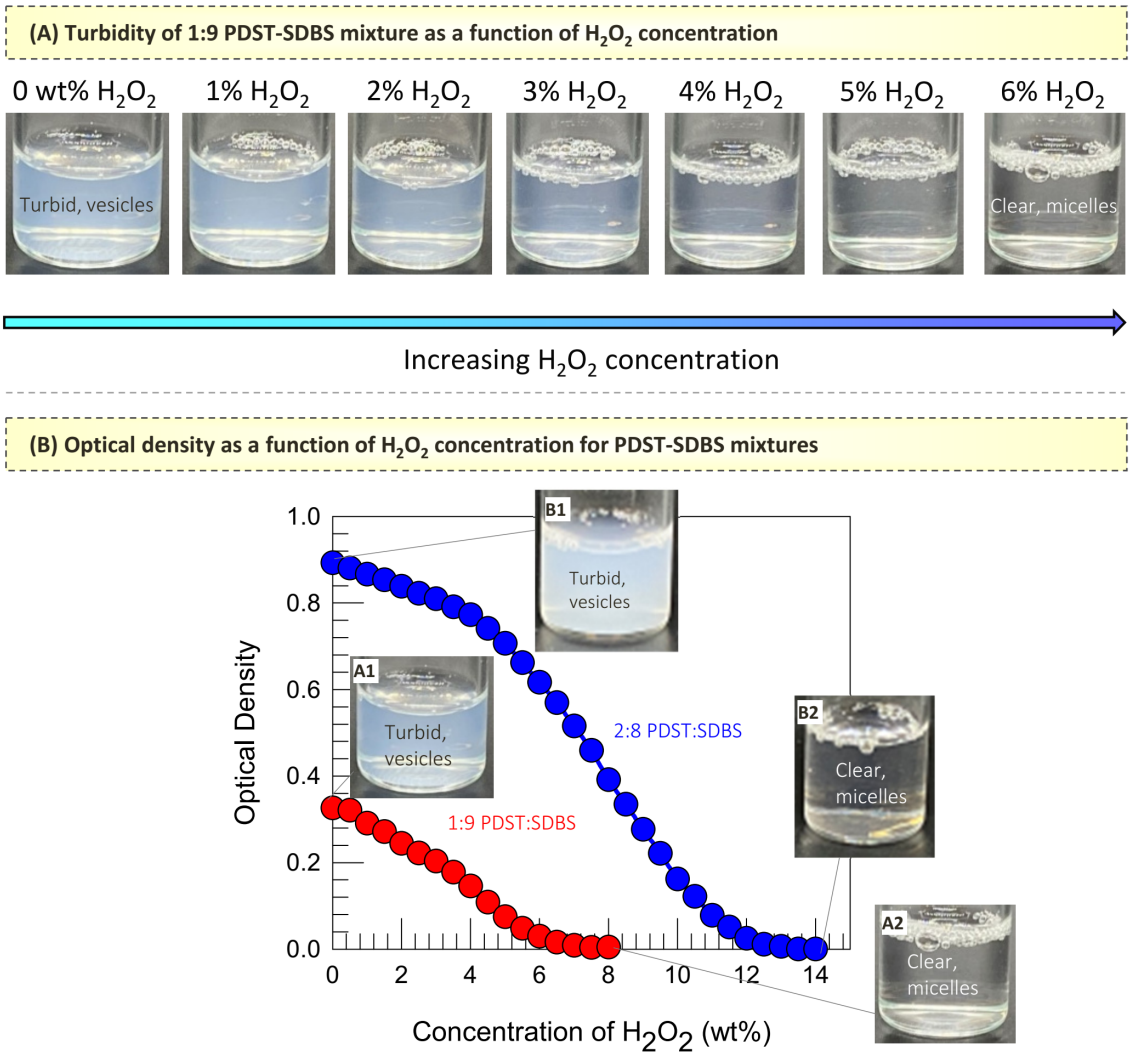

Figure 5.6. ROS-induced transformation of vesicles to micelles detected by turbidity measurements. (A) Photos showing the turbidity of 1% mixtures of 1:9 PDST-SDBS vesicles with increasing H_2O_2 concentration. The sample turns from turbid to clear, indicating the transformation of vesicles to micelles. (B) Optical density at a wavelength of 500 nm as a function of H_2O_2 concentration for 1:9 and 2:8 PDST:SDBS mixtures. As the H_2O_2 increases, the turbidity decreases to zero for both samples. Photos A1 and B1 show the turbid vesicle samples, while Photos A2 and B2 show the clear micellar solutions (with 8 and 14% added H_2O_2, respectively).

Figure 5.6B plots the OD of the 1:9 and 2:8 samples as a function of H_2O_2 added. The OD decreases with H_2O_2 for both samples in a sigmoidal decay. The 1:9 sample becomes transparent (OD ~ 0) at 6% H_2O_2 and above (see Photos A1 vs. A2) while the 2:8 sample turns

transparent at 14% H_2O_2 and above (see Photos B1 vs. B2). The optical changes signify a vesicle-to-micelle transition induced by ROS. It is worth mentioning that the decrease in turbidity is instantaneous at high H_2O_2, indicating that when there are numerous ROS, the transformation from large vesicles to small micelles occurs very fast. In the literature, most studies that have reported an ROS-response from thioether groups require incubation with H_2O_2 for long periods (typically hours).[51,52,55,58,132,133]

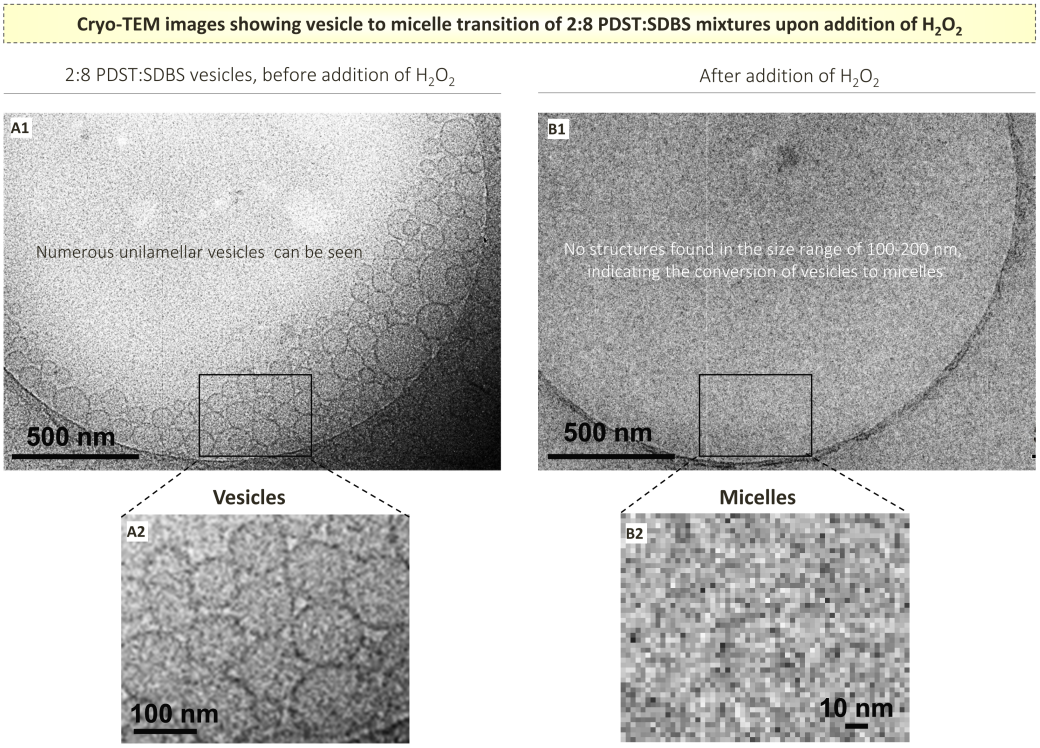

Figure 5.7. Cryo-TEM images showing the vesicle to micelle transition induced by ROS. The images are of 1% 2:8 PDST:SDBS before and after the addition of 15% H_2O_2. Photos A1 and A2 show unilamellar vesicles with sizes of 100-200 nm. Photo B1 shows the absence of structures in the 100-200 nm range. Photo B2 is a magnified image of Photo B1 with dark spots possibly indicating small (~ 5 nm) micelles.

We used cryo-TEM to conclusively prove the transformation of vesicles to micelles. Figure 5.7 shows cryo-TEM micrographs of the 2:8 PDST:SDBS sample, before and after

addition of 15% H_2O_2. In the initial bluish sample, numerous unilamellar vesicles are seen. Together with the DLS and turbidity data, this confirms that vesicles exist in these catanionic mixtures. After the vesicles are exposed to H_2O_2, the sample becomes clear and photos B1 and B2 show no structures in the size range of 100 nm and above. When this image is magnified further, black spots seem to be present, which may indicate spherical micelles (~ 5 nm in size). It should be noted that spherical micelles are very hard to image by cryo-TEM.[49] Overall, cryo-TEM provides clear support for the presence of vesicles, and it is also clear that these vesicles are transformed into much smaller structures, which have to be micelles.

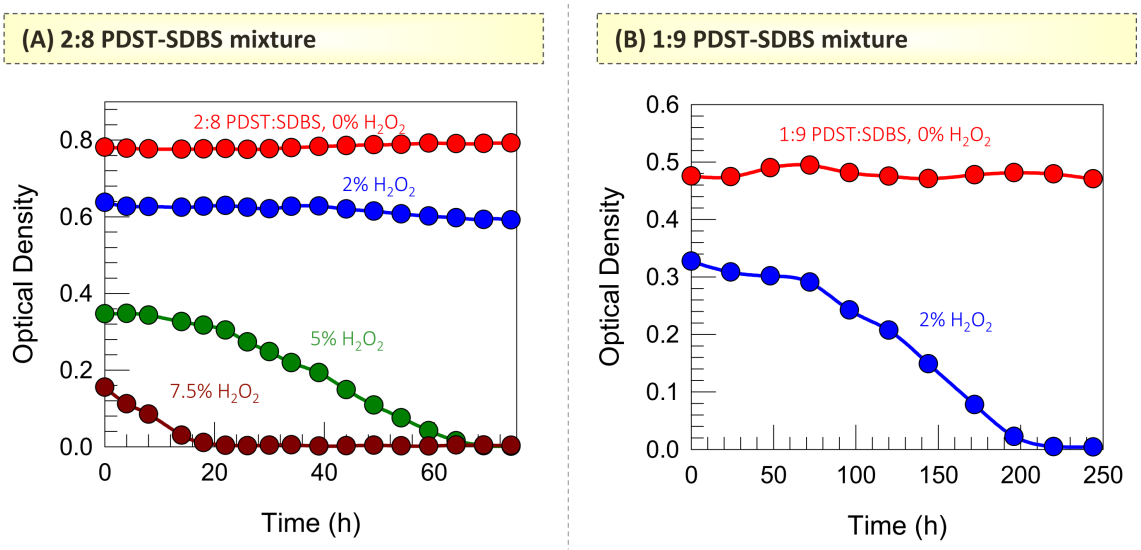

Figure 5.8. Kinetics of vesicle to micelle transitions. (A) OD of a 2:8 PDST:SDBS mixture vs. time after addition of 0, 2, 5, and 7.5% H_2O_2. (B) OD of a 1:9 PDST:SDBS mixture vs. time after addition of 0, and 2% H_2O_2.

We then studied the kinetics of the H_2O_2 induced vesicle to micelle transitions at various H_2O_2 concentrations. In all cases, the initial (t = 0) OD reading is much lower after the addition of H_2O_2 and the higher the H_2O_2, the lower the initial OD. Thereafter, in the case of the 2:8 sample (Figure 5.8A), there is hardly any change in turbidity with time at 2% H_2O_2, but the OD

drops to zero for 5% H_2O_2 over 70 h and at 7.5% H_2O_2 over 20 h. A similar trend is also observed for the 1:9 sample (Figure 5.8B). In this case, in the presence of 2% H_2O_2, the OD drops to zero over 240 h. These results indicate that the transformation from vesicles to micelles can be achieved at low H_2O_2 concentrations and can be tuned to occur over a long period of time. This feature of the vesicles may be useful in time-dependent drug-release applications.

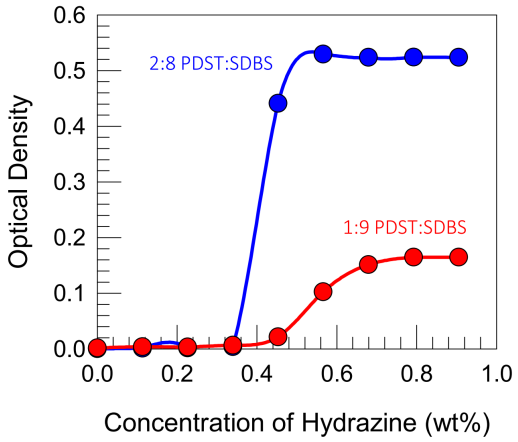

Figure 5.9. Reverse transition from micelles to vesicles by adding a reducing agent. OD of 1:9 and 2:8 PDST:SDBS micelles (prepared by adding 15% H_2O_2 and incubating for 2 days) after adding different concentrations of hydrazine, a reducing agent. The increase in OD at high hydrazine reflects the re-formation of vesicles.

Considering the above results, the following mechanism seems to be at play for the ROS-responsive behavior of the vesicles. As reported in the literature, and as shown in Figure 5.5B, ROS will transform the hydrophobic thioether in the tail to hydrophilic sulfoxide or sulfone groups. This will make the PDST molecule more soluble in water and also less amphiphilic. Initially, the PDST molecule is insoluble by itself in the aqueous buffer at room temperature (Photo B1, Figure 5.5B). However, after exposure to ROS, the PDST completely dissolves in the buffer (Photo B2). In terms of CPP and self-assembly, the oxidized PDST cannot stay in the

bilayer any more as it is hydrophilic and therefore it will exit the bilayer. Thus, the only amphiphile left is SDBS, with a CPP ~ 1/3 and it will thus form spherical micelles. This can explain the vesicle to micelle transition.

Next, we tested whether the transformation of vesicles to micelles could be reversed by a reducing agent such as hydrazine. Hydrazine has been studied previously for its ability to reduce sulfoxide or selenoxide groups into sulfide or selenide groups.[147] For this experiment, 1:9 and 2:8 PDST:SDBS micelles are first made by adding 15% H_2O_2 to the vesicle samples and allowing the system to equilibrate for a couple of days. This ensures complete conversion of thioether to sulfoxide groups. Figure 5.9 shows that the initial OD is almost zero indicating clear micellar solutions. Upon adding hydrazine, the OD increases along a sigmoidal curve until it reaches a plateau. This plateau indicates that all the micelles have been converted to vesicles again, and the samples appear bluish. DLS also confirms the presence of vesicles with average diameters of 180 nm and 120 nm for the 1:9 and 2:8 samples, respectively. These data show that the micelles can indeed be reverted to vesicles by adding reducing agents.

5.3.4 Temperature-Induced Vesicle to Micelle Transition

Next, we report the effect of temperature on the 1:9 and 2:8 PDST:SDBS samples, both of which contain vesicles at room temperature (Figure 5.2). Upon heating, the initially bluish samples (Photos a1 and b1, Figure 5.10A) transform into clear solutions at 40°C and 60°C (Photos a2 and b2). Moreover, when cooled back to room temperature, the samples again become bluish (Photos a3 and b3). This indicates that the vesicle to micelle transition is a thermo-reversible process. Systematic OD studies as a function of temperature are reported in

Figure 5.10B. The OD drops gradually and falls to zero by about 40°C and 60 °C respectively for the 1:9 and 2:8 samples.

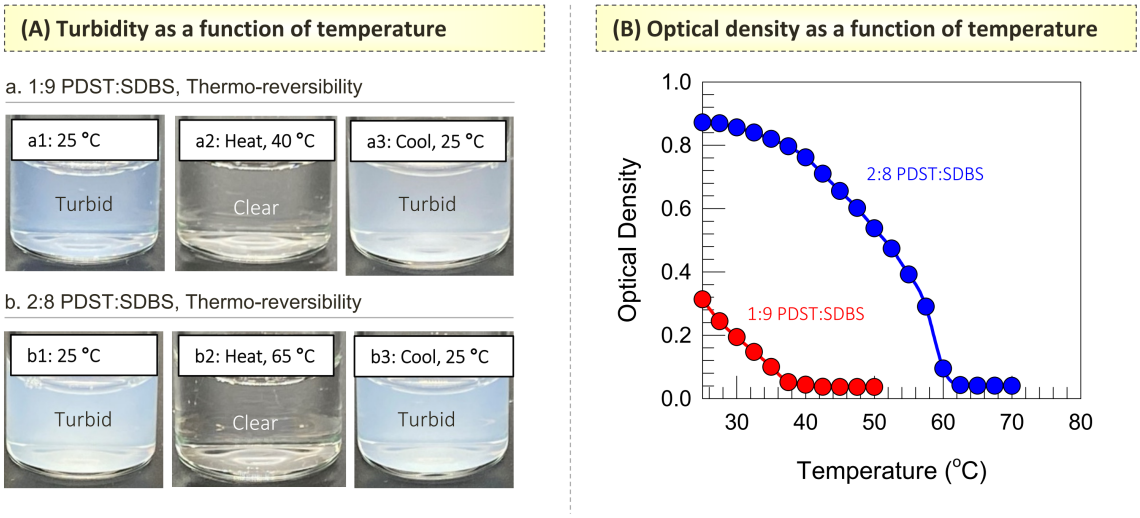

Figure 5.10. Thermo-reversible transformation of vesicles and micelles detected by turbidity measurements. (A) Photos showing the turbidity of 1:9 and 2:8 PDST:SDBS samples at various temperatures. (B) OD vs. temperature for these samples.

The mechanism for these changes likely involves the solubility of PDST as a function of temperature. Figure 5.5C shows that PDST is insoluble in buffer at room temperature, but dissolves upon heating to 60°C. This suggests that PDST becomes hydrophilic at high temperatures and if it is not amphiphilic anymore, it cannot remain in the bilayer. Thus, the only amphiphile left will be SDBS, with a CPP ~ 1/3, and it will hence form spherical micelles, just as in the case of ROS as a stimulus. This can explain the vesicle to micelle transition upon heating and its reverse upon cooling.

5.3.5 Dye Release Studies

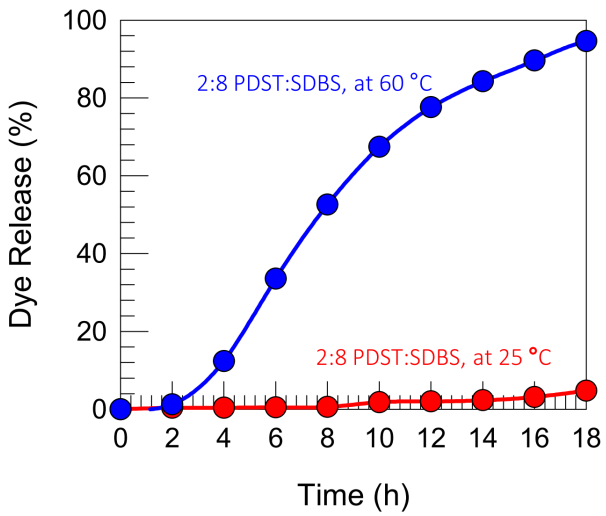

Figure 5.11. Solute release from PDST-SDBS mixtures at different temperatures. Cumulative dye release (% of the total) as a function of time from dialysis bags containing 1% of 2:8 PDST-SDBS mixtures at 25°C and 60°C. Only 5% of the dye gets released over a period of 18 h at 25°C. In contrast, 95% of the dye gets released over the same period at 60 °C.

Finally, the utility of vesicle-to-micelle transitions is shown by release studies. A well-studied cationic dye, Rhodamine 6G, is used as a model solute.[148] 1 mM of this dye was added to an SDBS-containing buffer solution, followed by the addition of PDST to form 2:8 PDST:SDBS vesicles. The dye will be mainly sequestered on the anionic surfaces of the vesicles.[149,150] The vesicles are placed in dialysis bags with a 100 kDa cutoff. We then exploit the fact that the vesicles will be responsive to temperature – thus we place one bag at 25°C (when the vesicles will remain as vesicles) and the other at 60°C (when the vesicles will be converted to micelles). Figure 5.11 plots the cumulative dye release (as a percentage of the total) as a function of time at the two temperatures. At 25°C, only 5% of the dye is released from the dialysis bag over 18 h. This slow release is likely because the dye remains bound to the vesicles, which are too large (~

100 nm) to pass through the dialysis membrane. At 60°C, 95% of the dye is released from the dialysis bag over the same 18 h period. This is because the vesicles are converted to micelles at 60°C. The micelles being only about 5 nm (~ 24 kDa) leak out of the dialysis membrane. This result shows that vesicles can keep solutes *encapsulated for long periods at room temperature, followed by rapid release of solutes by increasing the temperature*. Such a finding could be of importance in pharmaceutical applications, and it is one way to exploit a vesicle-to-micelle transition.

5.4 Conclusions

In this chapter, we have successfully demonstrated a multi-stimuli responsive catanionic vesicles system, prepared by simply mixing two commercially available and low-cost oppositely charged amphiphilic molecules, PDST and SDBS. The obtained vesicles exhibited UV light, ROS, and temperature responsiveness. PDST is the responsive cationic amphiphilic molecule here and is a commonly used photoinitiator and a photoacid generator. In the presence of UV light, PDST loses its positive charge and becomes hydrophobic. Another striking feature is that PDST contains a thioether group in its hydrophobic tail. Notably, the presence of ROS such as H_2O_2 induces the conversion of the thioether group to sulfoxide or sulfone group in the PDST molecule and thereby makes it hydrophilic. Likewise, the presence of the thioether group also increases its solubility at high temperatures. Overall, the chemistry changes or increase in solubility of PDST in the presence of external triggers such as light, ROS, and temperature, results in a decrease in the critical packing parameter and complete disruption of vesicles into smaller micelles. These transformations were observed using cryo-TEM and turbidity measurements. Furthermore, we also show that the transformation from catanionic vesicles to micelles is both redox reversible and thermo-reversible. Most importantly, the dye release experiments have demonstrated that cationic solutes can be easily encapsulated and sequestered by these negatively charged SDBS rich vesicles, and the resulting solute-loaded vesicles exhibited superior *temperature-responsive burst release of payloads* by disrupting the vesicle membranes into smaller micelles. Such multi-stimuli responsive vesicles provide unique opportunities in the field of targeted drug delivery.

Chapter 6
Recommendations and Future Work

6.1 Project Summary

In this dissertation, we have created *'smart' skins or membranes around soft aqueous structures such as hydrogels and vesicles.* These novel designs are inspired by soft aqueous structures with *'smart' membranes or skins found in nature*, including cells, organelles, fruits and vegetables, and human skin. All the structures synthesized in this work are synthesized by simple synthesis techniques using inexpensive, commercially available materials, making them easy to scale-up for industrial applications. We are successful in achieving some of the idealized release profiles from these structures, including *a hermetic seal followed by burst release*, and *a perfect cyclical on-off release* of various hydrophilic small molecule solutes. Our studies contribute towards pushing the frontiers in the fields of hydrogels and vesicles to achieve idealized release profiles that could not be realized thus far. Such materials have the potential to be used in various industrial formulations for encapsulating small-molecule solutes such as drugs, agrochemicals, flavor-ingredients, or cosmetic agents.

In Chapter 3, we presented a simple technique which allows any hydrogel of arbitrary composition and geometry to be encased by a thin, transparent 'skin'. Using our technique, we showed that a thin polymeric layer (~ 10 to 200 μm in thickness) grows outward from the core, and the entire process can be completed in a few minutes. We also demonstrated that the presence of the skin completely prevented the solutes in the gel core from leaking out into the external solution. Moreover, *the solutes can be released in a burst-release fashion upon peeling*

off the skin or by placing in a polar organic solvent such as ethanol. Thus, the *idealized release profile of hermetic seal followed by burst release* was achieved using the protective skin-covered hydrogel system. Furthermore, we showed that the properties of the skin including its thickness and its mechanical properties are all tunable. This ability to grow a skin readily around any given hydrogel is likely to prove useful in numerous applications, such as in controlled release of various hydrophilic small molecule solutes.

In Chapter 4, we employed the inside-out technique to form '*smart' skins equipped with redox-responsive properties around hydrogels*. Like the protective skins created in chapter 3, the initial skin achieved *hermetic seal of solutes*. Additionally, we showed that in the presence of oxidants, the skin became hydrophilic, and thereby 'turned on' the release of solutes out of the gel. We also showed that the release rate of various solutes can be easily controlled by changing the parameters such as skin thickness, solute, and oxidant concentrations. We then demonstrated that the solute release can be 'turned off' at any time by adding a reducing agent by reversing the chemistry of the skin to its hydrophobic state. Thus, using our smart skin, *the idealized release profile of "on-off" release of solutes out of a gel was achieved*. We also showed that the technique used for synthesizing smart skins around hydrogels can be extended to *create thin flat smart membranes*. These membranes can be employed as rate controlling barriers for achieving controlled release of small molecule solutes. Moreover, such stimuli-responsive membranes are envisaged to play paramount roles in several applications such as separations, water treatment, and drug delivery.

In Chapter 5, we synthesized catanionic vesicles that are formed by the self-assembly of two oppositely charged single-tail amphiphilic molecules. Especially, we developed low-cost, simple, *multi-stimuli responsive catanionic vesicle containers* made from commercially available amphiphilic molecules: the cationic (4-phenylthiophenyl)diphenylsulfonium triflate (PDST), and the anionic sodium dodecylbenzene sulfonate (SDBS). The PDST molecule is a light, temperature, and ROS responsive amphiphilic molecule, that is a commonly used photoinitiator and a photo-acid generator. We showed that in the presence of these stimuli (light, temperature, and ROS), these vesicles were successfully transformed into smaller micelles due to the changes in the critical packing parameter (CPP). Utilizing this transformation, we demonstrated that *negligible release of positively charged solutes was obtained at ambient conditions* due to strong electrostatic interactions with the negatively charged vesicles, whereas, when heated to high temperatures, *burst release of the solutes was achieved* due to the conversion to micelles. Thus, the *idealized release profile of zero release (negligible) followed by burst release* was achieved using these catanionic vesicles.

6.2 Recommendations for Future Work

6.2.1 Zero-order release from skin-covered hydrogels

In Chapters 3 and 4, we demonstrate that skin-covered hydrogels can be used to achieve idealized release profiles such as hermetic seal followed by burst release and cyclical on-off release of solutes. For majority of the controlled drug delivery applications, in addition to the cyclical on-off release of solutes, *zero order release of encapsulated therapeutics over extended periods* is the overarching goal. However, hydrogel-mediated zero-order release has not been achieved so far.[151] Therefore, we propose to further study the utility of skin-covered hydrogels for achieving zero-order release of various hydrophilic solutes.

In most drug delivery systems, the drugs are released in a first-order manner leading to a rapid increase in systemic drug concentrations. As a result, undesirable side effects are often observed and moreover, increased dosing frequencies are needed to achieve the necessary therapeutic effect. Zero-order drug delivery systems have the potential to overcome these issues by releasing the drugs at a constant rate; thereby maintaining drug concentrations within the therapeutic window for an extended period. Figure 6.1 shows the ideal zero-order cumulative release profile as well as the ideal release rate profile. Till date, researchers have explored several ways to accomplish zero-order release,[151] however, majority of them are complex, time-consuming, and difficult to manufacture. Here, we propose to design a simple skin-covered hydrogel system that provides zero-order release of various water-soluble solutes. Our synthesis technique involves inside-out strategy to synthesize skin-covered hydrogels. For a zero-order release to occur, the skin is made mostly from a hydrophobic monomer mixed with small amounts of a hydrophilic monomer. We believe that addition of hydrophilic monomer will

generates hydrophilic domains in the skin that will improve the skin's permeability to solutes slightly so as to achieve a zero-order response. Additionally, we also think that it is possible to adjust the zero-order release rate by tuning the thickness of the skin and the concentration of the hydrophilic monomer. We believe that the ability to predictively tune the zero-order release rate of various hydrophilic solutes from skin-covered hydrogels could be of great importance in controlled release drug delivery applications.

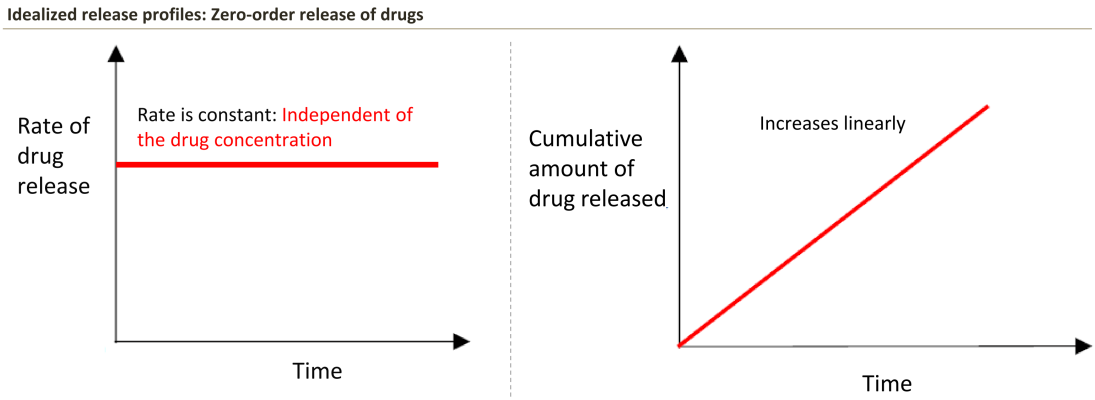

Figure 6.1. Zero-order release from skin-covered hydrogels. Idealized zero-order release profiles showing the release rate and cumulative amount of drug released as functions of time.

6.2.2 Skin-covered hydrogels at microscale

For fully unleashing the potential of skin-covered hydrogels, especially for drug delivery applications, it is worthy to extend the technique to form skins around micrometer-sized hydrogels.[33] In this regard, a simple, high throughput microfluidic technique such as the stop-flow lithography (SFL) could be potentially used.[152] SFL technique involves forming stationary layers of monomer inside a PDMS microfluidic channel for brief periods of time before being flushed out. Figure 6.2 shows the typical setup of a SFL consisting of a computer-controlled flow setup with a 3-way valve that allows for stop and flow modes and a UV source that provides

specified exposure times. The flow is first briefly stopped and then the UV source is irradiated to achieve polymerization of the monomer droplets. Next, the UV irradiation is turned off (by closing the shutter), while the flow is resumed, and the polymerized particles are flushed out. These steps are repeated in a cyclic manner to continuously produce polymer particles.

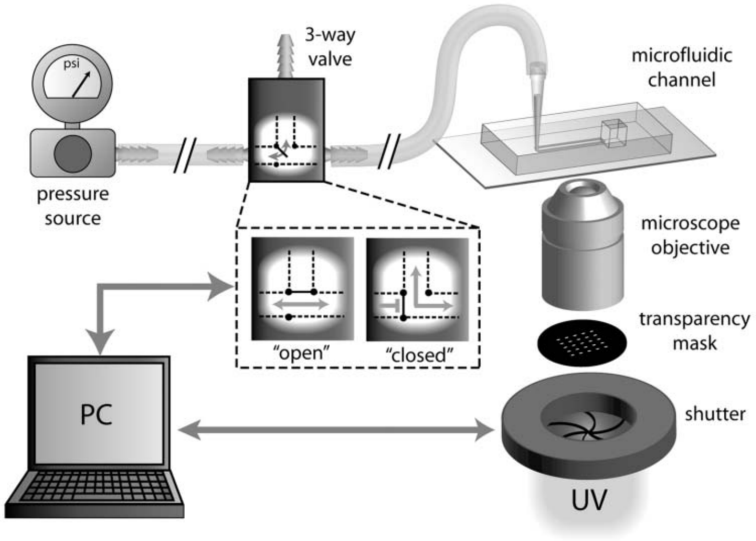

Figure 6.2. Stop-flow lithography setup. Schematic showing the stop-flow lithography setup with computer-controlled stop and flow modes achieved using a 3-way value along with a computer-controlled UV irradiation mechanism. Adapted from Dendukuri et al.[152]

We propose that by combining stop-flow lithography technique for forming polymeric particles with co-axial microfluidic flow of water and monomer phases, hydrogels with uniform polymer skins can be formed in a high-throughput fashion. Briefly, pre-polymer hydrogel solution loaded with initiator molecules will be flowed through the inner capillary while the monomer solution will flow through the outer capillary in the same direction. When both the solutions are contacted at low rates, individual monodisperse droplets of water in oil are produced at the tip of the inner capillary orifice.[153] These upstream droplets in monomer solution will then be stopped briefly using the SFL technique and will be subjected to UV irradiation to

form hydrogels with uniform polymer skins. Next, the flow will be resumed to push out to microscale skin-covered hydrogels into a reservoir solution. In this way, unform micrometer-sized skin-covered hydrogels can be produced in a high-throughput fashion. By using biocompatible and biodegradable chemistries of the hydrogels and the skins, these capsules can have wide range of applications in controlled drug delivery applications.

6.2.3 Smart-skins with different chemistries

In chapter 4, we can observe that slightly high concentrations of H_2O_2 and Vitamin C are needed to alter the chemistry of the smart skins covering hydrogels. So, we propose to further examine different oxidizing and reducing agents in addition to the above two. Additionally, we also plan to try different chemistries of monomers that can give rise to such responsive skins, including those containing disulfide groups or groups with selenium (Se) or tellurium (Te).[51] Many such monomers are known to have a faster response to oxidizing agents. Incidentally, selenium is an element with biological relevance as it plays an important role in maintaining the body's response to several diseases.[57] These studies will be useful in achieving smart skins with the ability to tightly control the rates of release of encapsulated solutes. Moreover, these chemistries can be even extended to synthesize flat thin polymer membranes and may prove useful in several applications dealing with smart polymer membranes.

6.2.4. Radiation-responsive smart vesicle membranes

Using the multi-stimuli responsive vesicles fabricated in the chapter 5, we propose to further investigate their ability as radiation-responsive materials. Radiation therapy (RT) and chemotherapy are currently the main modes of treating cancer. In RT, high-energy radiation

(such as X-rays) is delivered locally to the tumor, sparing the surrounding healthy tissue. Chemotherapy, in contrast, refers to the systemic administration of tumor-killing chemicals in a non-specific manner. RT is often the first line of treatment against a variety of cancers. Despite many advances in RT and chemotherapy, however, current cancer treatment remains rather ineffective. For example, Non-Small Cell Lung Cancer (NSCLC) is the most commonly diagnosed cancer in the United States with more than 220,000 new diagnoses expected over the coming year. The overall survival rate of patients from NSCLC, five years past diagnosis, is only 15% (lung cancer fact sheet, American lung association). Using the ROS-responsive vesicles, we propose a route to dramatically improve the efficacy of RT. Our idea is to use the same high-energy radiation to locally deliver therapeutic agents to the tumor cells. In effect, we propose to supplement RT with local chemotherapy in one step. If this concept is successful, it has the potential to make cancer treatment simpler and more effective.

In conventional RT, the damage to cancer cells is caused by generation of reactive oxygen species (ROS) such as singlet oxygens ($^1O_2$), which arise when X-rays hit the fluid (water) in tumor cells.[131,154] These ROS are believed to damage DNA, ultimately leading to cell death. We propose to exploit our ROS-responsive cationic vesicles to demonstrate radiation induced transformation to micelles. These vesicles will infiltrate the tumor, and under RT, they will be disrupted, thus releasing their payload into the tumor due to their conversion into micelles.

We will first subject the PDST-SDBS catanionic vesicles at various concentrations to X-rays at dose rates ranging from 100 to 1000 MU/min, with the total dose ranging from 0 to 10

Gy. The effects of radiation on vesicle size and permeability will be studied. The kinetics of solute release from the vesicles core will be assayed with a model dye (calcein) as well as with carboplatin. We will work with A549 adenocarcinoma cells, and these will be infiltrated with carboplatin-bearing vesicles, then irradiated with X-rays. The working hypothesis here is that the ROS will disrupt the vesicles, thereby releasing carboplatin into the cells. Control experiments will be done with radiation alone or free carboplatin alone. Over a range of radiation doses, we expect the fraction of cells killed by radiation alone to be low, whereas a much greater fraction of cells will be killed by the carboplatin released into the cells from the disrupted liposomes. Overall, any future studies on release of drugs from the catanionic vesicles using high energy radiation would be a very interesting work.

References

[1] Hoare, T. R.; Kohane, D. S. "Hydrogels in drug delivery: Progress and challenges." *Polymer* **2008**, *49*, 1993-2007.

[2] Shewan, H. M.; Stokes, J. R. "Review of techniques to manufacture micro-hydrogel particles for the food industry and their applications." *J. Food. Eng.* **2013**, *119*, 781-792.

[3] Wang, A. Z.; Langer, R.; Farokhzad, O. C. "Nanoparticle Delivery of Cancer Drugs." *Annu. Rev. Med.* **2012**, *63*, 185-198.

[4] Torchilin, V. P. "Recent advances with liposomes as pharmaceutical carriers." *Nat. Rev. Drug Discovery* **2005**, *4*, 145-160.

[5] Fathi, M.; Mozafari, M. R.; Mohebbi, M. "Nanoencapsulation of food ingredients using lipid based delivery systems." *Trends Food Sci. Technol.* **2012**, *23*, 13-27.

[6] Betz, G.; Aeppli, A.; Menshutina, N.; Leuenberger, H. "In vivo comparison of various liposome formulations for cosmetic application." *Int. J. Pharm.* **2005**, *296*, 44-54.

[7] Reza Mozafari, M.; Johnson, C.; Hatziantoniou, S.; Demetzos, C. "Nanoliposomes and Their Applications in Food Nanotechnology." *J. Liposome Res.* **2008**, *18*, 309-327.

[8] Brazel, C. S.; Peppas, N. A. "Pulsatile local delivery of thrombolytic and antithrombotic agents using poly(N-isopropylacrylamide-co-methacrylic acid) hydrogels." *J. Control. Release* **1996**, *39*, 57-64.

[9] Dinarvand, R.; D'Emanuele, A. "The use of thermoresponsive hydrogels for on-off release of molecules." *J. Control. Release* **1995**, *36*, 221-227.

[10] Zarket, B. C.; Raghavan, S. R. "Onion-like multilayered polymer capsules synthesized by a bioinspired inside-out technique." *Nat. Commun.* **2017**, *8*, 193.

[11] Goertz, J. P.; DeMella, K. C.; Thompson, B. R.; White, I. M.; Raghavan, S. R. "Responsive capsules that enable hermetic encapsulation of contents and their thermally triggered burst-release." *Mater. Horiz.* **2019**, *6*, 1238-1243.

[12] Ren, X.-D.; Hao, X.-Y.; Li, H.-C.; Ke, M.-R.; Zheng, B.-Y.; Huang, J.-D. "Progress in the development of nanosensitizers for X-ray-induced photodynamic therapy." *Drug Discov. Today* **2018**, *23*, 1791-1800.

[13] Abdul Kadir, L.; Stacey, M.; Barrett-Jolley, R. "Emerging Roles of the Membrane Potential: Action Beyond the Action Potential." *Front. Physiol.* **2018**, *9*, 1661-1661.

[14] Murota, H.; Matsui, S.; Ono, E.; Kijima, A.; Kikuta, J.; Ishii, M.; Katayama, I. “Sweat, the driving force behind normal skin: An emerging perspective on functional biology and regulatory mechanisms.” *J. Dermatol. Sci.* **2015**, *77*, 3-10.

[15] Lu, A. X.; Oh, H.; Terrell, J. L.; Bentley, W. E.; Raghavan, S. R. “A new design for an artificial cell: polymer microcapsules with addressable inner compartments that can harbor biomolecules, colloids or microbial species.” *Chem. Sci.* **2017**, *8*, 6893-6903.

[16] Igarashi, T.; Nishino, K.; Nayar, S. “The Appearance of Human Skin.” *Found. Trends Comput. Graph. Vis.* **2007**, *3*, 1-95.

[17] Yang, N. J.; Hinner, M. J. “Getting across the cell membrane: an overview for small molecules, peptides, and proteins.” *Methods mol. biol.* **2015**, *1266*, 29-53.

[18] Gadsby, D. C. “Ion channels versus ion pumps: the principal difference, in principle.” *Nat. Rev. Mol. Cell Biol.* **2009**, *10*, 344-352.

[19] Liu, Z.; Wang, W.; Xie, R.; Ju, X.-J.; Chu, L.-Y. “Stimuli-responsive smart gating membranes.” *Chem. Soc. Rev.* **2016**, *45*, 460-475.

[20] Kabashima, K.; Honda, T.; Ginhoux, F.; Egawa, G. “The immunological anatomy of the skin.” *Nat. Rev. Immunol.* **2019**, *19*, 19-30.

[21] Baker, L. B. “Physiology of sweat gland function: The roles of sweating and sweat composition in human health.” *Temperature* **2019**, *6*, 211-259.

[22] Kim, G.; Gardner, C.; Park, K.; Zhong, Y.; Jin, S. “Human-Skin-Inspired Adaptive Smart Textiles Capable of Amplified Latent Heat Transfer for Thermal Comfort.” *Adv. Intell. Syst.* **2020**, *2*, 2000163.

[23] Li, J.; Wong, W.-Y.; Tao, X.-m. “Recent advances in soft functional materials: preparation, functions and applications.” *Nanoscale* **2020**, *12*, 1281-1306.

[24] van der Gucht, J. “Grand Challenges in Soft Matter Physics.” *Front. Phys.* **2018**, *6*.

[25] Payne, G. F.; Kim, E.; Cheng, Y.; Wu, H.-C.; Ghodssi, R.; Rubloff, G. W.; Raghavan, S. R.; Culver, J. N.; Bentley, W. E. “Accessing biology's toolbox for the mesoscale biofabrication of soft matter.” *Soft Matter* **2013**, *9*, 6019-6032.

[26] Whitesides, G. M.; Grzybowski, B. “Self-Assembly at All Scales.” *Science* **2002**, *295*, 2418-2421.

[27] Yadav, S.; Sharma, A. K.; Kumar, P. “Nanoscale Self-Assembly for Therapeutic Delivery.” *Front. Bioeng. Biotechnol.* **2020**, *8*.

[28] Tanaka, T. “Gels.” *Sci. Am.* **1981**, *244*, 124-36, 138.

[29] Osada, Y.; Gong, J.-P. "Soft and Wet Materials: Polymer Gels." *Adv. Mater.* **1998**, *10*, 827-837.

[30] Ahmed, E. M. "Hydrogel: Preparation, characterization, and applications: A review." *J. Adv. Res.* **2015**, *6*, 105-121.

[31] Zhao, X.; Chen, X.; Yuk, H.; Lin, S.; Liu, X.; Parada, G. "Soft Materials by Design: Unconventional Polymer Networks Give Extreme Properties." *Chem. Rev.* **2021**, *121*, 4309-4372.

[32] Lin, C.-C.; Metters, A. T. "Hydrogels in controlled release formulations: Network design and mathematical modeling." *Adv. Drug Deliv. Rev.* **2006**, *58*, 1379-1408.

[33] Li, J.; Mooney, D. J. "Designing hydrogels for controlled drug delivery." *Nat. Rev. Mater.* **2016**, *1*, 16071.

[34] Quesada-Pérez, M.; Maroto-Centeno, J. A.; Forcada, J.; Hidalgo-Alvarez, R. "Gel swelling theories: the classical formalism and recent approaches." *Soft Matter* **2011**, *7*, 10536-10547.

[35] Tang, G.; Zhou, B.; Li, F.; Wang, W.; Liu, Y.; Wang, X.; Liu, C.; Ye, X. "Advances of Naturally Derived and Synthetic Hydrogels for Intervertebral Disk Regeneration." *Front. Bioeng. Biotechnol.* **2020**, *8*.

[36] Augst, A. D.; Kong, H. J.; Mooney, D. J. "Alginate Hydrogels as Biomaterials." *Macromol. Biosci.* **2006**, *6*, 623-633.

[37] Lee, K. Y.; Mooney, D. J. "Alginate: Properties and biomedical applications." *Prog. Polym. Sci.* **2012**, *37*, 106-126.

[38] Jen, A. C.; Wake, M. C.; Mikos, A. G. "Review: Hydrogels for cell immobilization." *Biotechnol. Bioeng.* **1996**, *50*, 357-364.

[39] Gasperini, L.; Mano, J. F.; Reis, R. L. "Natural polymers for the microencapsulation of cells." *J. R. Soc. Interface* **2014**, *11*, 20140817.

[40] Rinaudo, M. "Main properties and current applications of some polysaccharides as biomaterials." *Polym. Int.* **2008**, *57*, 397-430.

[41] Hirokawa, Y.; Tanaka, T. "Volume phase transition in a nonionic gel." *J. Chem. Phys.* **1984**, *81*, 6379-6380.

[42] Esser-Kahn, A. P.; Odom, S. A.; Sottos, N. R.; White, S. R.; Moore, J. S. "Triggered Release from Polymer Capsules." *Macromolecules* **2011**, *44*, 5539-5553.

[43] Wang, H.-C.; Zhang, Y.; Possanza, C. M.; Zimmerman, S. C.; Cheng, J.; Moore, J. S.; Harris, K.; Katz, J. S. "Trigger Chemistries for Better Industrial Formulations." *ACS Appl. Mater. Interfaces* **2015**, *7*, 6369-6382.

[44] Ahn, S.-k.; Kasi, R. M.; Kim, S.-C.; Sharma, N.; Zhou, Y. "Stimuli-responsive polymer gels." *Soft Matter* **2008**, *4*, 1151-1157.

[45] Lombardo, D.; Kiselev, M. A.; Magazù, S.; Calandra, P. "Amphiphiles Self-Assembly: Basic Concepts and Future Perspectives of Supramolecular Approaches." *Adv. Condens. Matter Phys.* **2015**, *2015*, 151683.

[46] Israelachvili, J. N.; Mitchell, D. J.; Ninham, B. W. "Theory of self-assembly of hydrocarbon amphiphiles into micelles and bilayers." *J. Chem. Soc., Faraday Trans. 2* **1976**, *72*, 1525-1568.

[47] Mitchell, D. J.; Ninham, B. W. "Micelles, vesicles and microemulsions." *J. Chem. Soc., Faraday Trans. 2* **1981**, *77*, 601-629.

[48] Marques, E. F. "Size and Stability of Catanionic Vesicles: Effects of Formation Path, Sonication, and Aging." *Langmuir* **2000**, *16*, 4798-4807.

[49] Oh, H.; Javvaji, V.; Yaraghi, N. A.; Abezgauz, L.; Danino, D.; Raghavan, S. R. "Light-induced transformation of vesicles to micelles and vesicle-gels to sols." *Soft Matter* **2013**, *9*, 11576-11584.

[50] Liang, J.; Liu, B. "ROS-responsive drug delivery systems." *Bioeng. Transl. Med.* **2016**, *1*, 239-251.

[51] Saravanakumar, G.; Kim, J.; Kim, W. J. "Reactive-Oxygen-Species-Responsive Drug Delivery Systems: Promises and Challenges." *Adv. Sci.* **2016**, *4*, 1600124-1600124.

[52] Xu, Q.; He, C.; Xiao, C.; Chen, X. "Reactive Oxygen Species (ROS) Responsive Polymers for Biomedical Applications." *Macromol. Biosci.* **2016**, *16*, 635-646.

[53] Gao, F.; Xiong, Z. "Reactive Oxygen Species Responsive Polymers for Drug Delivery Systems." *Front. Chem.* **2021**, *9*.

[54] Hu, B.; Lian, Z.; Zhou, Z.; Shi, L.; Yu, Z. "Reactive Oxygen Species-Responsive Adaptable Self-Assembly of Peptides toward Advanced Biomaterials." *ACS Appl. Bio Mater.* **2020**, *3*, 5529-5551.

[55] Lee, S. H.; Gupta, M. K.; Bang, J. B.; Bae, H.; Sung, H.-J. "Current Progress in Reactive Oxygen Species (ROS)-Responsive Materials for Biomedical Applications." *Adv. Healthc. Mater.* **2013**, *2*, 908-915.

[56] Tao, W.; He, Z. “ROS-responsive drug delivery systems for biomedical applications.” *Asian J. Pharm. Sci.* **2018**, *13*, 101-112.

[57] Guo, S.; He, S.; Chen, Z.; Zhang, Y. “Reactive oxygen species-responsive vesicle formed by selenium-containing cationic surfactant and SDS.” *J. Mol. Liq.* **2019**, *277*, 672-680.

[58] Napoli, A.; Valentini, M.; Tirelli, N.; Müller, M.; Hubbell, J. A. “Oxidation-responsive polymeric vesicles.” *Nat. Mater.* **2004**, *3*, 183-189.

[59] Abbasi, M.; Mohammadizadeh, M. R.; Moradi, Z. “Reduction of Sulfoxides with Ascorbic Acid Catalyzed by NBS.” *Bull. Chem. Soc. Jpn.* **2016**, *89*, 405-407.

[60] Yakabe, S.; Hirano, M.; Morimoto, T. “One-Pot Reduction of Sulfoxides with NaBH4, CoCl2 · 6H2O Catalyst, and Moist Alumina.” *Synth. Commun.* **2011**, *41*, 2251-2255.

[61] Jag, M. *Organic spectroscopy : principles and applications*, 2nd ed. ed.; Alpha Science International Ltd.: Harrow, U.K., **2004**.

[62] Lee, K. Y.; Mooney, D. J. “Hydrogels for Tissue Engineering.” *Chem. Rev.* **2001**, *101*, 1869-1880.

[63] Sun, J.-Y.; Keplinger, C.; Whitesides, G. M.; Suo, Z. “Ionic skin.” *Adv. Mater.* **2014**, *26*, 7608-7614.

[64] Yang, C. H.; Chen, B.; Lu, J. J.; Yang, J. H.; Zhou, J.; Chen, Y. M.; Suo, Z. “Ionic cable.” *Extreme Mech. Lett.* **2015**, *3*, 59-65.

[65] Jang, K.-I.; Chung, H. U.; Xu, S.; Lee, C. H.; Luan, H.; Jeong, J.; Cheng, H.; Kim, G.-T.; Han, S. Y.; Lee, J. W.; Kim, J.; Cho, M.; Miao, F.; Yang, Y.; Jung, H. N.; Flavin, M.; Liu, H.; Kong, G. W.; Yu, K. J.; Rhee, S. I.; Chung, J.; Kim, B.; Kwak, J. W.; Yun, M. H.; Kim, J. Y.; Song, Y. M.; Paik, U.; Zhang, Y.; Huang, Y.; Rogers, J. A. “Soft network composite materials with deterministic and bio-inspired designs.” *Nat. Commun.* **2015**, *6*, 6566.

[66] Schroeder, T. B. H.; Guha, A.; Lamoureux, A.; VanRenterghem, G.; Sept, D.; Shtein, M.; Yang, J.; Mayer, M. “An electric-eel-inspired soft power source from stacked hydrogels.” *Nature* **2017**, *552*, 214-218.

[67] Yang, C.; Suo, Z. “Hydrogel ionotronics.” *Nat. Rev. Mater.* **2018**, *3*, 125-142.

[68] Martin, L. B. B.; Rose, J. K. C. “There's more than one way to skin a fruit: formation and functions of fruit cuticles.” *J. Exp. Bot.* **2014**, *65*, 4639-4651.

[69] Lara, I.; Belge, B.; Goulao, L. F. “A Focus on the Biosynthesis and Composition of Cuticle in Fruits.” *J. Agric. Food Chem.* **2015**, *63*, 4005-4019.

[70] Tang, J.; Li, J.; Vlassak, J. J.; Suo, Z. “Adhesion between highly stretchable materials.” *Soft Matter* **2016**, *12*, 1093-1099.

[71] Yuk, H.; Zhang, T.; Parada, G. A.; Liu, X.; Zhao, X. “Skin-inspired hydrogel–elastomer hybrids with robust interfaces and functional microstructures.” *Nat. Commun.* **2016**, *7*, 12028.

[72] Li, T.; Li, G.; Liang, Y.; Cheng, T.; Dai, J.; Yang, X.; Liu, B.; Zeng, Z.; Huang, Z.; Luo, Y.; Xie, T.; Yang, W. “Fast-moving soft electronic fish.” *Sci. Adv.* **2017**, *3*, e1602045.

[73] Tian, K.; Bae, J.; Bakarich, S. E.; Yang, C.; Gately, R. D.; Spinks, G. M.; in het Panhuis, M.; Suo, Z.; Vlassak, J. J. “3D Printing of Transparent and Conductive Heterogeneous Hydrogel–Elastomer Systems.” *Adv. Mater.* **2017**, *29*, 1604827.

[74] Wirthl, D.; Pichler, R.; Drack, M.; Kettlguber, G.; Moser, R.; Gerstmayr, R.; Hartmann, F.; Bradt, E.; Kaltseis, R.; Siket, C. M.; Schausberger, S. E.; Hild, S.; Bauer, S.; Kaltenbrunner, M. “Instant tough bonding of hydrogels for soft machines and electronics.” *Sci. Adv.* **2017**, *3*, e1700053.

[75] Feng, J.-F.; Chen, J.-L.; Guo, K.; Hou, J.-B.; Zhou, X.-L.; Huang, S.; Li, B.-J.; Zhang, S. “Leeches-Inspired Hydrogel–Elastomer Integration Materials.” *ACS Appl. Mater. Interfaces* **2018**, *10*, 40238-40245.

[76] Kim, S. H.; Jung, S.; Yoon, I. S.; Lee, C.; Oh, Y.; Hong, J.-M. “Ultrastretchable Conductor Fabricated on Skin-Like Hydrogel–Elastomer Hybrid Substrates for Skin Electronics.” *Adv. Mater.* **2018**, *30*, 1800109.

[77] Liu, Q.; Nian, G.; Yang, C.; Qu, S.; Suo, Z. “Bonding dissimilar polymer networks in various manufacturing processes.” *Nat. Commun.* **2018**, *9*, 846.

[78] Liu, T.; Liu, M.; Dou, S.; Sun, J.; Cong, Z.; Jiang, C.; Du, C.; Pu, X.; Hu, W.; Wang, Z. L. “Triboelectric-Nanogenerator-Based Soft Energy-Harvesting Skin Enabled by Toughly Bonded Elastomer/Hydrogel Hybrids.” *ACS Nano* **2018**, *12*, 2818-2826.

[79] Tian, K.; Bae, J.; Suo, Z.; Vlassak, J. J. “Adhesion between Hydrophobic Elastomer and Hydrogel through Hydrophilic Modification and Interfacial Segregation.” *ACS Appl. Mater. Interfaces* **2018**, *10*, 43252-43261.

[80] Xie, W.; Duan, J.; Wang, H.; Li, J.; Liu, R.; Yu, B.; Liu, S.; Zhou, J. “Ultra-stretchable, bio-inspired ionic skins that work stably in various harsh environments.” *J. Mater. Chem. A* **2018**, *6*, 24114-24119.

[81] Baker, A. B.; Bates, S. R. G.; Llewellyn-Jones, T. M.; Valori, L. P. B.; Dicker, M. P. M.; Trask, R. S. “4D printing with robust thermoplastic polyurethane hydrogel-elastomer trilayers.” *Mater. Des.* **2019**, *163*, 107544.

[82] Macron, J.; Gerratt, A. P.; Lacour, S. P. "Thin Hydrogel–Elastomer Multilayer Encapsulation for Soft Electronics." *Adv. Mater. Tecnol.* **2019**, *4*, 1900331.

[83] Yang, H.; Li, C.; Yang, M.; Pan, Y.; Yin, Q.; Tang, J.; Qi, H. J.; Suo, Z. "Printing Hydrogels and Elastomers in Arbitrary Sequence with Strong Adhesion." *Adv. Funct. Mater.* **2019**, *29*, 1901721.

[84] Daristotle, J. L.; Zaki, S. T.; Lau, L. W.; Ayyub, O. B.; Djouini, M.; Srinivasan, P.; Erdi, M.; Sandler, A. D.; Kofinas, P. "Pressure-Sensitive Tissue Adhesion and Biodegradation of Viscoelastic Polymer Blends." *ACS Appl. Mater. Interfaces* **2020**, *12*, 16050-16057.

[85] Sun, K.; Oh, H.; Emerson, J. F.; Raghavan, S. R. "A new method for centrifugal separation of blood components: Creating a rigid barrier between density-stratified layers using a UV-curable thixotropic gel." *J. Mater. Chem* **2012**, *22*, 2378-2382.

[86] Raghavan, S. R.; Hou, J.; Baker, G. L.; Khan, S. A. "Colloidal Interactions between Particles with Tethered Nonpolar Chains Dispersed in Polar Media: Direct Correlation between Dynamic Rheology and Interaction Parameters." *Langmuir* **2000**, *16*, 1066-1077.

[87] Cipriano, B. H.; Banik, S. J.; Sharma, R.; Rumore, D.; Hwang, W.; Briber, R. M.; Raghavan, S. R. "Superabsorbent Hydrogels That Are Robust and Highly Stretchable." *Macromolecules* **2014**, *47*, 4445-4452.

[88] Grassi, M.; Sandolo, C.; Perin, D.; Coviello, T.; Lapasin, R.; Grassi, G. "Structural Characterization of Calcium Alginate Matrices by Means of Mechanical and Release Tests." *Molecules* **2009**, *14*, 3003-3017.

[89] Hermansson, E.; Schuster, E.; Lindgren, L.; Altskär, A.; Ström, A. "Impact of solvent quality on the network strength and structure of alginate gels." *Carbohydr. Polym.* **2016**, *144*, 289-296.

[90] Baglioni, P.; Baglioni, M.; Bonelli, N.; Chelazzi, D.; Giorgi, R. "Chapter 9 - Smart Soft Nanomaterials for Cleaning." in *Nanotechnologies and Nanomaterials for Diagnostic, Conservation and Restoration of Cultural Heritage*; Lazzara, G., Fakhrullin, R., Eds.; Elsevier, **2019**; pp 171-204.

[91] Wu, Z.; Yang, X.; Wu, J. "Conductive Hydrogel- and Organohydrogel-Based Stretchable Sensors." *ACS Appl. Mater. Interfaces* **2021**, *13*, 2128-2144.

[92] Hoffman, A. S. "Hydrogels for biomedical applications." *Adv. Drug Deliv. Rev.* **2002**, *54*, 3-12.

[93] Mitura, S.; Sionkowska, A.; Jaiswal, A. "Biopolymers for hydrogels in cosmetics: review." *J. Mater. Sci.: Mater. Med.* **2020**, *31*, 50-50.

[94] Rudzinski, W. E.; Dave, A. M.; Vaishnav, U. H.; Kumbar, S. G.; Kulkarni, A. R.; Aminabhavi, T. M. "Hydrogels as controlled release devices in agriculture." *Des. Monomers Polym.* **2002**, *5*, 39-65.

[95] Campos, E. V. R.; de Oliveira, J. L.; Fraceto, L. F.; Singh, B. "Polysaccharides as safer release systems for agrochemicals." *Agron. Sustain. Dev.* **2015**, *35*, 47-66.

[96] Thompson, B. R.; Zarket, B. C.; Lauten, E. H.; Amin, S.; Muthukrishnan, S.; Raghavan, S. R. "Liposomes Entrapped in Biopolymer Hydrogels Can Spontaneously Release into the External Solution." *Langmuir* **2020**, *36*, 7268-7276.

[97] Vaishya, R.; Khurana, V.; Patel, S.; Mitra, A. K. "Long-term delivery of protein therapeutics." *Expert Opin. Drug Deliv.* **2015**, *12*, 415-40.

[98] Ahn, S. H.; Rath, M.; Tsao, C.-Y.; Bentley, W. E.; Raghavan, S. R. "Single-Step Synthesis of Alginate Microgels Enveloped with a Covalent Polymeric Shell: A Simple Way to Protect Encapsulated Cells." *ACS Appl. Mater. Interfaces* **2021**, *13*, 18432-18442.

[99] Sikdar, P.; Uddin, M. M.; Dip, T. M.; Islam, S.; Hoque, M. S.; Dhar, A. K.; Wu, S. "Recent advances in the synthesis of smart hydrogels." *Mater. Adv.* **2021**, *2*, 4532-4573.

[100] Huebsch, N.; Kearney, C. J.; Zhao, X.; Kim, J.; Cezar, C. A.; Suo, Z.; Mooney, D. J. "Ultrasound-triggered disruption and self-healing of reversibly cross-linked hydrogels for drug delivery and enhanced chemotherapy." *Proc. Natl. Acad. Sci.* **2014**, *111*, 9762-9767.

[101] Sun, N.; Sun, P.; Wu, A.; Qiao, X.; Lu, F.; Zheng, L. "Facile fabrication of thermo/redox responsive hydrogels based on a dual crosslinked matrix for a smart on–off switch." *Soft Matter* **2018**, *14*, 4327-4334.

[102] Zhang, J.; Zheng, Y.; Lee, J.; Hua, J.; Li, S.; Panchamukhi, A.; Yue, J.; Gou, X.; Xia, Z.; Zhu, L.; Wu, X. "A pulsatile release platform based on photo-induced imine-crosslinking hydrogel promotes scarless wound healing." *Nat. Commun.* **2021**, *12*, 1670.

[103] Kikuchi, A.; Okano, T. "Pulsatile drug release control using hydrogels." *Adv. Drug Deliv. Rev.* **2002**, *54*, 53-77.

[104] Campbell, S.; Maitland, D.; Hoare, T. "Enhanced Pulsatile Drug Release from Injectable Magnetic Hydrogels with Embedded Thermosensitive Microgels." *ACS Macro Lett.* **2015**, *4*, 312-316.

[105] Vertommen, M. A. M. E.; Cornelissen, H.-J. L.; Dietz, C. H. J. T.; Hoogenboom, R.; Kemmere, M. F.; Keurentjes, J. T. F. "Pore-covered thermoresponsive membranes for repeated on-demand drug release." *J. Membr. Sci.* **2008**, *322*, 243-248.

[106] Satarkar, N. S.; Hilt, J. Z. "Magnetic hydrogel nanocomposites for remote controlled pulsatile drug release." *J. Control. Release* **2008**, *130*, 246-251.

[107] Amoli-Diva, M.; Sadighi-Bonabi, R.; Pourghazi, K. "Switchable on/off drug release from gold nanoparticles-grafted dual light- and temperature-responsive hydrogel for controlled drug delivery." *Mater. Sci. Eng. C Mater. Biol. Appl.* **2017**, *76*, 242-248.

[108] Subraveti, S. N.; Raghavan, S. R. "A Simple Way to Synthesize a Protective "Skin" around Any Hydrogel." *ACS Appl. Mater. Interfaces* **2021**, *13*, 37645-37654.

[109] Xu, S.; Ng, G.; Xu, J.; Kuchel, R. P.; Yeow, J.; Boyer, C. "2-(Methylthio)ethyl Methacrylate: A Versatile Monomer for Stimuli Responsiveness and Polymerization-Induced Self-Assembly in the Presence of Air." *ACS Macro Lett.* **2017**, *6*, 1237-1244.

[110] Yao, Y.; Zhang, H.; Wang, Z.; Ding, J.; Wang, S.; Huang, B.; Ke, S.; Gao, C. "Reactive oxygen species (ROS)-responsive biomaterials mediate tissue microenvironments and tissue regeneration." *J. Mater. Chem. B* **2019**, *7*, 5019-5037.

[111] Zhao, D.; Zhou, Q.; Yang, K.; Yang, H.; Tang, Q.; Zhang, X. "An Injectable ROS-Responsive Self-Healing Hydrogel Based on tetra-poly(ethylene glycol)-b-oligo(l-methionine)." *Macromol. Chem. Phys.* **2019**, *220*, 1900106.

[112] Saini, B.; Sinha, M. K.; Dey, A. "Functionalized polymeric smart membrane for remediation of emerging environmental contaminants from industrial sources: Synthesis, characterization and potential applications." *Process Saf. Environ. Prot.* **2022**, *161*, 684-702.

[113] Nakayama, H.; Kaetsu, I.; Uchida, K.; Sakata, S.; Tougou, K.; Hara, T.; Matsubara, Y. "Radiation curing of intelligent coating for controlled release and permeation." *Radiat. Phys. Chem.* **2002**, *63*, 521-523.

[114] Wandera, D.; Wickramasinghe, S. R.; Husson, S. M. "Stimuli-responsive membranes." *J. Membr. Sci.* **2010**, *357*, 6-35.

[115] Golchoubian, H.; Hosseinpoor, F. "Effective oxidation of sulfides to sulfoxides with hydrogen peroxide under transition-metal-free conditions." *Molecules* **2007**, *12*, 304-311.

[116] Whitesides, G. M.; Boncheva, M. "Beyond molecules: Self-assembly of mesoscopic and macroscopic components." *Proc. Natl. Acad. Sci.* **2002**, *99*, 4769-4774.

[117] Mendes, A. C.; Baran, E. T.; Reis, R. L.; Azevedo, H. S. "Self-assembly in nature: using the principles of nature to create complex nanobiomaterials." *Wiley Interdiscip. Rev. Nanomed. Nanobiotechnol.* **2013**, *5*, 582-612.

[118] Rideau, E.; Dimova, R.; Schwille, P.; Wurm, F. R.; Landfester, K. "Liposomes and polymersomes: a comparative review towards cell mimicking." *Chem. Soc. Rev.* **2018**, *47*, 8572-8610.

[119] Domazet Jurašin, D.; Šegota, S.; Strasser, V.; Selmani, A.; Dutour Sikirić, M. "Recent Advances in Catanionic Mixtures." in *Application and Characterization of Surfactants*; IntechOpen, **2017**.

[120] Akbarzadeh, A.; Rezaei-Sadabady, R.; Davaran, S.; Joo, S. W.; Zarghami, N.; Hanifehpour, Y.; Samiei, M.; Kouhi, M.; Nejati-Koshki, K. "Liposome: classification, preparation, and applications." *Nanoscale Res. Lett.* **2013**, *8*, 102.

[121] Kuo, A.-T.; Chang, C.-H. "Recent Strategies in the Development of Catanionic Vesicles." *J. Oleo Sci.* **2016**, *65*, 377-384.

[122] Kaler, E. W.; Murthy, A. K.; Rodriguez, B. E.; Zasadzinski, J. A. N. "Spontaneous Vesicle Formation in Aqueous Mixtures of Single-Tailed Surfactants." *Science* **1989**, *245*, 1371-1374.

[123] Stagnoli, S.; Luna, M. A.; Villa, C. C.; Alustiza, F.; Niebylski, A.; Moyano, F.; Correa, N. M.; Falcone, R. D. "Unique catanionic vesicles as a potential "Nano-Taxi" for drug delivery systems. In vitro and in vivo biocompatibility evaluation." *RSC Adv.* **2017**, *7*, 5372-5380.

[124] Davies, T. S.; Ketner, A. M.; Raghavan, S. R. "Self-Assembly of Surfactant Vesicles that Transform into Viscoelastic Wormlike Micelles upon Heating." *J. Am. Chem. Soc.* **2006**, *128*, 6669-6675.

[125] Yang, Y.; Liu, L.; Huang, X.; Tan, X.; Luo, T.; Li, W. "Temperature-induced vesicle to micelle transition in cationic/cationic mixed surfactant systems." *Soft Matter* **2015**, *11*, 8848-8855.

[126] Ghosh, R.; Dey, J. "Vesicle-to-Micelle Transition in Aqueous Solutions of l-Cysteine-Derived Carboxylate Surfactants Containing Both Hydrocarbon and Poly(ethylene glycol) Tails." *Langmuir* **2017**, *33*, 543-552.

[127] González, Y. I.; Nakanishi, H.; Stjerndahl, M.; Kaler, E. W. "Influence of pH on the Micelle-to-Vesicle Transition in Aqueous Mixtures of Sodium Dodecyl Benzenesulfonate with Histidine." *J. Phys. Chem. B* **2005**, *109*, 11675-11682.

[128] Winterbourn, C. C. "Reconciling the chemistry and biology of reactive oxygen species." *Nat. Chem. Biol.* **2008**, *4*, 278-286.

[129] Valentine, J. S.; Gralla, E. B. "Introduction: Reactive Oxygen Species Special Feature." *Proc. Natl. Acad. Sci.* **2008**, *105*, 8178-8178.

[130] Zhou, Z.; Song, J.; Nie, L.; Chen, X. "Reactive oxygen species generating systems meeting challenges of photodynamic cancer therapy." *Chem. Soc. Rev.* **2016**, *45*, 6597-6626.

[131] Deng, W.; Chen, W.; Clement, S.; Guller, A.; Zhao, Z.; Engel, A.; Goldys, E. M. "Controlled gene and drug release from a liposomal delivery platform triggered by X-ray radiation." *Nat. Commun.* **2018**, *9*, 2713.

[132] Du, Y.; He, W.; Xia, Q.; Zhou, W.; Yao, C.; Li, X. "Thioether Phosphatidylcholine Liposomes: A Novel ROS-Responsive Platform for Drug Delivery." *ACS Appl. Mater. Interfaces* **2019**, *11*, 37411-37420.

[133] Geven, M.; d'Arcy, R.; Turhan, Y.; El Mohtadi, F.; Alshamsan, A.; Tirelli, N. "Sulfur-based oxidation-responsive polymers. Chemistry, (chemically selective) responsiveness and biomedical applications." *Eur. Polym. J.* **2021**, *149*, 110387.

[134] Denkova, A. G.; Liu, H.; Men, Y.; Eelkema, R. "Enhanced Cancer Therapy by Combining Radiation and Chemical Effects Mediated by Nanocarriers." *Adv. Ther.* **2020**, *3*, 1900177.

[135] Cao, Y.; Hu, X.-Y.; Li, Y.; Zou, X.; Xiong, S.; Lin, C.; Shen, Y.-Z.; Wang, L. "Multistimuli-Responsive Supramolecular Vesicles Based on Water-Soluble Pillar[6]arene and SAINT Complexation for Controllable Drug Release." *J. Am. Chem. Soc.* **2014**, *136*, 10762-10769.

[136] Li, W.; Yang, Y.; Liu, L.; Tan, X.; Luo, T.; Shen, J. "Dual stimuli-responsive self-assembly transition in zwitterionic/anionic surfactant systems." *Soft Matter* **2015**, *11*, 4283-4289.

[137] Li, S.; Chu, X.; Hao, A.; Shang, N.; Wang, C. "A triply-responsive supramolecular vesicle fabricated by α-cyclodextrin based host–guest recognition and double dynamic covalent bonds." *Soft Matter* **2018**, *14*, 9923-9927.

[138] Ma, M.; Xu, S.; Xing, P.; Li, S.; Chu, X.; Hao, A. "A multistimuli-responsive supramolecular vesicle constructed by cyclodextrins and tyrosine." *Colloid Polym. Sci.* **2014**, *293*.

[139] Xing, L.-B.; Yu, S.; Wang, X.-J.; Wang, G.-X.; Chen, B.; Zhang, L.-P.; Tung, C.-H.; Wu, L.-Z. "Reversible multistimuli-responsive vesicles formed by an amphiphilic cationic platinum(ii) terpyridyl complex with a ferrocene unit in water." *Chem. Commun.* **2012**, *48*, 10886-10888.

[140] Zhang, Y.; Uthaman, S.; Song, W.; Eom, K. H.; Jeon, S. H.; Huh, K. M.; Babu, A.; Park, I.-K.; Kim, I. "Multistimuli-Responsive Polymeric Vesicles for Accelerated Drug Release in Chemo-photothermal Therapy." *ACS Biomater. Sci. Eng.* **2020**, *6*, 5012-5023.

[141] Zhou, J.; Tang, Q.; Zhong, J.; Lei, Z.; Luo, H.; Tong, Z.; Jiang, G.; Liu, X. "Construction of glucose and H2O2 dual stimuli-responsive polymeric vesicles and their application in controlled drug delivery." *J. Mater. Sci.* **2018**, *53*.

[142] Monney, B.; Hess-Dunning, A. E.; Gloth, P.; Capadona, J. R.; Weder, C. "Mechanically adaptive implants fabricated with poly(2-hydroxyethyl methacrylate)-based negative photoresists." *J. Mater. Chem. B* **2020**, *8*, 6357-6365.

[143] Dektar, J. L.; Hacker, N. P. "Photochemistry of triarylsulfonium salts." *J. Am. Chem. Soc.* **1990**, *112*, 6004-6015.

[144] Danino, D.; Bernheim-Groswasser, A.; Talmon, Y. "Digital cryogenic transmission electron microscopy: an advanced tool for direct imaging of complex fluids." *Colloids Surf. A: Physicochem. Eng. Asp.* **2001**, *183-185*, 113-122.

[145] Danino, D. "Cryo-TEM of soft molecular assemblies." *Curr. Opin. Colloid Interface Sci.* **2012**, *17*, 316-329.

[146] Höfer, M.; Liska, R. "Photochemistry and initiation behavior of phenylethynyl onium salts as cationic photoinitiators." *J. Polym. Sci. A: Polym. Chem.* **2009**, *47*, 3419-3430.

[147] Zhang, Y.; Liu, L.; Liu, X.; Fang, Y. "Reversibly Switching Wormlike Micelles Formed by a Selenium-Containing Surfactant and Benzyl Tertiary Amine Using CO2/N2 and Redox Reaction." *Langmuir* **2018**, *34*, 2302-2311.

[148] Sugiarto, I.; Isnaeni; Putri, K. "Analysis of dual peak emission from Rhodamine 6G organic dyes using photoluminescence." *J. Phys. Conf. Ser.* **2017**, *817*, 012047.

[149] Danoff, E. J.; Wang, X.; Tung, S.-H.; Sinkov, N. A.; Kemme, A. M.; Raghavan, S. R.; English, D. S. "Surfactant Vesicles for High-Efficiency Capture and Separation of Charged Organic Solutes." *Langmuir* **2007**, *23*, 8965-8971.

[150] Wang, X.; Danoff, E. J.; Sinkov, N. A.; Lee, J.-H.; Raghavan, S. R.; English, D. S. "Highly Efficient Capture and Long-Term Encapsulation of Dye by Catanionic Surfactant Vesicles." *Langmuir* **2006**, *22*, 6461-6464.

[151] Laracuente, M.-L.; Yu, M. H.; McHugh, K. J. "Zero-order drug delivery: State of the art and future prospects." *J. Control. Release* **2020**, *327*, 834-856.

[152] Dendukuri, D.; Gu, S. S.; Pregibon, D. C.; Hatton, T. A.; Doyle, P. S. "Stop-flow lithography in a microfluidic device." *Lab Chip* **2007**, *7*, 818-828.

[153] Shah, R. K.; Shum, H. C.; Rowat, A. C.; Lee, D.; Agresti, J. J.; Utada, A. S.; Chu, L.-Y.; Kim, J.-W.; Fernandez-Nieves, A.; Martinez, C. J.; Weitz, D. A. "Designer emulsions using microfluidics." *Mater. Today* **2008**, *11*, 18-27.

[154] Akamatsu, K. “Development of ‘leaky’ liposome triggered by radiation applicable to a drug reservoir and a simple radiation dosimeter.” *Appl. Radiat. Isot.* **2013**, *74*, 144-151.